UNIVERSITY OF CALIFORNIA SAN DIEGO

Therapeutic Functions of Bioengineered, Enucleated Cells

A dissertation submitted in partial satisfaction of the
requirements for the degree Doctor of Philosophy

in

Biomedical Sciences

by

Christina Nicole Alarcón

Committee in charge:

Professor Richard L. Klemke, Chair
Professor Jack Bui
Professor Peter Ernst
Professor Victor Nizet
Professor Maurizio Zanetti

2020

The Dissertation of Christina Nicole Alarcón is approved, and it is acceptable in quality and form for publication on microfilm and electronically:

_____

_____

_____

_____

_____

Chair

University of California San Diego
2020

DEDICATION

With eternal gratitude to God, my family, friends, mentors, and colleagues.
Without you, I would not be who I am today.

TABLE OF CONTENTS

LIST OF FIGURES

LIST OF TABLES

ACKNOWLEDGEMENTS

I humbly acknowledge Professor Richard L. Klemke for his input as thesis advisor and chair of my thesis committee. His vision and enthusiasm for the therapeutic possibilities of enucleated cells guided this project.

I gratefully acknowledge members of the Klemke Lab, who provided invaluable resources, support, assistance, and camaraderie during this long project. I specifically recognize Bei Liu and Felicia Watson for their help and teamwork on all the mini-projects and multitasking involved in this intricate platform technology. I also enthusiastically thank Huawei Wang for his constant mentorship, support, and guidance during my growth as a scientist in this lab.

This work was supported by the National Institutes of Health (NIH) grants R01 CA097022, CA184594 and CA182495 to Richard Klemke, and Center for Drug Discovery and Innovation at UC San Diego to Richard Klemke. Christina N. Alarcón was supported by NIH 5T32 OD17863-4, a postdoctoral research training grant for veterinary scientists, and a short-term, much-appreciated stipend support from the UC San Diego Biomedical Sciences Program. Imaging and analysis was in part performed at the UCSD School of Medicine Microscopy Core (NS047101) and UCSD Moores Cancer Center Tissue Technology Shared Resource Core (CCSG Grant P30CA23100). Human primary bone marrow MSCs were obtained from Texas A&M Health Science Center College of Medicine Institute for Regenerative Medicine (NIH P40OD011050).

Portions of this work are included in a patent submission (U.S. Provisional Patent Application Serial No. 62/542,133 by Richard Klemke and Huawei Wang) and the Cytonus Therapeutics, Inc.[1] website (Richard Klemke).

The Introduction and Chapters 1-5, in part, have been submitted for publication of the material as it may appear in Nature Biotechnology, H. Wang, C.N. Alarcón, B. Liu, F. Watson, S.

Searles, C. Lee, J. Keys, W. Pi, D. Allen, J. Lammerding, J.D. Bui, and R.L. Klemke, 2020. The dissertation author was the co-primary investigator and co-first author of this paper.

VITA

2006	Bachelor of Arts, Stanford University
2006-2008	Life Science Research Assistant, Stanford University
2012	Doctor of Veterinary Medicine, University of California, Davis
2012-2015	Veterinary Anatomic Pathology Resident, University of California, Davis
2017	Diplomate, American College of Veterinary Pathologists
2020	Doctor of Philosophy, University of California San Diego

ABSTRACT OF THE DISSERTATION

Therapeutic Functions of Bioengineered, Enucleated Cells

by

Christina Nicole Alarcón

Doctor of Philosophy in Biomedical Sciences

University of California San Diego, 2020

Professor Richard Klemke, Chair

Cell-based therapies hold tremendous potential to treat cancer, inflammatory conditions, and degenerative diseases. However, despite a few notable successes, cell-based therapies face key clinical barriers, including cell source heterogeneity, inefficient directed migration (homing) to target tissues, cell dosing or controllability, inability to affect tissue microenvironments, and patient safety. Bioengineering may potentially enhance cell capabilities, but raises safety concerns regarding the control of genetically engineered cells in vivo. Therefore, bioengineering methods to improve cell-based therapy efficacy must prioritize predictable behavior and safety.

To address these issues, the Klemke Laboratory developed a platform technology that couples cell bioengineering with cell enucleation (mass removal of nuclei) to enhance cellular function and controllability. By adapting methods developed in the 1970s, mesenchymal stromal cells (MSCs) were enucleated by ultracentrifugation in discontinuous Ficoll gradients containing

cytochalasin B. Combining cell bioengineering with enucleation both decreases the risk of engraftment and oncogenesis, and provides opportunities for customized pre- and/or post-enucleation bioengineering. We named these bioengineered, enucleated cells "Cargocytes™".

Cargocytes were characterized by absent nuclei, viability for 2-3 days, functional protein translational machinery, retention of receptor expression, and directional migration, and then further investigated via bioengineering with therapeutically-relevant properties. For in vitro studies, Cargocytes were bioengineered and then examined for secretion of functional cytokines and expression of functional chemokine receptors. Next, Cargocytes in vivo abilities were examined in two independent mouse models. First, bioengineered Cargocytes injected intratumorally in a mouse breast cancer model produced functional antitumor cytokine that slowed tumor progression and increased animal survival. Second, bioengineered Cargocytes injected intravenously in a mouse ear inflammation model both homed to the site of inflammation and produced functional anti-inflammatory cytokine that reduced inflammation. This suggests that bioengineered, enucleated cells are more efficacious than non-engineered cells, and lacking nuclei uniquely contributes to safety and controllability in vivo.

To my knowledge, therapeutic bioengineering of enucleated cells has not been previously described, and Cargocytes represent a unique entity in the cell-based therapy field as either a stand-alone or adjuvant therapy. By retaining biologically important cell-like functions yet with advantages like small size and defined lifespan, Cargocytes potentially resolve key barriers currently limiting cell-based therapies.

Introduction: Cell-Based Therapies in the Treatment of Diseases

1 The potential promise and problems in cell-based therapies

Cell-based therapies are a field of medicine and research in which cells from a patient (autologous) or from a donor (allogeneic) are isolated, purified, enhanced, or modified in order to have a therapeutic effect when transplanted or transferred into the patient. Early scientific attempts at cell-based therapy in the 1880s and 1930s involved injection of animal cells into human patients to reduce aging or treat cancer, and while these treatments produced no validated or documented success, these ideas paved the way for future development of hormone therapies and stem cell therapies.[2] The first successful, medically-validated use of cell therapy in humans was a bone marrow transplant between identical twins in the 1950s, which spurred the maturation of the hematopoietic stem cell (HSC) field for the treatment of blood disorders.[3] By 2014, HSC emerged as the most common cell-based therapy in clinical trials, followed by mesenchymal stromal cells (MSCs), lymphocytes, and dendritic cells.[4] With recent technologic advances, cell-based therapies are poised to become an additional "pillar" of therapeutic healthcare, alongside the traditional pillars of pharmaceuticals (small molecules and drugs), biologics (hormones, antibodies, gene therapies), and medical devices.[5]

Cell-based therapies hold incredible promise to treat many types of disease, such as cancer, inflammatory conditions, and degenerative diseases. Compared to conventional pharmaceuticals and biologics, cells possess the ability to physically respond to, interact with, and regulate their microenvironment,[6, 7] such as through cell-cell junctions, tunneling nanotubes, extracellular vesicles, expression of surface molecules, and release or receipt of signaling molecules. Despite over 1,300 listed cell therapy clinical trials,[8] the Food and Drug Administration (FDA) to date has only approved 14 cell therapy products, including eight hematopoietic progenitor cell (HPC, HSC),

two chimeric antigen receptor T cell (CAR T), and four other cell types (fibroblasts, keratinocytes, chondrocytes, dendritic cells).[9, 10] This discrepancy between the intensity of cell therapy research and the list of FDA-approved products can be attributed to clinical barriers in achieving reproducible efficacy and safety, wherein selection of patient population, donor cell heterogeneity and efficacy, scalability and effect of cell culturing protocols, quality control and standardization of cell products, and administration technique all affect the ultimate variability and therefore outcome of clinical trials.[11] While some of these barriers can be addressed on an institutional level, such as through randomizing patients to treatment groups or defining more rigorous patient eligibility criteria, our laboratory focused on addressing the efficacy and safety of the therapeutic cell itself. Because one prominent constraint to cell therapies is the inability to achieve an appropriate number of viable, therapeutically efficacious cells at the target site, we posed the following question: How can we improve the in vivo efficacy, reproducibility, and safety of cell therapies?

2 Bioengineering to improve efficacy and controllability in cell-based therapies

The variability in properties of therapeutic cells arises from multiple sources. Aside from potential differences between different donors, there can also be significant intrinsic heterogeneity of cells from the same donor between cells harvested from different tissue sources,[12] and individual cells within a clonal population.[13] Additionally, ex vivo culture techniques and the tissue microenvironment can influence the overall in vivo efficacy of cells.[14] Once in the body, cell therapies face problems related to cell trafficking and biodistribution, homing and targeting to desired sites, and tissue penetration.[15] In an ideal scenario, it would be possible to control cell proliferation and death, cell migration and homing to target sites, targeted effects, cell-cell communication and response to signals, and production and secretion of bioengineered therapeutic

products.[7] To achieve these goals, methods like bioengineering can be harnessed to improve both the consistency, quality, specificity, and efficacy of cell-based therapeutics.[15-17] In this field, bioengineering refer to genetic or non-genetic modification of cells to produce a desired therapeutic effect. As a few examples, T cells infected with viral vectors to express endogenous or synthetic surface markers (chimeric antigen receptors) became CAR T cells able to bind specific targets;[18]coating cells with nanopolymers embedded with adhesion molecules improved extravasation into target tissues;[19]and cells transfected with mRNAs encoding the cytotoxic TRAIL ligand induced death of tumor cells.[20] In the context of precision medicine, bioengineering might include reverse-engineering a therapeutic cell based on the genetic signature, antigen expression, cytokine profile, or disease state of the patient. Given the wide variety of manipulations available to modify cells, our question was refined: How can bioengineering be applied to more specifically improve the efficacy, reproducibility, and safety of cell-based therapies?

While bioengineering can address many pitfalls inherent in cell-based therapies, it is still necessary to address the controllability of cell behavior in vivo. This is of particular importance in pluripotent stem cell therapies like human embryonic stem cells or induced pluripotent stem cells (iPSC), which have the potential to differentiate, proliferate, and in some cases, transform into tumors.[21-23] The FDA has recognized the uncertainty in this rapidly-evolving field, and issued a consumer alert warning about the risks involved in the unregulated use of stem cells.[24] There is also the possibility that transplantation of donor DNA can eventually elicit immune reactions.[25, 26] To address controllability and patient safety, some cell-based therapies include irradiation of cells to induce irreversible DNA damage,[27, 28] on-switches,[29] or bioengineering with an apoptosis-inducing suicide switch.[30-32] However, irradiation can induce production of undesirable cytokines[33] or compromise cellular functions, and suicide switches can fail[34] or introduce problems

such as immunogenicity, slow onset, no prevention of toxicity, and potentially eradicate cells prematurely.[29] Therefore, our lab considered alternative methods to reduce or even remove the risk of DNA, and specifically engineered DNA, in cell-based therapies. This led us to explore the process of cell enucleation, in which the nucleus is removed from the cell. Theoretically, removing the cell nucleus would prevent in vivo transfer of genomic DNA without inducing additional cell damage, avoid de novo gene synthesis for undesired reprogramming in disease microenvironments, and ultimately control the lifespan and behavior of the cell. To determine the feasibility of enucleating therapeutic cells, I evaluated previous work detailing the methods to generate enucleated cells and their characteristics.

3 History of mass cell enucleation

Cell enucleation describes the process of removing the nucleus from a cell body. In the context of somatic cell nuclear transfer, the donor oocyte is enucleated using microsurgical, chemically-assisted, or centrifugation techniques.[35] However, these methods are generally inefficient for larger scale (mass) enucleation of somatic cells. Other methods for cell enucleation were developed in the 1960s, when S.B. Carter described the effects of cytochalasin B, a cell-permeable toxic metabolite isolated from the mold *Helminthosporium dematioideum*, upon mouse L (fibroblast) cells grown on conventional tissue culture dishes. At different concentrations and incubation times, cytochalasin B induced mitotic division without cellular cleavage, decreased cell mobility, and eventually, led to spontaneous nuclear extrusion.[36] During nuclear extrusion, the nucleus becomes condensed and enclosed in a thin rim of cell membrane as it separates from the cell body, loosely connected by a thin stalk of plasma membrane. Complete extrusion occurs if the stalk is severed, but extrusion is reversible if the cytochalasin B is removed while the stalk is still intact.[37]

Following Carter's discovery, cytochalasin B was applied to a wide range of cell types with variable enucleation success,[38] although generally, mouse cells were more susceptible than human cells and other species. In 1972, Prescott et. al. increased the yield of enucleated cells by combining cytochalasin B treatment with high gravitational force equivalent (g-force) via ultracentrifugation to enucleate cells grown on rigid surfaces[39] such as flasks or dishes,[40-50] tubes,[51, 52] or coverslips.[39, 53-62] It is assumed that the force of ultracentrifugation aids in severing the stalk tethering the cell membrane-coated nucleus (karyoplast) to the plasma membrane encasing the remnant cytoplasm (cytoplast).[39] While ultracentrifugation improved the overall enucleation efficiency, the total yield was limited by the surface area upon which the cells were plated, and also decreased if cells or cytoplasts detached from the surface during centrifugation. In pilot experiments, I also encountered these shortcomings when enucleating cells grown on plastic inserts or dishes.

In 1975, Wigler and Weinstein described a method for mass enucleation of cells by ultracentrifugation in suspensions of discontinuous gradients of Ficoll containing cytochalasin B.[63] Ficoll 400 (Chemical Abstracts Service Number 26873-85-8) is a synthetic, highly branched polysaccharide polymer characterized as high molecular weight, neutral (non-ionic), hydrophilic, and water soluble with low osmolality and low membrane permeability.[64] Based on these properties, Ficoll is gentler on cells compared to sucrose gradients, so while it is primarily used as a density gradient media to separate or isolate cell populations or organelles, it also has applications in electrophoresis, hybridization, cryopreservation, and immunologic studies.[65] According to Wigler and Weinstein's method, concentrations of Ficoll (25%, 17%, 16%, 15%, and 12.5%) made with cytochalasin B were layered into centrifuge tubes. After equilibration, cells grown on plastic dishes were harvested and suspended in additional 12.5% Ficoll with cytochalasin B, layered onto the existing gradients, and ultracentrifuged at ~100,000 *g*. Distinct bands of cellular components

were found to aggregate in the different layers: cellular debris banded in the 0-12.5% Ficoll layer interface, cytoplasts aggregated in the 15-17% layer, and karyoplasts banded at the 17-25% interface. From these experiments, they concluded that cytochalasin B was necessary to generate viable cytoplasts, but the process required greater centrifugal forces than those used in enucleation of cells adherent to flat surfaces. However, this method dramatically improved both the total and relative yields of cytoplasts (up to 70% of input cells were recovered as cytoplasts) and consistency of generating cytoplasts of high purity (high efficiency, minimal contamination with remnant cells or nuclei). Theoretically, the yield is only limited by the band capacity of the gradient, although I found that the enucleation protocol had to be adapted for each cell type to achieve optimized enucleation. Further information on adaptation of this protocol is provided in Chapter 1.

Since Wigler and Weinstein's publication, additional enucleation protocols have used other density gradients such as Percoll[66] or colloidal silica[67] on various cell types.[68] However, the reproducibility, large yield, and high enucleation efficiency of cell in Ficoll gradients made it an attractive choice for my investigation of enucleated cells. For these studies, it was important to define the capabilities of enucleated cells before proposing how these functions could be harnessed for therapeutic benefit.

4 Characteristics and uses of enucleated cells

Early on, it was recognized that cytoplasts retain many key morphologic and behavioral characteristics of nucleated cells. The karyoplast is composed of a nucleus surrounded by a small portion of cell membrane and scant cytoplasm containing only ribosomes, mitochondria, and small pieces of endoplasmic reticulum, so while it can attach to a plastic surface, it is not motile.[56 60] In contrast, cytoplasts are rimmed by plasma membrane and retain all cytoplasmic organelles minus the nucleus, and therefore can attach to plastic and are motile.[56, 60, 61] Cytoplasts are viable for up

to 2-3 days.[39, 60] By microscopy, cytoplasts attach to plastic, spread, retain cellular shape, perform pinocytosis, exhibit contact inhibition, and are motile, even after trypsinization and replating.[53] Compared to parental cells, cytoplasts perform similar cellular functions (albeit sometimes at lower levels), such as assembly of microtubules and cytoplasmic fibers,[61] propensity to spread as a monolayer or overlapping,[59] incorporation of amino acids into proteins,[39, 68, 69] and expression of cell surface antigens.[70]

Cytoplasts are useful for studying the nuclear-cytoplasmic roles in the metabolism or localization of subcellular components,[52, 68] cell migration,[71] replication and development of viruses viruses,[39, 54, 68, 72] and host response to infectious agents.[73] There is a large body of literature defining the properties of enucleated human neutrophils/granulocytes, termed cytokineplasts (selected references).[74-78] Additionally, cytoplasts are used in fusion studies of heterologous nuclei or cytoplasts into nucleated cells or cytoplasts, a process that generates hybrid cells known as cybrids.[79, 80] All of these published studies characterized cytoplast properties or functions in vitro only, with the exception of neutrophil cytoplasts in a rat neonatal sepsis model[81] and enucleated tumor cells used as a tumor vaccine in mice.[46]

5 Proposed therapeutic use of bioengineered, enucleated cells (Cargocytes)

Based on their manifold capabilities, we were intrigued with the idea of not only using cytoplasts in vivo, but bioengineering them to have specific therapeutic functions. While the technology to generate cytoplasts is not new compared to the cutting-edge field of cell bioengineering, the combination of these techniques to produce cytoplasts with therapeutic properties is a novel approach to cell-based therapy. We coined the term "Cargocyte™" when referring to cells that are bioengineered and enucleated for therapeutic applications. The bioengineering can be applied either pre- or post-enucleation, with examples of this workflow and

potential bioengineering strategies listed on the graphical abstract (Fig. 1).

Based on the broad potential of bioengineering to customize and enhance cells for therapeutic use, the need to preserve the controllability and safety of bioengineered cells in vivo, and previous studies showing that enucleated cells can perform many important cellular functions for a limited time, I hypothesized that Cargocytes would be amenable to bioengineering with specific clinically-relevant functions, such as production of immunomodulatory cytokines and expression of homing receptors that would ultimately produce an in vivo effect. To test these hypotheses, I first validated basic functional characteristics of Cargocytes, and then evaluated their bioengineered capabilities in two mouse models in vivo. In vitro assays that validate basic properties and feasibility of bioengineering Cargocytes are described in Chapter 1. Bioengineering constructs and enhancements to in vitro performance are provided in Chapter 2. In vivo use of Cargocytes producing antitumor cytokines in a mouse breast cancer model is presented in Chapter 3. Finally, in vivo effects of Cargocytes homing to sites of inflammation in a mouse ear inflammation model are detailed in Chapter 4.

Concepts in the Introduction, in part, have been submitted for publication of the material as it may appear in Nature Biotechnology, H. Wang, C.N. Alarcón, B. Liu, F. Watson, S. Searles, C. Lee, J. Keys, W. Pi, D. Allen, J. Lammerding, J.D. Bui, and R.L. Klemke, 2020. The dissertation/thesis author was the co-primary investigator and co-first author of this paper.

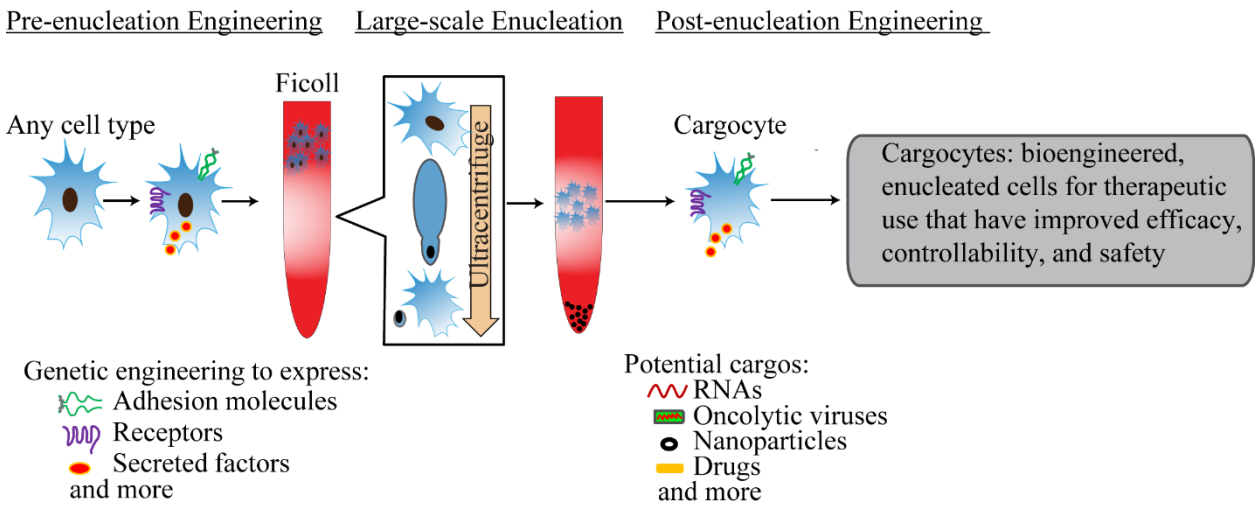

Figure 1: Schematic of example workflow when generating bioengineered, enucleated cells for therapeutic use (Cargocytes). Note that bioengineering can occur pre-and post-enucleation and also include multiple combinations (layers) of engineering.

Chapter 1: Endogenous Capabilities of Enucleated Mesenchymal Stromal Cells

1.1 Therapeutic properties of Mesenchymal Stromal Cells

Based on previous studies indicating that ultracentrifugation of cells in Ficoll with cytochalasin B could produce large numbers of relatively pure populations of enucleated cells, I attempted enucleation of a variety of cell types, including human, mouse, and cancer cell lines (Table 1). After examining both the initial enucleation potential of the various cells, and factoring in the known bioengineering capability and therapeutic potential of the cell type, our work focused on the enucleation and bioengineering of mesenchymal stromal cells (MSCs), which are these second most commonly used cell in current cell-based clinical trials after HSCs.[4] To my knowledge, MSCs have not been previously reported to be enucleated.

Mesenchymal stromal cells, previously termed mesenchymal stem cells,[82] are a heterogeneous groups of cells that were first isolated from bone marrow in the 1960s and described as adherent, non-hematopoietic, fibroblast-like stromal cells capable of osteogenic differentiation.[83, 84] Since that time, MSCs have been isolated from almost every tissue,[85, 86] and although their exact lineage is still debatable, it is likely of pericyte (perivascular) or fibroblast origin.[87-89] Although there is no definitive characterization or classification for MSCs, the International Society for Cell Therapy (ISCT) consensus statement indicates that MSCs should be adherent to plastic, display select surface markers, and differentiate along adipogenic, osteogenic, and chondrogenic lines.[90]

MSCs hold great promise as a cell-based therapy due to their intrinsic ability to immunomodulate the disease microenvironment,[91] secrete disease-fighting products,[92] signal or recruit other disease-fighting cells, and differentiate or regenerate in damaged tissues.[93] In fact, it has been proposed that MSCs should be called medicinal signaling cells,[94] since they have such a

great ability to immunomodulate and recruit other cells in disease. Unlike embryonic stem cells, MSCs do not raise ethical concerns because they can be isolated from almost any post-natal tissue,[86] and isolated in high numbers from bone marrow, adipose, umbilical cord blood, and menstrual blood.[93] MSC are considered to be immune evasive rather than truly immunopriviledged,[95] and their low immunogenicity is derived from a low but upregulatable basal expression of human leukocyte antigen (HLA) class I and lack of HLA class II. Finally, MSCs are considered relatively safe because they do not form teratomas[96-98] and it is thought that their main mechanism of action is through paracrine-mediated effects rather than cell engraftment,[99, 100] the so-called "hit-and-run" hypothesis.

1.2 Limitations to current MSC therapies

Current MSC therapies face many problems common to other cell-based therapy applications, including cell heterogeneity, in vivo homing, and overall efficacy.[101, 102] MSC heterogeneity in humans and mice has been described between donors (based on age, health, gender),[103-110] within individual donors,[111-113] between site of harvest (bone marrow, adipose, umbilical cord, cord blood),[114-117] and time and method of ex vivo culturing.[106, 118-123] In particular, there is conflicting evidence that long-term culturing of MSCs affects phenotype, aneuploidy, and immunogenicity, [124, 125] but the secretome can also be altered by time in suspension, formulation of the delivery vehicle, and exposure to adjuvant.[126]

Despite their incredible endogenous capabilities and efficacy in treating a variety of diseases,[127, 128] the intrinsic and extrinsic MSC heterogeneity likely contributes to the variability of outcomes in clinical trials. While they were initially reported to have great homing to bone marrow, tumors, and sites of inflammation,[129, 130] MSCs can also be reprogrammed in disease environments to have cancer-promoting effects[131-134] or inconsistent homing to desired tissues.

Until recently, MSC clinical trials most commonly used bone marrow (BM)-derived cells, [135] but now perinatal (umbilical cord blood, UC) predominate, and adipose-derived (AD) MSCs are also rising in popularity.

Based on the plentiful endogenous therapeutic properties of MSCs, we selected these cells as a prototype for Cargocyte generation, in which their functions could be specifically expanded or enhanced. In our lab, standard two dimensional (2D) tissue culture of primary BM and UC MSCs was laborious and cells reached senescence within six passages[136] without reaching adequate numbers for mass enucleation. We therefore examined the feasibility of using AD MSCs, which were identified in the 1960s and characterized in the early 2000s.[137] AD MSCs require minimally-invasive methods of collection, and net a high yield of cells with delayed senescence and relatively fast expansion in cell culture. Additionally, AD MSCs may be even less immunogenic than BM MSCs,[138] although they may have some differences in therapeutic potential.[139-141] To reduce cell senescence and heterogeneity, I performed experiments with a commercially-available,[142] adipose-derived, human MSC cell line immortalized with telomerase reverse transcriptase (hTERT).[143] These cells fulfill the (ISCT) criteria, grow relatively fast with consistent morphology in culture, and survive cryopreservation.[144]

I adapted the Wigler enucleation protocol to optimize the yield and efficiency of enucleated hTERT MSCs (hT-MSCs) as a therapeutic prototype for bioengineering. Since cytoplasts were previously reported to retain many cellular features and functions of the parental cells, I hypothesized that hTERT MSC-derived Cargocytes would also retain key cell properties, specifically in regards to cell surface marker expression and functionality of cytoplasmic organelles that would convey ability to secrete proteins and migrate.

1.3 Materials and Methods for enucleation of MSCs

1.3.1 Protocol for culturing MSCs

Human telomerase reverse transcriptase (hTERT)-immortalized, adipose-derived mesenchymal stromal cells (hereinafter referred to as "hT-MSC") were purchased from ATCC (#SCRC-4000™). Primary human BM-derived MSCs were obtained through Texas A&M College of Medicine's Institute for Regenerative Medicine. Primary human UC-derived MSCs were a generous gift from Dr. Mana Parast (UCSD). MSCs were cultured in complete culture medium (CCM) including alpha MEM (Gibco #12561) supplemented with 16.5% Premium FBS (Atlanta Biologics S1150), 1% HEPES (Gibco #15630), 1% Glutamax 100X (Gibco #35050), and 1% Anti-Anti 100X (Gibco #15240). hT-MSCs were authenticated by IDEXX Laboratories. All cell stocks tested mycoplasma negative by PCR.

1.3.2 Protocol for enucleation of MSCs in suspension

The following protocol was adapted from Wigler et. al.[63] One day (24 hours) prior to enucleation, hT-MSCs were seeded at 2.5M cells per 15cm-diameter plate (Olympus 25-203) covered with 15ml of CCM. Stocks of 50% (weight/weight) Ficoll PM400 (GE Healthcare 17-0300-500) were made by dissolving grams of Ficoll in ultrapure water (Invitrogen 10977-015) by continual magnetic stirring for 24 hours at room temperature, followed by 30 minutes of autoclaving. Once cooled, the mixture was stirred again for consistency, the refractive index (RI, 1.4230-1.4290) measured on a refractometer (Reichert 13940000), and then aliquoted and stored at -20°C. Stock 2X MEM was prepared by adding 20% 10X MEM (Gibco, 11430-030), 5.9% Sodium Bicarbonate (7.5%, Gibco, 25080-094), 2% 100X Pen-Strep (Gibco 15140-122) and 72% ultrapure water (Invitrogen 10977-015) and filtering through 0.22um membrane flask (Olympus 25-227) before aliquoting for storage at 4°C. Stock cytochalasin B (Sigma Aldrich C6762) was made by dissolving powdered cytochalasin B in DMSO (Sigma D2650) at 10 mg/ml, then

aliquoted and stored at -20°C. The night before enucleation (6-18 hours prior), Ficoll gradients were made by adding cytochalasin B (stock diluted to 2mg/ml in DMSO) to 2X MEM at 20 µg/ml (RI 1.3383 ± 0.0001), and then diluting it 1:1 with 50% Ficoll to make 25% Ficoll (1.3800 ±0.0005). Additional layers were made by diluting 25% Ficoll with 1X MEM (2X MEM containing cytochalasin B diluted 1:1 with ultrapure water) to make 17%, 16%, 15%, and 12.5% volumes. Layers were individually incubated for 1 hour at 37°C and then gradients were carefully poured into 13.2ml ultracentrifuge tubes (Beckman Coulter, #344059) from bottom to top as 2ml 25%, 2ml 17%, 0.5ml 16%, 0.5ml 15%, and 2ml 12.5% Ficoll. Tubes and leftover 12.5% and 1X were incubated overnight at 37°C.

The day of enucleation, subconfluent MSCs were harvested by washing with PBS (Gibco 14190-144), adding 5ml Accutase (Innovative Cell Technologies, Inc., AT104) until cells detached, then washing in CCM at 1,200 rpm (IEC-CL2 centrifuge) for 5 mins, re-suspending in PBS for counting cell number. Cells were pelleted again and thoroughly resuspended at 20M per 3.2ml 12.5% Ficoll, then filtered through a 40um cell strainer (Falcon 352340) and layered onto the prepared gradients in the centrifuge tube. The layers were topped with 1ml 1X MEM and carefully placed into pre-warmed SW41 swinging buckets. Buckets were balanced to ±0.05g, then the caps loosened during a 45 minute incubation at 37°C. Caps were tightened and buckets loaded onto a pre-warmed SW41 rotor in a Beckman Coulter L8-60M ultracentrifuge for 60 mins at 26,000rpm (~103,000 x g), 31°C, and slow acceleration/deceleration (setting 7). Cargocytes were collected with low-binding pipette tips from the mid-12.5 to 1X layers (layer 1) and 16 to 15/12.5% interface (layer 2) in Stemfull low cell adhesion tubes (Sbio MS90150Z) and diluted with at least 1:3 volumes of warm serum-free MSC medium. Tubes were gently inverted to mix the collected Ficoll layers with diluent, then pelleted for 10 mins at 1,200 rpm (IEC-CL2). The second and third

washes used 10ml of serum free media at 1,200 rpm for 6 minutes. Cytoplasts were counted and viability determined by Trypan blue exclusion (0.4%, Invitrogen T10282) on a Countess automated cell counter (Invitrogen) and a small aliquot used to determine enucleation efficiency (purity, % enucleated cells from total population present) via staining with Vybrant Dyecycle Green (1:4000, Invitrogen V35004) on an epifluorescent microscope (Nikon Eclipse Ti). Diameters of Cargocytes and parental MSCs were determined by the NIS-Elements AR 3.0 software (Nikon). Cargocytes were either used immediately for in vitro or in vivo assays (freshly isolated), plated for assays at various later timepoints, or resuspended at 1M/ml in CCM with 10% DMSO for cryopreservation. Cargocytes and cells were frozen by controlled cooling at -1°/minute in an insulated container in the -80° freezer overnight, and then transferred to liquid nitrogen storage.

1.3.3 Protocol for flow cytometry of surface receptors pre- and post-enucleation

MSCs or Cargocytes were resuspended in fluorescence-activated cell sorting (FACS) buffer (pH 7.4 PBS, 0.5mM EDTA and 0.5% BSA) and stained with indicated antibodies (Table 2) for 40 minutes on ice. After washing with FACS buffer 3 times, samples were analyzed by the flow cytometry machine FACS Canto II (BD). Isotype matched IgG was used for negative control.

2.3.4 Protocol for immunofluorescent antibody staining of cytoskeleton and organelles

MSCs or Cargocytes were cultured on fibronectin-coated (10µg/ml) Chambered Coverglass (ThermoFisher, # 155383) at subconfluent density. Cells were fixed in 4% Paraformaldehyde Solution (PFA, ThermoFisher, #AAJ19943K2), and permeabilized with 0.2% Triton X-100 (Sigma Aldrich, #T8787) in PBS, then stained with indicated concentrations of antibodies (Table 2) and DAPI as previously described.[145] After staining, fluorescent images were taken using Nikon Eclipse Ti epi-fluorescence microscope or Olympus FV1000 confocal

microscope and analyzed with the Image J Fiji software.

1.3.5 Protocol for transfection of synthesized mRNAs

Green fluorescent protein (GFP) and Gaussia Luciferase (Gluc) mRNAs were synthesized by TriLink Biotechnologies. The protein coding sequence was flanked by 5'- and 3'-untranslated regions (UTRs) from mouse α-globin. Full substitution of pseudouridine was used to synthesize transcripts. After adding 5' cap structure (CleanCap® AG) and 3' poly(A) tail (120A), the synthesized mRNAs were purified with silica membrane. The pre-made mRNAs from TriLink were directly used for mRNA transfection. Briefly, 1 µg synthesized mRNA was added to 49 µl warm opti-MEM and separately 4 µl Lipofectamine 3000 (ThermoFisher, # L3000008) was added to 46 µl Opti-MEM. The Lipofectamine and mRNA solutions were incubated separately for 5 minutes, then mixed together and incubated for another 15 minutes at room temperature (RT). MSCs or Cargocytes were resuspended in CCM without antibiotics at 1E6 cells/ml. 100 µl of mixed mRNA + Lipofectamine-3000 solution was added to 1ml MSC or Cargocyte suspension, mixed thoroughly and incubated at 37°C for 30 minutes. After transfection, MSCs or Cargocytes were washed twice with CCM. GFP-transfected MSCs or Cargocytes were plated in 6-well-plate (1E5 per well) and GFP expression was analyzed with the epifluorescence microscope (Nikon Eclipse Ti) or by flow cytometry. For Gluce mRNA, transfected MSCs or Cargocytes were plated in 24-well-plate (25,000 per well, 1 ml CCM media). Conditioned medium was taken 48 hours after transfection, and luciferase activity was determined as relative luminometer units (RLU) using BioLux Gaussia Luciferase Assay Kit (NEB, E3300) on GloMax 96 microplate luminometer (Promega)

1.3.6 Protocol for transwell migration and invasion assays

Boyden chamber assays[146] for directional movement were performed using fibronectin–

coated (Sigma Aldrich, #F1141) inserts with 8 µm pore membranes (Corning, #10167000). MSCs or Cargocytes were resuspended in serum free media with 0.25% BSA (Sigma Aldrich, #126593), and placed in the upper chamber (5E4 cells per well). The lower chambers were filled with serum free media with 10% FBS (Atlanta Biologicals, #S11550). After 2 hours, the inserts were removed and the upper surface of the membrane and chamber were wiped with cotton swabs to remove cells that did not migrate to the bottom side of the membrane. The membranes were stained with crystal violet staining solution (Sigma Aldrich, #HT90132) containing 2% ethanol, and then removed from the insert and mounted on glass microscope slides. The migrated cells present on the underside of the membrane were counted using light microscopy at 400X magnification. The loading control for each condition was MSCs or Cargocytes directly plated into 24-well plates (2E4 cells per well) to count cells that attached to the plate (i.e. no inserts were used). The number of cells migrating to the underside of a membrane was ratioed back to the number of cells in the loading control as a measure of the migrational ability of MSCs or Cargocytes.

Invasion assays were performed using CultreCoat® 24 Well Medium BME Cell Invasion Assay (Trevigen, #3482-024-K) kit with 8 µm pore size. Cells were prepared and loaded into chambers per manufacturer recommendations. Briefly, MSCs or Cargocytes were cultured overnight media with 0.5% FBS, then trypsinized, washed, and resuspended in media with 0.5% FBS, and then placed in the upper chambers (4E4 cells per well) of rehydrated cell invasion inserts. The lower chambers were filled with media with 10% FBS. After 24 hours, inserts were removed and the upper surface of the membrane and chamber were wiped with cotton swabs to remove cells that did not invade into the BME. The membranes were stained with crystal violet staining solution (Sigma Aldrich, #HT90132) containing 2% ethanol, and then removed from the insert and mounted on glass microscope slides. The migrated cells present on the underside of the membrane

were counted using light microscopy at 400X magnification. The loading control for each condition was MSCs or Cargocytes directly plated into 24-well plates (2E4 cells per well) to count cells that attached to the plate (i.e. no inserts were used). The number of cells migrating to the underside of a membrane was ratioed back to the number of cells in the loading control as a measure of the migrational ability of MSCs or Cargocytes.

1.3.7 Protocol for 3D migration in microfluidic mevice

Confined migration assays were performed using a microfluidic device as previously described.[147, 148] The device consists of alternating parallel migration channels of either 5μm height and constrictions 1 to 2 μm width (confined migration) or 5 μm height and 15 μm width (unconfined migration). Devices were assembled as previously described and coated with a solution of 10 μg/ml of fibronectin 24 hours prior to experiments[148]. Four hours prior to imaging, 3E4 MSCs or Cargocytes were stained with Hoechst 33342 (1:4000 v/v), then seeded into microfluidic devices and allowed to migrate along an FBS gradient (2% to 16.5%). Imaging was performed on a Zeiss LSM700 laser scanning confocal microscope with a 20x air objective. Cells and devices were imaged for 14 hours at 10 minute intervals in a temperature controlled stage (37C°). The time required for cells to migrate through an individual constriction was quantified manually from images and was defined as starting at the first frame that the anterior portion of a cell entered a constriction and ending with the first frame after the cell posterior passed through the constriction.

1.3.8 Protocol for select biodistribution and lung trapping

MSCs labeled with LifeAct RFP were grown by two dimensional (2D) or 3D methods (see Section 4.1 and 4.5.2 for information about 3D culturing) and enucleated to produce 2D or 3D-cultured Cargocytes. For flow cytometry analyses, MSCs or Cargocytes labeled with LifeAct RFP

were stained with 10 µM Vybrant DiD (Invitrogen, #V22887) following manufacturer's instructions prior to intravenous (IV) injection of 1M MSCs or Cargocytes. Animals were euthanized 24 hours after MSC or Cargocyte injection. Lungs, spleen, and liver were removed and each placed in 2 ml digestion buffer containing collagenase I solution (0.5 mg/ml collagenase (Sigma Aldrich, #C9891-100MG), 20 µg/ml DNase, 5% FBS in PBS). After incubation at 37°C for 1 hour, tissues were ground with a pestle in a 70 µm cell strainer (Biopioneer, #DGN258368). When no large tissue pieces remained intact, strainers were washed with 2 ml of 1% FBS, 2 mM EDTA in PBS. Cells were then treated with 1X RBC lysis buffer (Biolegend, # 420301) for 2 minutes, washed with PBS, and analyzed by flow cytometry machine FACS Canto II (BD). 7-AAD staining was not performed in this experiment due to overlapping signal with the RFP wavelength in the channels available.

1.4: Characterization of MSC-derived Cargocytes

Based on previously published descriptions of cytoplasts of various cell types, I hypothesized that enucleated hT-MSCs (Cargocytes) would retain many characteristics of the parental cell line, such as cell surface marker expression, and functional organelles. Therefore, Cargocytes should have short-term viability, express exogenous proteins, and migrate.

My optimized enucleation protocol consistently produced a high yield (80-90%) of Cargocytes with >95% enucleation efficiency (purity, absent nuclei) (Table 1). Cargocytes collected from Ficoll layer 2 lack nuclei (Fig. 2a), and therefore are smaller than parental cells in suspension (Fig. 2b). They exclude Trypan blue for up to 72 hours without proliferating (Fig. 2c), even after thawing from cryopreservation (Fig 2d). Similar to parental cells over a period of 48 hours, Cargocyte have cell membrane surface receptor expression of CD44, CD90, CD105, and CD166, with absent CD45 expression (Fig. 2e). After enucleation, Cargocytes can attach and

spread on plastic dishes, where they display organized F-actin and α-tubulin cytoskeletons (Fig 2f) and presence of organelles including Golgi, ER, mitochondria, lysosomes, and endosomes (Fig. 2g).

To test Cargocyte ability to translate exogenous mRNAs, Cargocytes were transfected with green fluorescent protein (GFP) mRNA, and their production of GFP was similar to parental cells (Fig. 3a, b). Similarly, Cargocytes transfected with Gaussia luciferase (Gluc) mRNA had Gluc activity comparable to parental MSCs (Fig. 3c). In 2D migration assays, Cargocytes migrated towards gradients of FBS similar to parental cells in Boyden chambers (Fig. 3d, e), even after recovery from cryopreservation (Fig. 3f). Similarly, Cargocytes invaded through Matrigel-coated inserts (Fig. 3f, g). In a 3D microfluidic chamber, Cargocytes moved faster and more effectively towards a FBS gradient, whereas parental cells frequently stopped at narrow constrictions due to inflexible nuclear size (Fig. 4a, b). Finally, when Cargocytes were injected intravenously into mice, fewer were detected in the lungs but more were present in the spleen and liver compared to parental MSCs (Fig. 4c).

1.5 Conclusions about MSC-derived Cargocyte basic capabilities

Without a nucleus, Cargocytes are incapable of cellular division but can survive up to 72 hours in vitro, which means they have a defined population and lifespan. With more precise control over cell proliferation and ultimate viability, Cargocytes may have more controlled behavior in vivo. Although a full panel of MSC markers was not performed, Cargocytes displayed similar cell surface profiles as parental cells, indicating that enucleation does not disrupt endogenous receptor profiles. In these experiments, it is important to underscore that we were not attempting to prove that Cargocytes are still MSCs because without a nucleus, they cannot undergo differentiation. Although Cytoplast viability was quantified only with Trypan blue exclusion, their ability to

express surface receptors and migrate at 48 hours strongly indicates their viability because these processes require an intact cell membrane and ATP.

With intact cytoskeletal organization and retention of key organelles, Cargocytes possess the cellular machinery for protein translation and cell migration, which was further evidenced by GFP expression and migration in Boyden chamber assays. Of the organelles identified by immunofluorescent antibodies, the Golgi and ER in particular demonstrate functional ability to translate exogenous proteins. Importantly, this includes both cytoplasmic (GFP) and secreted (Gluc) proteins, as many therapeutically-relevant proteins are produced in these forms. Based on basal receptor expression, cytoskeletal organization, and cytoplasmic functionality, Cargocytes have an endogenous motility that can be classified as migration (directional and functional movement) towards a non-specific chemoattractant like FBS. The maintenance of viability and migration after cryopreservation have important implications for the ability to ship and store Cargocytes for biobanking or widespread distribution. In fact, migration studies in the microfluidic study were performed by shipping cryopreserved vials of Cargocytes and MSCs from California to New York, where they were thawed and imaged in the microfluidic device as shown.

Although a recent study suggested that cytoplasts can migrate in 2D but not in 3D collagen gels,[71] our analysis shows that Cargocytes migrate in both 2D Boyden chambers and 3D microfluidic chambers. In our lab, we observed that Cargocytes must first attach and spread in order to migrate, which they do preferentially on fibronectin-coated substrates rather than collagen-coated ones (unpublished observations).

A full biodistribution study has not yet been completed (in progress), but the decreased number of Cargocytes present in the mouse lungs at 24 hours suggests that they experience less lung trapping after intravenous injection. This may be due to Cargocytes' decreased size compared

to parental cells, as well as lack of the rigid nucleus,[149] which prevented cells from migrating through constrictions in the 3D microfluidic device (Fig. 4a). These features theoretically could allow for easier passage through small pulmonary capillaries. Additionally, the fact that Cargocytes labeled with a vital dye are detectable in tissue contributes to the evidence that Cargocytes are viable in vivo. These properties are examined in more detail in Chapter 4 for homing following intravenous injection.

Together, these experiments indicate that Cargocytes perform biologically important cellular properties and functions like protein translation, receptor expression, and cell migration, as previously reported in the cytoplast literature. I next investigated Cargocyte therapeutic potential by characterizing the biofunctional properties of bioengineered Cargocytes.

Chapter 1, in part, has been submitted for publication of the material as it may appear in Nature Biotechnology, H. Wang, C.N. Alarcón, B. Liu, F. Watson, S. Searles, C. Lee, J. Keys, W. Pi, D. Allen, J. Lammerding, J.D. Bui, and R.L. Klemke, 2020. The dissertation author was the co-primary investigator and co-first author of this paper.

Figure 2: Cargocytes retain cell-like structure and organization.

(**a**) hTERT MSCs labeled with LifeAct RFP (red) were enucleated by ultracentrifugation in Ficoll gradients and stained with Vybrant Green vital dye (green) for epifluorescent (top) and phase contrast (bottom) microscopy. Arrowhead = nucleus, arrow = Cargocyte without nucleus. Scale bar 20 µm. (**b**) Bar graph shows average diameter of MSCs or Cargocytes in suspension. Mean ± SEM; n=80. P value, two-tailed unpaired t-test. (**c**) Graphs show the percentage of viable hT-MSCs or freshly-isolated Cargocytes versus initial population over time. Mean ± SEM; n=6 biological replicates. (**d**) Graphs show the percentage of viable hT-MSCs or Cargocytes recovered following 1 month of cryopreservation versus initial population over time. Mean ± SEM; n=6 biological replicates. (**e**) Graphs show MSC and Cargocyte surface expression of indicated markers analyzed by FACS with FlowJo. Parental MSC= nucleated MSCs from which Cargocytes were derived; Isotype control= MSC stained with isotype-matched IgG. 2hr/24hr/48hr Cargocyte= MSC-derived Cargocyte analyzed at indicated timepoints post-enucleation; Representative results from 3 independent experiments. (**f**) Fluorescent confocal images of hT-MSCs and Cargocytes stained with rhodamine phalloidin to visualize the F-actin cytoskeleton (left), or anti-α-Tubulin antibody to visualize the microtubule network (right), and DAPI to visualize the nucleus. Arrows point to the F-actin cytoskeleton; arrowheads point to the microtubule network. Scale bar, 50 µm. (**g**) Fluorescent images of MSCs or Cargocytes stained with indicated subcellular organelle antibodies (green, arrows) and DAPI (blue). Mitochondria, anti-AIF (Apoptosis-inducing factor); Lysosome, anti-LAMP1 (Lysosome-associated membrane protein 1); Golgi, anti- RCAS1 (Receptor binding cancer antigen expressed on SiSo cells); Endoplasmic Reticulum (ER), anti-PDI (Protein disulfide isomerase); Endosome, anti-EEA1 (Early Endosome Antigen 1). Arrows point to indicated organelles. Scale bar= 50 µm.

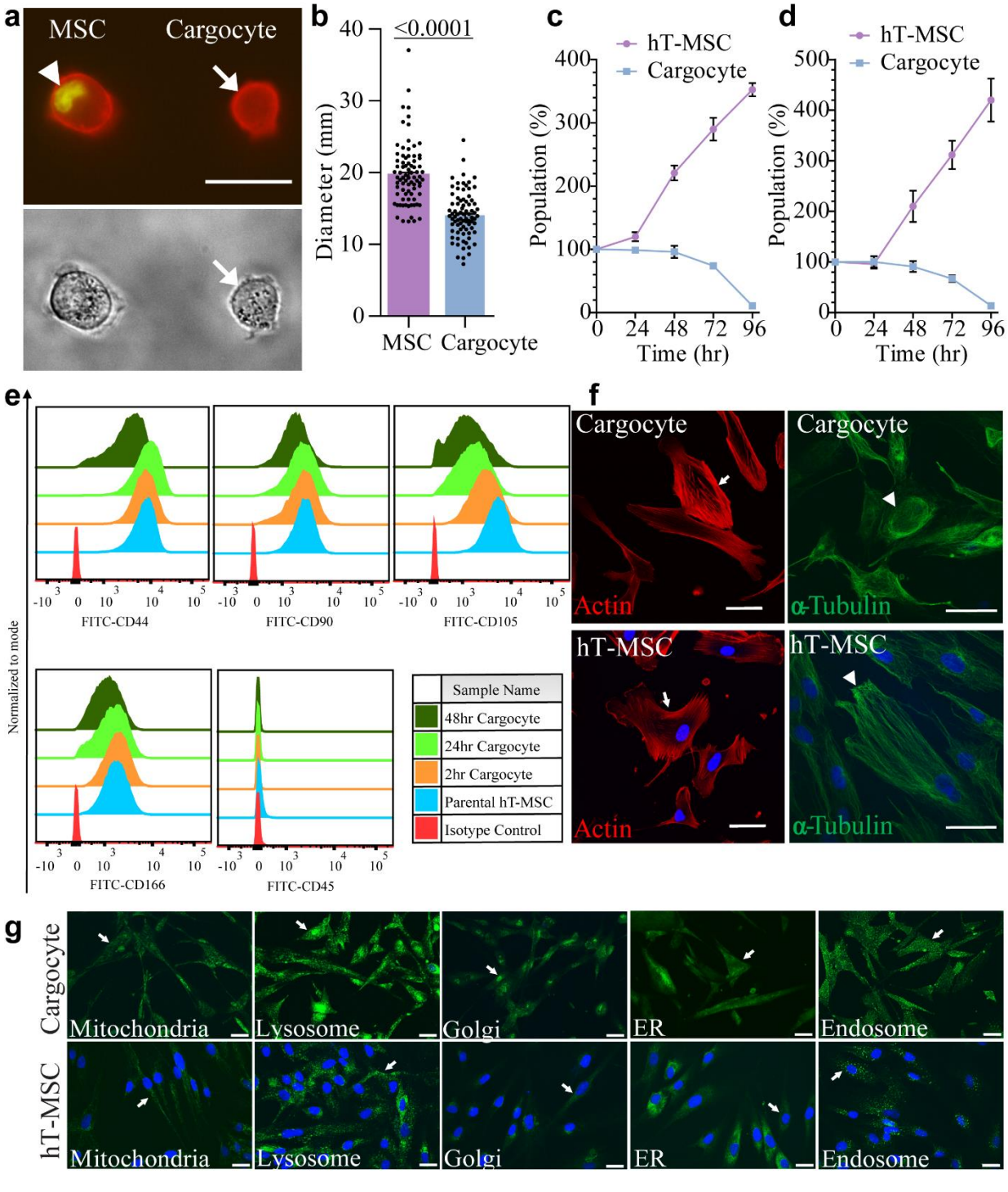
a
MSC
Cargocyte
b
≤0.0001
Diameter (mm)
MSC
Cargocyte
c
hT-MSC
Cargocyte
Population (%)
Time (hr)
d
hT-MSC
Cargocyte
Population (%)
Time (hr)
e
Normalized to mode
FITC-CD44
FITC-CD90
FITC-CD105
FITC-CD166
FITC-CD45
Sample Name
48hr Cargocyte
24hr Cargocyte
2hr Cargocyte
Parental hT-MSC
Isotype Control
f
Cargocyte
Actin
Cargocyte
α-Tubulin
hT-MSC
Actin
hT-MSC
α-Tubulin
g
Cargocyte
hT-MSC
Mitochondria
Lysosome
Golgi
ER
Endosome

Figure 3: Cargocytes retain important cellular functions and can be bioengineered.

(**a**) Epifluorescent images show LifeAct RFP (red) hT-MSCs or Cargocytes stained with Hoechst 33342 (blue) 24h post-transfection with GFP (green) mRNA. Representative results of 3 independent experiments. Scale bar, 50 µm. (**b**) Bar charts show the mean fluorescent intensity (MFI) of GFP (left) or GFP positive ratio (right) of cells treated as in (**a**) and analyzed by flow cytometry. Mean ± SEM; n=6 biological replicates; Data pooled from 2 independent experiments; P value, two-tailed unpaired t-test. **(c)** Bar graph shows Gaussia luciferase (Gluc) activity in conditioned medium from MSCs or Cargocytes 48h post-transfection with Gluc mRNA. RLU=Relative luminometer units. Mean ± SEM; n=6 biological replicates; Data pooled from 2 independent experiments; P value, two-tailed unpaired t-test (**d**) MSCs/Cargocytes migrated in Boyden chambers towards fetal bovine serum (FBS) gradients for 2 hours. Representative brightfield images of MSCs or Cargocytes that migrated to the underside of 8.0 □m porous filters were stained with Crystal Violet. **(e)** Bar graph represents the ratio of migrated MSCs or freshly isolated Cargocytes treated as in (d) versus loading control (MSCs/Cargocytes seeded on fibronectin-coated plates). Mean ± SEM; n=10 independent fields from 3 biological replicates. **(f)** Bar graph represents the ratio of migrated MSCs or Cargocytes treated as in (**d**) when recovered following 1 month of cryopreservation versus loading control (MSCs/Cargocytes seeded on fibronectin-coated plates). Mean ± SEM; n=10 independent fields from 3 biological replicates. **(g)** MSCs/Cargocytes invaded through Matrigel-coated Boyden chambers to migrate towards FBS gradient. Representative brightfield images of MSCs or Cargocytes that invaded through the Matrigel to the underside of 8.0 µm porous filters were stained with Crystal Violet. **(h)** Bar graph represents the ratio of invading MSCs or Cargocytes treated as in (g) versus loading control. Mean ± SEM; n=18 independent fields from 6 biological replicates. For (**d**), (**e**), (**f**), (**g**), and (**h**): Results representative of at least 3 independent experiments. All statistics are two-way ANOVA with Tukey's multiple comparisons test. P values shown above the bars.

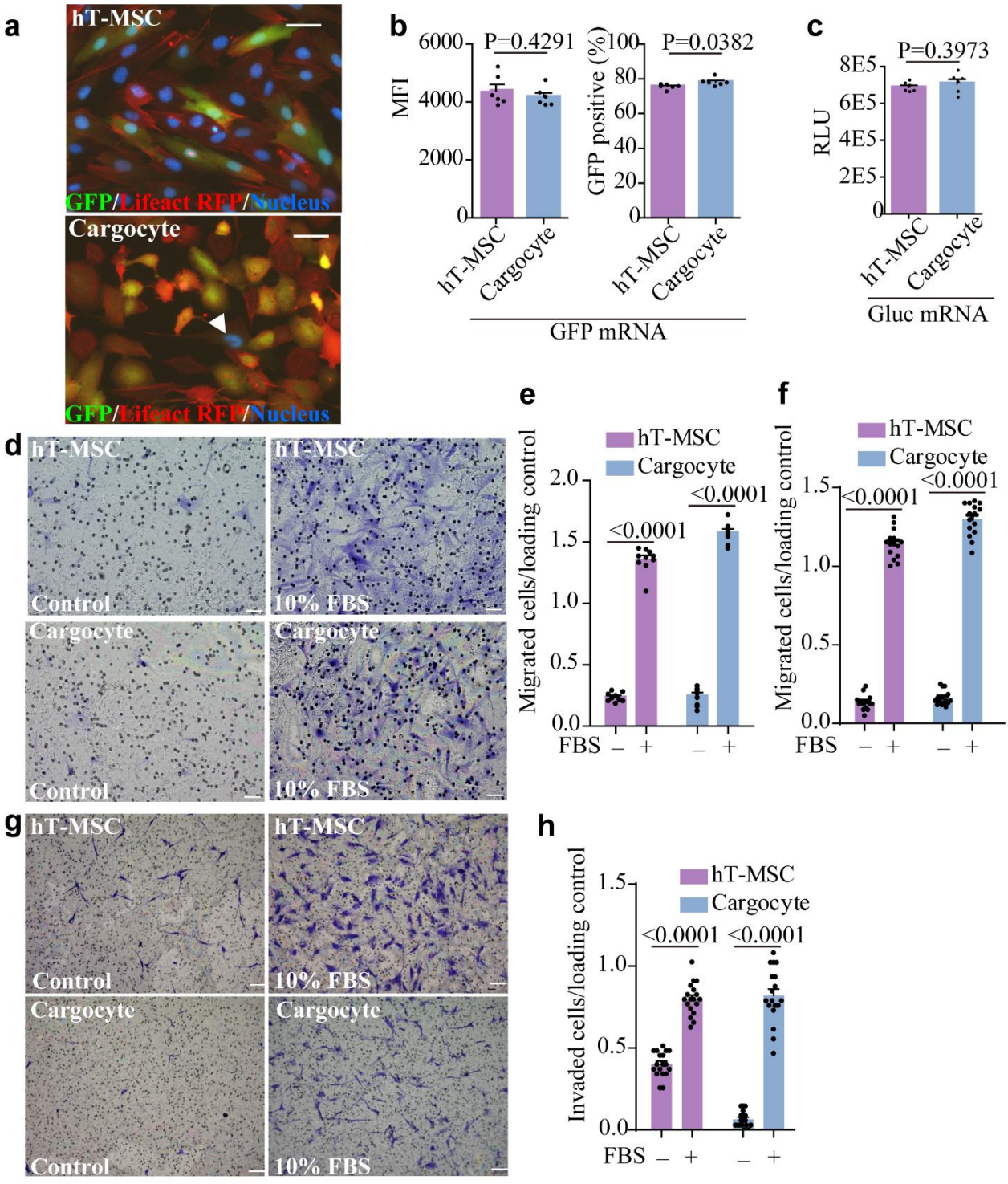
a
hT-MSC
GFP/Lifeact RFP/Nucleus
Cargocyte
GFP/Lifeact RFP/Nucleus
b
MFI
6000
4000
2000
0
P=0.4291
hT-MSC
Cargocyte
GFP positive (%)
100
80
60
40
20
0
P=0.0382
hT-MSC
Cargocyte
GFP mRNA
c
RLU
8E5
6E5
4E5
2E5
0
P=0.3973
hT-MSC
Cargocyte
Gluc mRNA
d
hT-MSC
hT-MSC
Control
10% FBS
Cargocyte
Cargocyte
Control
10% FBS
e
Migrated cells/loading control
hT-MSC
Cargocyte
2.0
1.5
1.0
0.5
0.0
≤0.0001
≤0.0001
FBS – + – +
f
Migrated cells/loading control
hT-MSC
Cargocyte
1.5
1.0
0.5
0.0
≤0.0001
≤0.0001
FBS – + – +
g
hT-MSC
hT-MSC
Control
10% FBS
Cargocyte
Cargocyte
Control
10% FBS
h
Invaded cells/loading control
hT-MSC
Cargocyte
1.5
1.0
0.5
0.0
≤0.0001
≤0.0001
FBS – + – +

Figure 4: Cargocytes migrate in 3D in vitro and in vivo

(**a**) Time-lapse image sequence of hT-MSCs (bottom) and Cargocytes (top) moving through constrictions along an FBS gradient in a microfluidic device. F-actin cytoskeleton (red) was labeled with LifeAct-RFP and cell nucleus (blue) was stained with Hoechst 33342. Arrows point to migrating Cargocytes and arrowheads point to hT-MSC nuclei trapped in the confined constrictions. Scale bar, 50 μm. Experiment performed in the lab of Jan Lammerding by Jeremy Keys. (**b**) Bar graph shows the average time required for MSCs and Cargocytes treated as in (**a**) to migrate through an individual microfluidic constriction. Data for both confined (≤2 μm ×5 μm) and unconfined (15μm ×5 μm) constrictions are shown. Mean ± SEM. Data pooled from 3 independent experiments. Exact number in each group shown above the bar. P value, one-way ANOVA with Bonferroni's multiple comparison tests. (**c**) LifeAct RFP MSC were cultured by two dimensional (2D) or 3D methods, then ultracentrifuged in Ficoll to generate 2D or 3D-derived Cargocytes. 2D and 3D MSCs and Cargocytes were stained with DiD intravital dye and IM were administered intravenously in BALB/c mice. 24 hours after injection, organs were harvested for FACS analysis. Bar graphs represent number of DiD stained, RFP+ MSCs or Cargocytes per 5x10E5 events. NS= not significant; * = $p<0.05$, **=$p< 0.01$, *** = $p<0.001$.

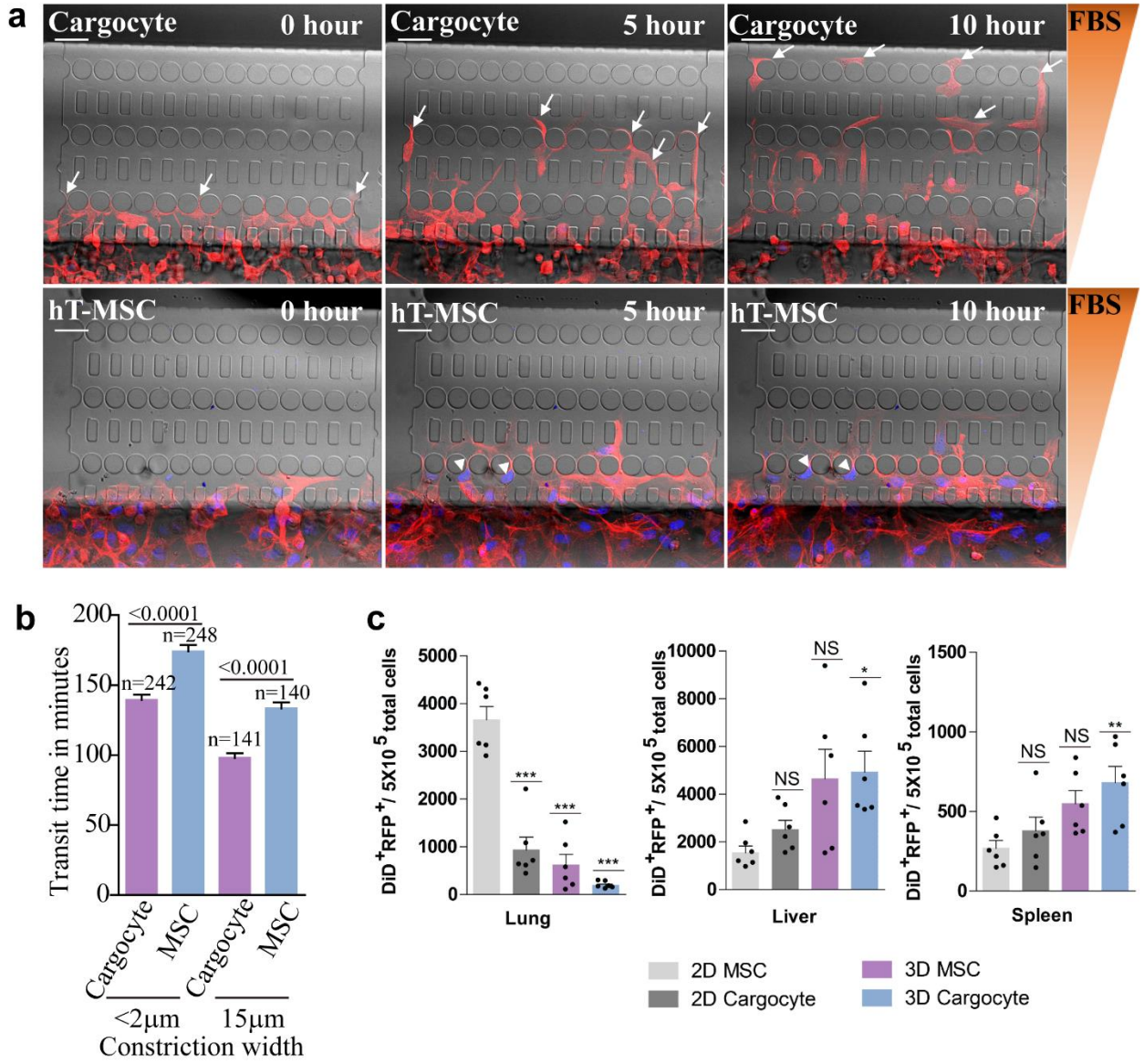
a
Cargocyte 0 hour
Cargocyte 5 hour
Cargocyte 10 hour
FBS
hT-MSC 0 hour
hT-MSC 5 hour
hT-MSC 10 hour
FBS
b
Transit time in minutes
200
150
100
50
0
<0.0001
n=248
n=242
<0.0001
n=140
n=141
Cargocyte
MSC
Cargocyte
MSC
<2μm
15μm
Constriction width
c
DiD+RFP+/ 5X10^5 total cells
Lung
Liver
Spleen
***
NS
*
**
2D MSC
2D Cargocyte
3D MSC
3D Cargocyte

Table 1: Enucleation efficiency and viability of mammalian cells following ultracentrifugation in Ficoll density gradients.

Cell Origin	Cell name	Enucleation Efficiency	Recovery Rate	Viability after 24 hours	Yield per tube
MSC cells	hT-MSC (hTERT)	>95%	80%-90%	>95%	12-15M
	UC-MSC (primary)	85%-90%	60%-80%	>90%	10-15M
	BM-MSC (primary)	50%-85%	20%-50%	50%-75%	~8M
	D1 MSC	>95%	40%-80%	>90%	5M-10M
NK cells	NK-92	70%-90%	20%-40%	20%-40%	~5M
Macrophages	RAW 264.7	85%-95%	40%-70%	20%-40%	~15M
Neutrophils	HL-60	60%-98%	20%-40%	60%-80%	~15M
Fibroblasts	L929	70%-90%	50%-70%	70%-90%	~15M
	NIH3T3	70%-80%	40%-50%	70%-80%	~9M

Enucleation efficiency (%) = number enucleated cells versus total number of cells in population retrieved from the tube. Enucleation was detected by epifluorescent microscopy as absence of fluorescent nuclear dye staining;

Recovery rate (%) = number enucleated cells retrieved out of the tube versus initial number of cells input for enucleation;

Viability after 24 hours = live enucleated cells versus total population as measured by the Trypan blue dye exclusion test;

Yield per tube = total number of enucleated cells harvested from each 13 ml centrifuge tube; M = million cells

hT-MSC = human hTERT immortalized adipose-derived mesenchymal stromal cells;

BM-MSC = human primary bone marrow-derived mesenchymal stromal cells;

UC-MSC = human primary umbilical cord mesenchymal stromal cells;

D1 MSC = mouse bone marrow stromal precursor cells;

NK = natural killer cells.

Table 2. List of Antibodies and Concentrations

Primary antibodies				
Name	**Host Species**	**Catalog**	**Vendor**	**Application and dilution**
anti-h/mSTAT4	Mouse	MAB5287	R&D	Western Blot, 1:1000
anti P-STAT4 (Y693)	Rabbit	4134S	Cell Signaling Technology	Western Blot, 1:1000
anti STAT3 (124H6)	Mouse	9139S	Cell Signaling Technology	Western Blot, 1:1000
anti P-STAT3	Rabbit	91315	Cell Signaling Technology	Western Blot, 1:1000
anti GAPDH	Rabbit	ab22555	Abcam	Western Blot, 1:10000
anti RCAS1 (Golgi)	Rabbit	12290T	Cell Signaling Technology	Immunostaining, 1:100
anti AIF (Mitochondria)	Rabbit	5318T	Cell Signaling Technology	Immunostaining, 1:100
anti EEA1 (Endosome)	Rabbit	3288T	Cell Signaling Technology	Immunostaining, 1:100
anti LAMP1 (Lysosome)	Rabbit	9091T	Cell Signaling Technology	Immunostaining, 1:100
anti PDI (C81H6) (ER)	Rabbit	3501T	Cell Signaling Technology	Immunostaining, 1:100
Cy3 Anti-Human Mitochondria clone 113-1	Mouse	MAB1273C3	Millipore	Immunostaining, 1:100
FITC anti-mouse CD31 Antibody	Rat	102506	Biolegend	Immunostaining, 1:100
Alexa-647 Human Nuclear Antigen Antibody (235-1)	Mouse IgG1 Kappa	NBP2-34525AF647	Novus Biologicals	Immunostaining, 1:100
CD8a Monoclonal Antibody (4SM16)	Rat	14-0195-82	ThermoFisher	Immunohistochemistry, 1:100
Anti-CD4 antibody	Rabbit	183685	Abcam	Immunohistochemistry, 1:100
FOXP3 Monoclonal Antibody (FJK-16s)	Rat	14-5773-82	ThermoFisher	Immunohistochemistry, 1:100
anti-CD44	Mouse IgG2A	965614	R&D	FACS, 1:20

Table 2. List of Antibodies and Concentrations, continued.

Name	Host Species	Catalog	Vendor	Application and dilution
anti-CD90	Mouse IgG2A	965609	R&D	FACS, 1:20
anti-CD105	Mouse IgG1	965611	R&D	FACS, 1:20
anti-CD166	Mouse IgG1	965613	R&D	FACS, 1:20
anti-CD45	Mouse IgG1	965616	R&D	FACS, 1:20
APC anti-human CXCR4	Mouse IgG2A	306510	Biolegend	FACS, 1:100
PE/Cy7 anti-human CD184 (CXCR4)	Mouse IgG2a, κ	306513	Biolegend	FACS, 1:100
Alexa Fluor 647 anti-mouse CD192 (CCR2)	Rat IgG2b, κ	150604	Biolegend	FACS, 1:100
PE rat anti-mouse CD162 (PSGL-1)	Lewis IgG1, κ	555306	BD	FACS, 1:100
R-Phycoerythrin AffiniPure Goat Anti-Human IgG	Goat	109-115-098	Jackson ImmunoResearch	FACS, 1:100
Purified Mouse P-Selectin - IgG Fusion Protein	IgG Fusion Protein	555294	BD	FACS, 1:50
E-selectin-human IgG fusion protein	IgG Fusion Protein	575-ES-100	R&D systems	FACS, 1:100
APC anti-mouse NK-1.1 Clone: PK136	Mouse IgG2a, κ	108710	Biolegend	FACS, 1:50
APC anti-mouse CD8a Clone: 53-6.7	Rat IgG2a, κ	100712	Biolegend	FACS, 1:50
APC/Cyanine7 anti-mouse CD45 Clone: 30-F11	Rat IgG2b, κ	103116	Biolegend	FACS, 1:100
PE anti-mouse CD45.2 Clone 104	Mouse (SJL) IgG2a, κ	109808	Biolegend	FACS, 1:50
APC/Cy7 anti-mouse CD4 Clone: RM4-5	Rat IgG2a, κ	100526	Biolegend	FACS, 1:50

Table 2. List of Antibodies and Concentrations, continued.

Name	Host Species	Catalog	Vendor	Application and dilution
PE/Cy7 anti-mouse CD3 Clone: 17A2	Rat IgG2b, κ	100219	Biolegend	FACS, 1:50
APC anti-mouse I-A/I-E Clone: M5/114.15.2	Rat IgG2b, κ	107614	Biolegend	FACS, 1:100
PE anti-mouse F4/80 Clone: BM8	Rat IgG2a, κ	123110	Biolegend	FACS, 1:100
FITC anti-mouse Ly-6C Clone: HK1.4	Rat IgG2c, κ	128006	Biolegend	FACS, 1:50
PE/Cy7 anti-mouse CD25 Clone: PC61	Rat IgG1, λ	102016	Biolegend	FACS, 1:100
APC anti-mouse Foxp3 Clone: FJK-16s	Rat IgG2b, κ	# 17-5773-82	ThermoFisher	FACS, 1:20
PerCP anti-mouse CD4 Clone GK1.5	Rat IgG2b, κ	100432	Biolegend	FACS, 1:100
Purified anti-mouse CD16/32 Antibody	Rat IgG2a, λ	101302	Biolegend	Fc Blocking, 1:1000
IgG controls				
Mouse IgG1 Negative Control Antibody, clone 1E2.2	Mouse IgG1κ	CBL600	Chemicon	FACS, 1:100
Mouse IgG2a Isotype Control from murine myeloma	Mouse IgG2a,k	M5409	Sigma	FACS, 1:100
PE Mouse IgG2a, κ Isotype Ctrl (FC)	Mouse IgG2a, κ	400213	Biolegend	FACS, 1:100
PE Mouse IgG1, κ Isotype Ctrl (FC)	Mouse IgG1, κ	400113	Biolegend	FACS, Immunostaining, 1:100
FITC Mouse IgG1, κ Isotype Ctrl (FC)	Mouse IgG1, κ	400110	Biolegend	FACS, 1:100

Table 2. List of Antibodies and Concentrations, continued.

Name	Host Species	Catalog	Vendor	Application and dilution
FITC Mouse IgG2a, κ Isotype Control	Mouse IgG2a, κ	554647	BD	FACS, 1:100
APC Mouse IgG1, κ Isotype Ctrl (FC)	Mouse IgG1, κ	400122	Biolegend	FACS, Immunostaining, 1:100
APC Rat IgG2a, κ Isotype Ctrl	Rat IgG2a, κ	400511	Biolegend	FACS, 1:100
Alexa Fluor 488 Rat IgG2a, κ Ctrl Clone: RTK2758	Rat IgG2a, κ	400525	Biolegend	FACS, 1:100
PE/Cy7 Mouse IgG2a, κ Isotype Ctrl	Mouse IgG2a, κ	400232	Biolegend	FACS, 1:100
Secondary antibodies				
HRP- Goat anti Rabbit IgG	Goat	111-035-003	Jackson ImmunoResearch	WB (1:10000)
HRP- Goat anti mouse IgG	Goat	115-036-068	Jackson ImmunoReserarch	WB (1:10000)
Alexa Flour 488 goat anti-mouse IgG (H+L)	Goat	A11001	Invitrogen	FACS, 1:200
Alexa Flour 647 goat anti-mouse IgG1	Goat	A21240	Invitrogen	FACS, 1:200
Alexa Flour 488 Goat anti-Rabbit IgG (H+L)	Goat	A11008	Invitrogen	Immunostaining, 1:500
In Vivo antibodies				
InVivoMAb anti-mouse PD-1 (CD279)	Armenian Hamster IgG	BE0033-2	BioXcell	In Vivo, 100 mcl of 2.0 mg/ml per injection
InVivoMAb Armenian hamster IgG isotype control, anti-glutathione S-transferase	Armenian hamster IgG	BE0260	BioXcell	In Vivo, 100 mcl of 2.0 mg/ml per injection

Chapter 2 Pre- and Post-enucleation Bioengineering of Cargocytes

2.1 Bioengineering Cargocyte immunomodulatory functions

In addition to characterizing the endogenous potential of MSC-derived Cargocytes, this work also endeavored to determine the ability to bioengineer Cargocytes with specific function-enhancing properties, starting with the evaluation of protein translation, receptor expression, and chemotaxis. Because MSCs have many important innate immunomodulatory functions, I focused on the bioengineering of immunomodulatory cytokines and chemokine receptors. Since time in culture and exposure to disease microenvironments can alter the immunomodulatory functions of MSCs, it is important for bioengineering to either restore or stabilize endogenous immunomodulatory properties, as well as potentially impart new immunomodulatory functions.

2.1.1 Immunomodulatory cytokines

Cytokines are a large family of soluble proteins secreted mainly by leukocytes that exert key immunomodulatory functions by autocrine, paracrine, or endocrine means.[150] Despite their potent activities, most endogenous cytokines have a short serum half-life and low bioavailability,[151] which in a therapeutic setting necessitates either administering high exogenous doses that risk toxicity, or bioengineering with stabilizing modalities such as binding with fusion proteins, antibody complexes, polyethylene glycol (PEGylation), or mutagenesis.[152] The balance of cytokines in health is carefully maintained, which partly explains why therapeutic administration of cytokines is often difficult to predict and control.[153] In particular, cell-based therapies that attempt to stimulate the immune system, such as CAR T cells, can have serious adverse events like cytokine release syndrome secondary to massive leukocyte stimulation and activation.[154] Therefore, effective cytokine therapies must address cytokine stability and delivery as well as ways to maintain or control the delicate immunoregulatory balance in vivo.

To address cytokine stability, our strategy used Cargocytes as delivery vehicles[155] for locoregional production of the cytokine. Theoretically, this would reduce off-target effects and increase site-specific effects by more precisely confining the cytokine at the region of interest. To produce these cytokines, Cargocytes would be transfected with synthesized mRNA and then cytokine production and biofunctionality determined. Although Cargocytes translated exogenous proteins GFP and Gluc, more complex proteins like cytokines required careful design of the synthesized mRNA strands to maximize strand integrity, initiation of translation, and efficiency of translation. Therefore, we designed cytokine mRNA through TriLink BioTechnologies[156] to included artificial caps to increased capping efficiency, a Kozak sequence[157] for increased translation efficiency, 5'UTR and 3'UTR of alpha globin to increase the stability, and a pseudouridine modification to improve overall stability and translation efficiency.

We bioengineered production of prototypical pro- or anti-inflammatory interleukins (IL): IL-12 is an immunostimulatory cytokine with antitumor activity,[158] whereas IL-10 is an anti-inflammatory cytokine.[159] Bioactive IL-12 is a heterodimer (IL-12p70) composed of two covalently linked subunits (p35 and p40),[160] so successful production of protein requires translation of two mRNA strands. When secreted IL-12 binds to the IL-12 receptor, it signals through the JAK-STAT pathway to activate STAT4 .[161] Downstream effects of this activation include regulation of cell-mediated immune responses, as well as innate immune modulation. IL-10 is a non-covalently linked homodimer that uniquely binds the IL-10RA receptor, which is mainly expressed on leukocytes. It also signals through JAK-STAT pathways to activate predominantly STAT3.[162] Its main targets are macrophages and monocytes to either decrease the production of pro-inflammatory cytokines or increase the production of anti-inflammatory ones. Additional details about IL-12 and IL-10 as therapeutic agents in vivo are found in Chapter 3

(mouse breast cancer model) and Chapter 4 (mouse inflammation model), respectively.

2.1.2 Chemokine receptors and endothelial adhesion molecules

Chemokines are chemotactic cytokines that help direct cell migration to specific locations. They signal through G-protein-coupled receptors (GPCRs) and play an important role in cell homing (directed migration, including to the tissue of origin), tissue homeostasis and embryogenesis, and disease states like inflammatory conditions and cancer.[163] Since MSCs frequently express low basal levels of homing receptors during ex vivo expansion, strategies to enhance in vivo homing have predominantly utilized preconditioning in culture to upregulate endogenous receptor expression, or bioengineering to express homing receptors for chemoattractants expressed in specific tissues.[155]

The CXCR4/SDF-1α axis is important for MSC endogenous homing to several types of tissues, including bone marrow. C-X-C chemokine receptor type 4 (CXCR4, CD184) directs homing of MSCs, leukocytes, and some cancer cells towards its cognate ligand, SDF-1α (CXCL12)[163]. SDF1-α is predominantly expressed in immunoregulatory organs such as bone marrow, lungs, lymph nodes, heart, thymus, and liver, although it can also be upregulated in sites of tissue injury or disease.[163] To improve in vivo homing, MSCs have been previously bioengineered with lentiviruses to increase CXCR4 expression on the surface.[164] We used a similar strategy by infecting MSCs with lentiviruses encoding CXCR4 (MSC^{CXCR4}) and then examined functional receptor expression of Cargocytes ($Cargocyte^{CXCR4}$) after enucleation.

Another chemokine receptor we investigated is C-C chemokine receptor type 2 (CCR2, CD192), a chemokine receptor for chemokine ligand 2 (CCL2, monocyte chemoattractant protein, MCP-1) that directs monocytes, T cells, and dendritic cells to the sites of tissue damage, inflammation, and cancer.[165, 166] Although CCR2 is not normally expressed on MSCs, it has been

used as an exogenous homing receptor to target MSCs to regions of ischemia.[167] Since CCL2 can be increased in diseased tissues, we also used lentiviral bioengineering to express CCR2 on MSCs (MSC^{CCR2}) and then enucleated them ($Cargocyte^{CCR2}$).

Following systemic administration through intravenous (IV) injection, cell-based therapies must undergo steps similar to leukocyte extravasation in order to exit the vasculature into the tissue of interest.[155] One important step is the interaction with the endothelium for transmigration, which can be mediated by endothelial expression of adhesion molecules (P- and E-selectins) and expression of the P-selectin glycoprotein ligand (PSGL-1) on the therapeutic cell.[168] While MSCs do not express PSGL-1 endogenously,[169, 170] some studies found that mRNA transfection or glycoengineering of MSCs with PSGL-1 or sialyl-Lewis X (E-selectin ligand) increased homing to sites of inflammation.[171-173] We again used a lentivirus approach to express PSGL-1 and its fucosyltransferase (FUT-7) on the MSC surface (MSC^{PSGL-1}) prior to enucleation ($Cargocyte^{PSGL-1}$).

In addition to bioengineering MSC lines that expressed each of the chemokine receptors or endothelial adhesion molecule, we also created a cell line to simultaneously express all three (triple-engineered MSC, MSC^{Tri-E}) to determine the feasibility of multiple layers of bioengineering.

2.2 Materials and Methods for pre- and post-enucleation bioengineering

2.2.1 Protocol for IL-12 and IL-10 mRNA transfection

As in Section 1.3.5, mRNAs for human IL-10 and mouse IL-12a/IL-12b mRNAs were synthesized by TriLink Biotechnologies and transfected as previously described.

2.2.2 Protocol for cytokine ELISAs

Cytokines levels were determined by commercial enzyme-linked immunosorbent assay

(ELISA) kits for Human IL-10 (Biolegend, #430604) and Mouse IL-12 (p70) (Biolegend, #433604) according to manufacturer's instructions. Conditioned media were diluted in kit assay diluent. Absorbance was read on the µQuant plate reader (Biotek) according to kit instructions. Standard curves and cytokine concentrations were calculated in Microsoft Excel.

2.2.3 Protocol for cytokine western blots for in vitro bioactivity

RAW 264.7 cells (ATCC® TIB-71™) were purchased from ATCC and cultured in DMEM (Gibco, #11960) with 10% FBS. For human IL-10 bioactivity, RAW 264.7 macrophage cells were serum-starved overnight, exposed to indicated conditioned media or 1ng/ml recombinant human IL-10 protein (Biolegend, #571002) in CCM for 1 hour, and then lysed for western blot (WB) analysis. For mouse IL-12 bioactivity, freshly isolated splenocytes were exposed to indicated conditioned media or 10ng/ml recombinant mouse IL-12 protein (Biolegend, #577002) in CCM for 30 minutes, and then lysed for WB. Cell lysates were generated using standard methods with lysis buffer (50 mM HEPES, pH 7.4, 150 mM NaCl, 1% Triton X-100, 1% sodium deoxycholate, 0.1% SDS, 10% glycerol, cocktail protease inhibitors, PMSF and phosphatase inhibitors). Lysates were boiled in LDS sample buffer (ThermoFisher, # NP0008), resolved on Nupage 4%-12% gel (Thermofisher, #NP0323BOX), and transferred to nitrocellulose blotting membrane (GE Healthcare, #10600020). After blocking with 5% milk, the membrane was incubated with indicated primary antibodies. After incubating with corresponding HRP-conjugated secondary antibodies, blots were developed on HyBlot Autoradiography film (Denville Scientific, #E3012) with chemiluminescent substrate (ThermoFisher, # 34580). All the primary and secondary antibodies used for western blots are listed in Table 2.

2.2.4 Protocol for lentivirus-based cell transduction

Lentiviruses pLV-Hygro-EF1A hCXCR4, pLV-EF1A mCcr2, and pLV-Puro-EFS mPsgl-

1 P2A mFut7 were purchased from VectorBuilder (Table 3, vector maps and sequences available on the VectorBuilder website). Lentivirus rLV-Ubi-LifeAct RFP was purchased from Ibidi (#60141). Briefly, hTERT MSCs were transduced with lentivirus particles at 2 to 5 MOI in Opti-MEM medium (ThermoFisher, #31985088) with 8 µg/ml SureENTRY transduction reagent (Qiagen, #336921). After 4 hours of co-incubation, transduction complex was replaced with CCM. If necessary, drug selection was added to the cells 72 hours after virus transduction. To generate triple-engineered MSCs (mCcr2, hCXCR4 and mPsgl-1, named MSC^{Tri-E}), hT-MSCs were first infected with lentivirus pLV-Hygro-EF1A hCXCR4 and cultured under drug selection (50 µg/ml hygromycin) for two weeks. Surviving cells (designated MSC^{CXCR4}) were next infected with lentivirus pLV-Puro-EFS mPsgl-1 P2A mFut7 and cultured under drug selection (10 µg/ml puromycin) for another two weeks. Finally, surviving cells (designated $MSC^{CXCR4/PSGL-1}$) were infected with lentivirus pLV-EF1A mCcr2 to generate MSC^{Tri-E}, which were analyzed for surface expression of hCXCR4, mCcr2 and mPsgl-1 by flow cytometry.

2.2.5 Protocol for flow cytometry of surface receptors pre- and post-enucleation

As in Section 1.3.3, MSCs and Cargocytes were stained with indicated antibodies for 40 minutes on ice. After washing with FACS buffer 3 times, samples were analyzed by the flow cytometry machine FACS Canto II (BD). Isotype matched IgG was used for negative control. For FACS sorting of MSC^{Tri-E}, cells were simultaneously stained with FITC anti-human CXCR4, APC anti-mouse CCR2 and PE-anti mouse PSGL-1. Single cells with high expression of all 3 markers were sorted into 96-well plates with CCM using the BD FACSAria Fusion cell sorter at the UCSD Stem Cell Core. Nineteen fast-growing single cells clones were established from two 96-well plates, expanded and stocked in liquid nitrogen. Clone 19 was used for most in vivo experiments based on its high expression of all 3 markers and fast growth in culture.

For mouse P-selectin or E-selectin binding assays, resuspended MSCs or Cargocytes were incubated with purified mouse P-selectin- human IgG fusion protein (BD, #555294) or E-selectin-human IgG fusion protein (R&D systems, # 575-ES-100) in binding buffer (PBS with Calcium and Magnesium (ThermoFisher, # 14040133) and 0.5% BSA) on ice for an hour with gentle shaking. After washing with binding buffer for 3 times, MSCs or Cargocytes were then incubated with R-Phycoerythrin AffiniPure Goat Anti-Human IgG on ice for another hour with gentle shaking. After washing with binding buffer for 3 times, MSCs or Cargocytes were analyzed by FACS Canto II (BD). Purified Human IgG1 Isotype Control Recombinant Antibody was used for Isotype control.

2.2.6 Protocol for transwell chemotaxis assays

As in section 1.3.6, Boyden chambers were used to measure directional 2D migration. For cells bioengineered with CXCR4, concentrations of SDF1-α (0, 1, 10, or 100 ng/ml) were placed in the bottom chamber. For cells bioengineered with CCR2, 100 ng/ml was in the bottom.

2.3: Post-enucleation bioengineering of Cargocytes to secrete functional cytokines

Since Cargocytes translated exogenous mRNAs for GFP and Gluc into detectable and functional proteins, I hypothesized that Cargocytes would also have the ability to produce bioactive immunomodulatory cytokines like IL-12 and IL-10 in vitro. To bioengineer Cargocytes to secrete therapeutic proteins, I performed post-enucleation transfection of Cargocytes with synthesized mRNAs.

After enucleation, Cargocytes transfected with purified mouse IL-12 mRNA (Cargocyte IL-12, Fig. 5a) or human IL-10 mRNA (Cargocyte IL-10, Fig. 5b) produced detectable protein in conditioned media. However, the production of IL-12 was lower than parental cells (Fig. 5c) while levels of IL-10 were similar (Fig. 5d). When conditioned media from cytokine-secreting

Cargocytes was applied to target cells, it led to phosphorylation of the appropriate STAT (Fig. 5e, f).

2.4 Conclusions from bioengineering Cargocytes to secrete cytokines

Cargocytes successfully produced IL-12 and IL-10 following mRNA transfection, although the production of IL-12 was lower than parental cells. The most likely explanation for this decreased capability is that secretion of IL-12 requires translation of both strands of the heterodimeric protein. Since Cargocytes are smaller than cells, it is possible that their decrease volume both limited the total number of transfected mRNAs and decreased the odds of having the appropriate number of correlating paired mRNA strands to form the heterodimer. Despite this potential limitation to the total amount produced, it is still impressive that an enucleated cell was able to translate two separate mRNAs into a functional complex protein. The presence of phosphorylated STATs in leukocytes following treatment with cytokine-conditioned media suggests that the cytokines were appropriately able to signal their downstream activators in target cells. These results indicate that Cargocytes can be bioengineered to secrete bioactive proteins like complex immunomodulatory cytokines.

2.5: Pre-enucleation bioengineering of Cargocytes with chemokine receptors and adhesion molecules

Since Cargocytes retained parental cell surface markers after enucleation and can migrate, I tested the ability of Cargocytes to retain functional bioengineered chemokine receptors and endothelial adhesion molecules. I hypothesized that Cargocytes derived from MSCs bioengineered to express CXCR4, CCR2, and/or PSGL-1 would retain expression for at least 24 hours. Because Cargocytes retain migrational machinery, I also hypothesized that these functional markers would increase Cargocyte chemotaxis towards the cognate chemoattractant and have appropriate binding

with the adhesion ligand.

After lentiviral infection, drug selection, and FACS sorting for the highest expressors of each marker, each bioengineered MSC was enucleated to produce the corresponding Cargocyte, and then compared for marker expression and either chemotaxis or ligand binding. Cargocyte^{CXCR4} displayed similar CXCR4 expression as MSC^{CXCR4} at 2, 24, and 48 hours post-enucleation (Fig. 6a), and migrated in a dose-responsive fashion towards SDF-1α in Boyden chambers (Fig. 6b). This chemotaxis was more dramatic compared to the non-engineered hT-MSCs, especially at the higher doses of SDF-1α. Cargocyte^{CCR2} also displayed CCR2 expression, with a slight decrease at 2 hours, but similar expression to MSC^{CCR2} at 24 and 48 hours (Fig. 6c). Both Cargocyte^{CCR2} and MSC^{CCR2} showed strong chemotaxis towards a gradient of Ccl2 (Fig. 6d) compared to non-engineered hT-MSCs. Cargocyte^{PSGL-1} displayed surface PSGL-1 similar to MSC^{PSGL-1} at 2 hours, with gradual and slight left shifts at 24 and 48 hours (Fig. 6e left). Cargocyte^{PSGL-1} and MSC^{PSGL-1} bound P-selectins more strongly than E-selectins (Fig. 6e middle and right), with a gradual decrease in P-selectin binding by 48 hours. Cargocytes bioengineered to express all 3 markers simultaneously (Cargocyte^{Tri-E}) had similar expression profiles of individual markers as Cargocytes bioengineered with single marker expression. Additionally, Cargocyte^{Tri-E} were able to chemotax towards individual gradients of SDF1-α and Ccl2 (Fig. 6f) and bind P-selectin (Fig. 6g).

2.6 Conclusions from bioengineering Cargocytes with functional surface markers

As seen in previous studies, MSCs are amenable to genetic engineering through techniques like lentiviral infection to create stable overexpression of endogenous or exogenous receptors. In addition to generating MSC lines expressing chemokine receptors CXCR4, CCR2, and endothelial adhesion molecule PSGL-1, I found that Cargocytes generated from these bioengineered MSCs

were able to retain stable surface expression for 48 hours, indicating that Cargocytes can undergo pre-enucleation bioengineering. Importantly, these surface markers were functional, as evidenced by the chemotaxis of Cargocytes towards their cognate ligands, and the binding of P-selectin, and to a lesser extent, E-selectin. In fact, bioengineered Cargocytes migrated at similar levels to MSC^{CCR2} and even better than MSC^{CXCR4}, but always dramatically better than the non-engineered controls. Therefore, Cargocytes not only retain migrational machinery after enucleation, but also have enhanced directed migration when bioengineered with specific receptors, which has important implications for their ability to home in vivo. When bioengineered to express all 3 markers simultaneously, $Cargocyte^{Tri\text{-}E}$ still showed strong chemotaxis to gradients of SDF-1α, Ccl2, and binding to P-selectin. This indicates that Cargocytes can undergo multiple layers of bioengineering, and that these bioengineered surface molecules do not interfere with each other's functional abilities. In fact, the purpose of multilayered bioengineering is to simultaneously enhance multiple functional abilities of the cell in vivo.

Chapter 2, in part, has been submitted for publication of the material as it may appear in Nature Biotechnology, H. Wang, C.N. Alarcón, B. Liu, F. Watson, S. Searles, C. Lee, J. Keys, W. Pi, D. Allen, J. Lammerding, J.D. Bui, and R.L. Klemke, 2020. The dissertation author was the co-primary investigator and co-first author of this paper.

Figure 5: Bioengineered Cargocytes translate exogenous mRNAs to produce bioactive immunomodulatory cytokines.

(**a**) Schematic design of the mouse IL-12a and IL-12b mRNAs synthesized in vitro (**b**) Schematic design of the human IL-10 mRNA synthesized in vitro. For (**a**) and (**b**), Kozak sequence was added in front of the start codon of the IL-10 mRNA coding region (CDS). 5'UTR and 3'UTR of mouse alpha globin mRNA were added respectively to the 5' and 3' end of CDS. An artificial 5'Cap was added to the 5' end of mRNAs and the pseudouridine modification was engineered to increase mRNA stability. (**c**) Bar graph shows the secreted IL-12 concentration in conditioned media of IL-12 transfected MSCs (MSC-IL-12), Cargocytes (Cargocyte-IL-12) or non-transfected cells (Control MSC). Mean ± SEM; n=6 biological replicates. (**d**) Graph shows the secreted IL-10 concentration in conditioned media of IL-10 transfected MSCs (MSC-IL-10), Cargocytes (Cargocyte-IL-10), non-transfected cells (Control MSC) or control media. Mean ± SEM; n=6 biological replicates. (**e**) Mouse splenocytes were treated with indicated conditioned media or recombinant mouse IL-12 (p70) protein (10ng/ml) for 30 mins. The phosphorylation of Stat4 was determined by western blot. (**f**) Mouse RAW macrophage cells were treated with indicated conditioned media or recombinant IL-10 protein (1ng/ml) for 30 mins. The phosphorylation of Stat3 was determined by western blot. Western blots were run by Felicia Watson.

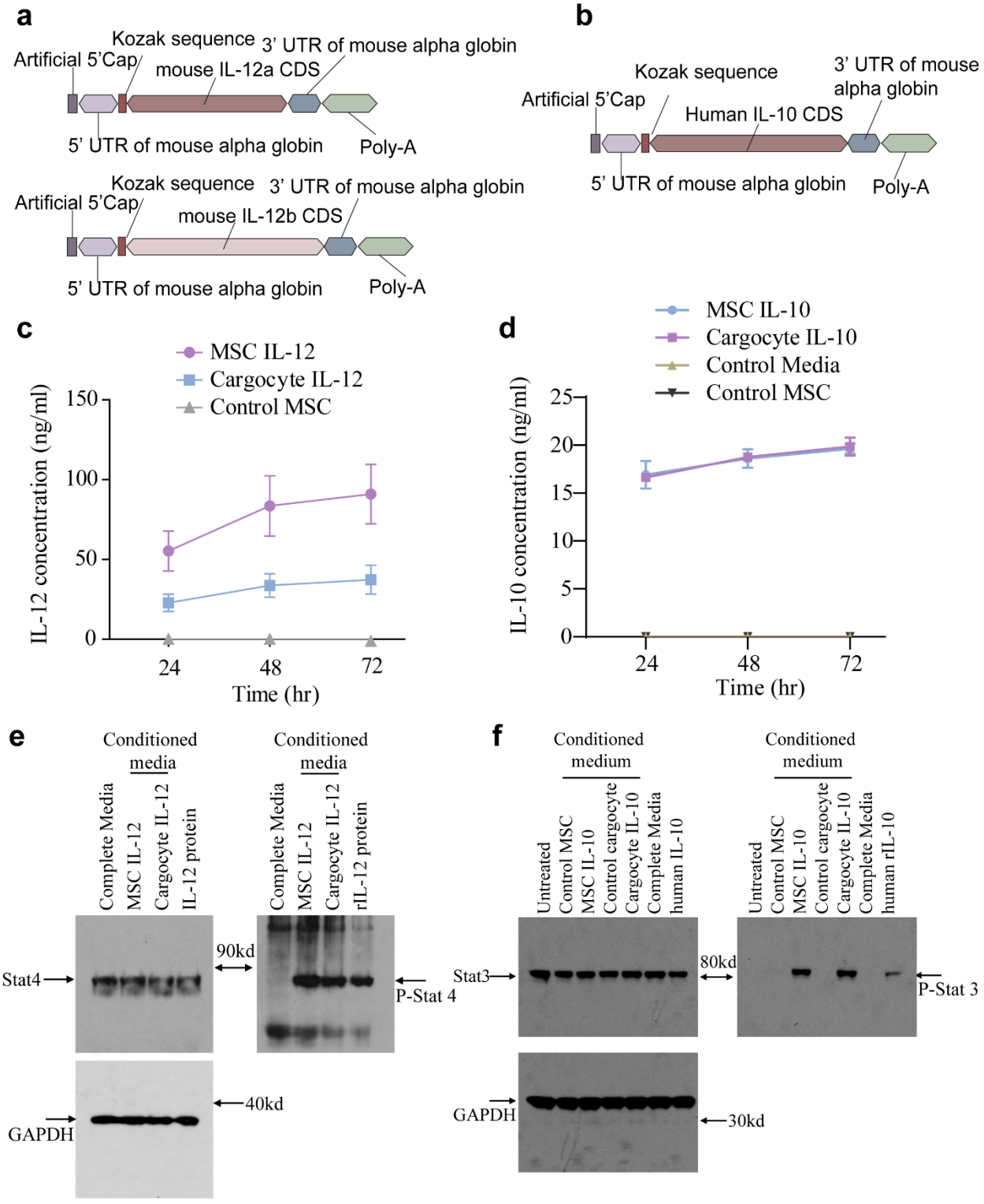
a
Artificial 5'Cap
Kozak sequence
mouse IL-12a CDS
3' UTR of mouse alpha globin
5' UTR of mouse alpha globin
Poly-A
Artificial 5'Cap
Kozak sequence
mouse IL-12b CDS
3' UTR of mouse alpha globin
5' UTR of mouse alpha globin
Poly-A
b
Artificial 5'Cap
Kozak sequence
Human IL-10 CDS
3' UTR of mouse alpha globin
5' UTR of mouse alpha globin
Poly-A
c
MSC IL-12
Cargocyte IL-12
Control MSC
IL-12 concentration (ng/ml)
150
100
50
0
24
48
72
Time (hr)
d
MSC IL-10
Cargocyte IL-10
Control Media
Control MSC
IL-10 concentration (ng/ml)
25
20
15
10
5
0
24
48
72
Time (hr)
e
Conditioned media
Complete Media
MSC IL-12
Cargocyte IL-12
IL-12 protein
Conditioned media
Complete Media
MSC IL-12
Cargocyte IL-12
rIL-12 protein
Stat4
90kd
P-Stat 4
GAPDH
40kd
f
Conditioned medium
Untreated
Control MSC
MSC IL-10
Control cargocyte
Cargocyte IL-10
Complete Media
human IL-10
Conditioned medium
Untreated
Control MSC
MSC IL-10
Control cargocyte
Cargocyte IL-10
Complete Media
human rIL-10
Stat3
80kd
P-Stat 3
GAPDH
30kd

Figure 6: Bioengineered Cargocytes express functional chemokine receptors and adhesion molecules that enhance chemotaxis and selectin binding, respectively.

(**a**) Graph shows cell surface expression of CXCR4 by flow cytometry. Data analyzed in Flowjo and normalized to mode. MSC^{CXCR4}, CXCR4 lentivirus-engineered hT-MSC; 2hr/24hr/48hr Cargocytes, MSC^{CXCR4}-derived Cargocytes analyzed at indicated timepoints after enucleation; hT-MSC, non-engineered; Isotype control, MSC^{CXCR4} stained with isotype-matching IgG. (**b**) MSCs and Cargocytes bioengineered as in (**a**) migrated in Boyden chambers towards the indicated concentrations of SDF-1α for 2 hours. Bar graph represents the ratio of migrated cells versus loading control (MSCs or Cargocytes seeded onto fibronectin-coated plates). Mean ± SEM; n=10 independent fields from 3 biological replicates. All statistics are two-way ANOVA with Bonferroni's correction for multiple testing. (**c**) Graphs show cell surface expression of CCR2 analyzed by flow cytometry. Data were analyzed in Flowjo and normalized to mode. MSC^{CCR2}, CCR2 lentivirus-engineered MSC; 2hr/24hr/48hr Cargocyte ^{CCR2}, MSC ^{CCR2}-derived Cargocytes analyzed at indicated timepoints after enucleation; Parental hT MSC, non-engineered; Isotype control, MSC ^{CCR2} stained with isotype matching IgG. (**d**) MSCs and Cargocytes bioengineered as in (**c**) migrated in Boyden chambers towards the indicated concentration of Ccl2 for 2 hours. Bar graph represents the ratio of migrated MSCs/Cargocytes versus loading control (MSCs or Cargocytes seeded onto fibronectin-coated plates). Mean ± SEM; n=10 independent fields from 3 biological replicates. P values, one-way ANOVA with Tukey's multiple comparisons test. (**e**) Graphs show cell surface expression of PSGL-1 (left), P-selectin binding (middle), and E-selectin binding (right) of MSCs or Cargocytes analyzed by flow cytometry. Data were analyzed in Flowjo and normalized to mode. MSC^{PSGL-1}, PSGL-1/Fut7 lentivirus-engineered MSC; 2hr/24hr/48hr Cargocyte $^{PSGL-1}$, MSC $^{PSGL-1}$-derived Cargocytes analyzed at indicated timepoints after enucleation; Parental hT MSC, non-engineered; Isotype control, MSC $^{PSGL-1}$ stained with isotype matching IgG. (**f**) CXCR4/CCR2/PSGL-1 lentivirus-engineered MSCs (MSC^{Tri-E}) and $Cargocytes^{Tri-E}$ migrated in Boyden chambers towards the indicated chemokine gradients for 2 hours. Bar graph represents the ratio of migrated MSCs/Cargocytes versus loading control (MSCs or Cargocytes seeded onto fibronectin-coated plates). Mean ± SEM; n=10 independent fields from 3 biological replicates. P values, one-way ANOVA with Tukey's multiple comparisons test. (**g**) Graphs show cell surface expression of PSGL-1 (left), P-selectin binding (middle), and E-selectin binding (right) of MSCs bioengineered as in (**e**) and Cargocytes bioengineered as in (**f**) and analyzed by flow cytometry. Data were analyzed in Flowjo and normalized to mode. 2hr/24hr/48hr $Cargocytes^{Tri-E\ C19}$, Cargocytes derived from MSC^{Tri-E} (CXCR4/CCR2/PSGL-1 lentivirus-engineered MSCs) analyzed at indicated timepoints after enucleation; MSC $^{PSGL-1}$, MSCs bioengineered as in (**e**); Isotype control, MSC $^{PSGL-1}$ stained with isotype matching IgG. MSCs. For (**a**) – (**g**), lentiviral constructs were designed by Huawei Wang.

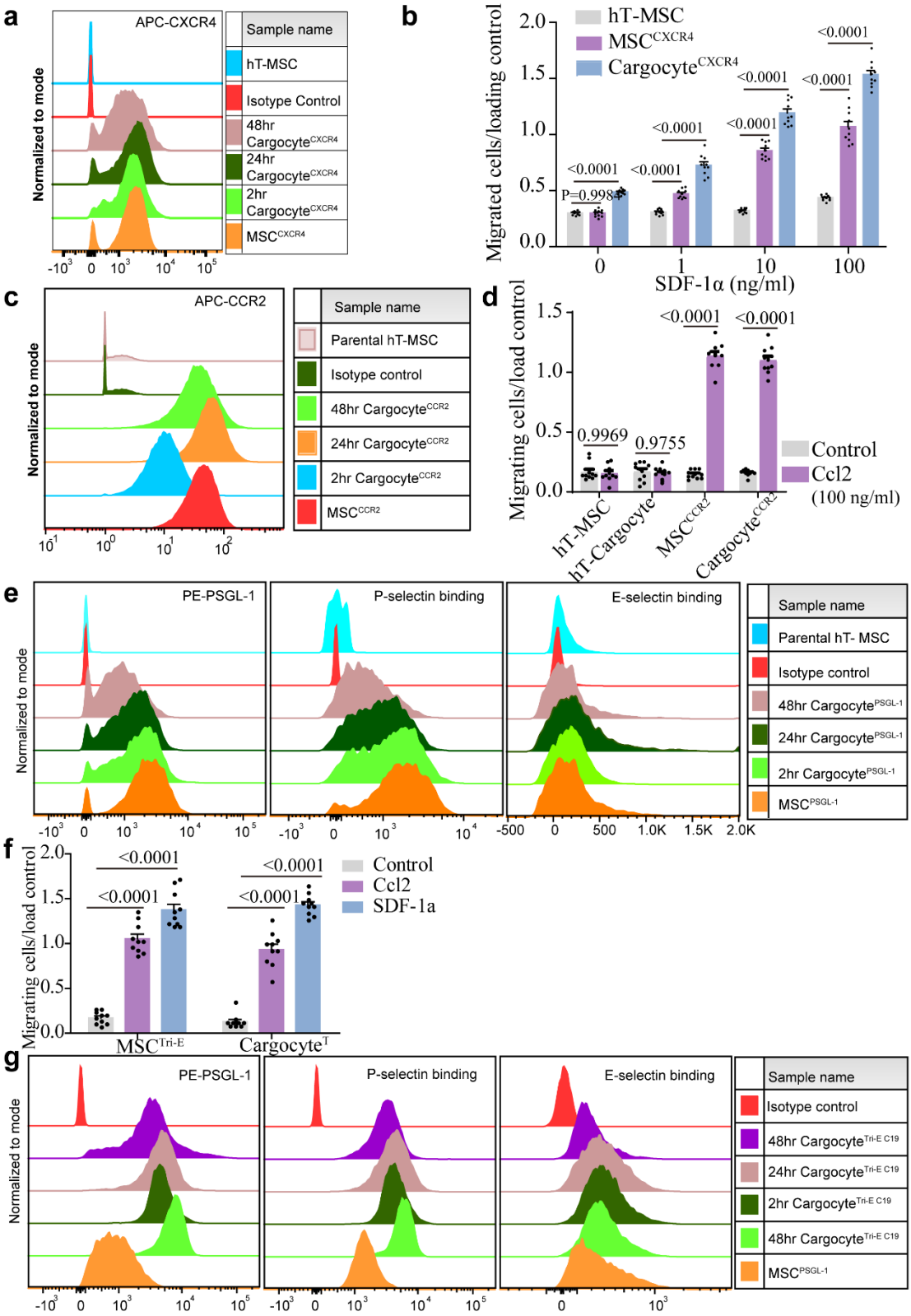
a
APC-CXCR4
Normalized to mode
Sample name
hT-MSC
Isotype Control
48hr Cargocyte^CXCR4
24hr Cargocyte^CXCR4
2hr Cargocyte^CXCR4
MSC^CXCR4
b
hT-MSC
MSC^CXCR4
Cargocyte^CXCR4
Migrated cells/loading control
SDF-1α (ng/ml)
P=0.998
<0.0001
c
APC-CCR2
Normalized to mode
Sample name
Parental hT-MSC
Isotype control
48hr Cargocyte^CCR2
24hr Cargocyte^CCR2
2hr Cargocyte^CCR2
MSC^CCR2
d
Migrating cells/load control
0.9969
0.9755
Control
Ccl2
(100 ng/ml)
hT-MSC
hT-Cargocyte
MSC^CCR2
Cargocyte^CCR2
e
PE-PSGL-1
P-selectin binding
E-selectin binding
Normalized to mode
Sample name
Parental hT- MSC
Isotype control
48hr Cargocyte^PSGL-1
24hr Cargocyte^PSGL-1
2hr Cargocyte^PSGL-1
MSC^PSGL-1
f
Migrating cells/load control
Control
Ccl2
SDF-1a
MSC^Tri-E
Cargocyte^T
g
PE-PSGL-1
P-selectin binding
E-selectin binding
Normalized to mode
Sample name
Isotype control
48hr Cargocyte^Tri-E C19
24hr Cargocyte^Tri-E C19
2hr Cargocyte^Tri-E C19
48hr Cargocyte^Tri-E C19
MSC^PSGL-1

Chapter 3: Cargocyte Antitumor Potential in a Preclinical Mouse Breast Cancer Model

3.1 Investigating Cargocyte delivery of IL-12 in vivo

Although bioengineering of Cargocytes validated some impressive in vitro capabilities, these cellular enhancements are meaningless as a therapeutic platform if it does not produce an effect in vivo. The next step was to administer Cargocytes in preclinical mouse models to determine if they could produce bioactive proteins in vivo. To investigate the ability of Cargocytes to secrete therapeutic factors in vivo, I used a mouse model of breast cancer and injected tumors with Cargocytes secreting IL-12. At various timepoints on various dosing schedules, I analyzed the amount of IL-12 produced within the tumor, as well as any functional response to the IL-12 secretion against the tumor. Based on Cargocyte ability to secrete bioactive IL-12 in vitro, I hypothesized that Cargocytes would produce IL-12 in vivo, even in a harsh tumor microenvironment. Because of its immunomodulatory effects, successful secretion of IL-12 should affect the endogenous leukocyte response to effect an antitumor response.

3.2 The E0771 Triple Negative Breast Cancer (TNBC) syngeneic C57Bl/6 mouse model

Triple negative breast cancer (TNBC) in humans often carries a poor prognosis because of early metastasis and unresponsiveness to hormone-targeting drugs.[174] The E0771 murine breast cancer cell line was originally isolated from a spontaneous medullary mammary adenocarcinoma in a C57Bl/6 mouse. [175, 176] Since its characterization in the 1940s, it has received renewed interest as a useful syngeneic mouse model of breast cancer that closely recapitulates the human disease. First, similar to invasive human breast cancers, E0771 tumors grow rapidly (tumors develop in 10-14 days) and subcutaneous/orthotopic transplants can both locally invade and/or metastasize to the lungs.[177] Second, E0771 cells are immunohistochemically similar to human TNBC due to the lack of estrogen, progesterone, and HER2/neu receptor expression. [178] Third, the mutational rate of

E0771s is within the upper range of mutational loads in human TNBCs, suggesting that tumor neoantigens are common. [179] Finally, E0771 tumors have immune profiles similar to human TNBCs, including intratumoral neutrophils and lymphocytes (predominantly FoxP3+ T regulatory cells (Tregs)), increased expression of programmed death ligand 1 (PD-L1) but only moderate response rates to single immune checkpoint inhibitors, [179] large induction of immunodysfunctional myeloid derived suppressor cells associated with poor prognosis, [180] low expression and production of pro-inflammatory IL-6, [181] and are poorly immunogenic and nonspecifically immunosuppressive (i.e. not tumor-antigen dependent). [177] Therefore, because E0771 tumors resemble human TNBC behavior and immunoprofiling, immunotherapies that effectively treat E0771 syngeneic preclinical models are predicted to have better clinical translation to human disease. Additionally, since the C57Bl/6 mouse strain is immunocompetent and has over 700 commercially available genetically engineered variants, this syngeneic model allows for testing multiple pathways and conditions involved in the immune response to breast cancer. [180]

In our studies, E0771 cells were subcutaneously (SQ) injected on the C57BL/6 mouse dorsolateral flank and allowed to grow for 14 days, then treated with intratumoral injection of Cargocytes transfected with IL-12 mRNA (Cargocyte-IL-12, Fig. 7a). In these experiments, tumors were harvested at different timepoints to assess effective Cargocytes delivery of IL-12 in the tumor.

3.3 Interleukin 12 and anti-PD-1 in cancer immunotherapy

Interleukin 12 (IL-12) is an immunomodulatory cytokine whose functions bridge both the innate and adaptive immune response. It was first described in 1989 as a natural killer (NK) cell stimulating factor[182] and in 1990 as a cytotoxic lymphocyte maturation factor,[183] alluding to its ability to promote the cell-mediated immune response, which is now known to include induction

of T helper 1 (Th1) differentiation and survival, and proliferation and enhancement of the effector functions of T cell, NK, and NK-T cells.[160] Additionally, IL-12 has anti-angiogenic activities, and induces secretion of IFN-γ, whose downstream pathways converge to decrease tumor progression.[160] Other downstream activators of IL-12 and IFN-γ include PD-L1 and CXCL9,[184, 185] which we used to indirectly identify bioactivity of IL-12.

Based on numerous preclinical studies showed significant IL-12 antitumor activity,[186] IL-12 was investigated as an anticancer agent. However, patients in early clinical trial had adverse reactions based on overstimulated immune responses, linked to dosing and IL-12 levels in the blood.[158] To reduce IL-12 toxicity[187] following systemic administration, further studies addressed ways to contain or deliver IL-12 locally, such as through PEGlyation, cell carriers like MSCs,[129, 158] or local administration, such as intratumoral (IT) injection. [188-191] After addressing some of the dosing and delivery problems, clinical trials with IL-12 alone still produced only modest effects,[160, 192] whereas combination of IL-12 with other therapies like immune checkpoint inhibitors had better results.

Tumors use activation of immune checkpoints to evade antitumor immune responses, whereas checkpoint inhibitors like antibodies to programmed cell death protein 1 (PD-1), PD ligand 1 (PD-L1) or cytotoxic T-lymphocyte-associated protein 4 (CTLA4, CD152) reverse this immunosuppression by interrupting these co-inhibitory signals expressed on the leukocyte or the cancer cell.[193] While PD-1 is widely expressed on T, B, and NK cells, there is conflicting evidence that breast cancer PD-L1 expression predicts survival,[194] and administration of anti-PD-1 (aPD-1) alone in TNBC clinical trials yielded overall response rates of less than 20%.[195] In particular, it seems that aPD-1 therapy success depends on crosstalk between T cells and dendritic cells, mediated by IL-12. [196] Since IL-12 and aPD-1 as single-agent therapies appear to be insufficient,

combination therapies (cytokine, radiation, vaccine, multiple checkpoint inhibitors, adjuvants, etc) are an area of active area of breast cancer and TNBC research.[197] Therefore, our immunotherapy strategy was to induce antitumor immune stimulation via IL-12 secretion coupled with reduced tumor-induced immunosuppression via aPD-1.

3.4 Antitumor leukocyte profiles

For many cancers, the presence of tumor-infiltrating leukocytes (TILs) is associated with a better prognosis because many leukocytes have endogenous antitumor activity. In TNBC, the presence of CD8+ T lymphocytes (cytotoxic T cells) or a high ratio of CD8+ T cells to FoxP3+ Tregs of favors a good prognosis and predicts a response to immunotherapies.[198] Although TNBC is the most immunogenic breast cancer subtype, its immunogenicity is still relatively low compared to other types of cancer (i.e. lower numbers of TILs), so immunotherapy is an attractive therapeutic modality to manipulate the immune system towards a more antitumor profile.[199] Aside from increasing CD8+T cells or decreasing FoxP3+Tregs, other important leukocyte populations include NK cells[200] and macrophages, where M1 polarized macrophages tend to have more antitumor effects than M2 polarized macrophages.[201] Additionally, the presence of CD4+T helper 2 cells is important for forming lasting antitumor immunity.[202] I hypothesized that the combination of IL-12 and aPD-1 would be able to increase recruitment of antitumor leukocytes into the E0771 tumors.

3.5: Materials and Methods for Cargocyte in vivo cytokine production

3.5.1 General protocol for establishing E0771 tumors in mice

E0771 murine breast cancer cells were purchased from CH3 Biosystems and cultured and tumors established as previously described[203]. Briefly, 1E6 E0771 cells were subcutaneously injected in the right flank of C57BL/6J male or female mice (8-12 weeks old) on Day 0 and allowed

to grow for 14 days to a tumor size of about 100 mm^3. Following IL-12 mRNAs transfection, 1E6 MSC IL-12, 3E6 Cargocyte IL-12, or vehicle only (PBS) were intratumorally (IT)-injected directly into the tumor centers in a total volume of 50 µl PBS.

3.5.2: Protocol for determining intratumoral IL-12 levels by ELISA

After establishment of tumors, animals with similarly-size tumors were IT-injected with MSC-IL-12, Cargocyte-IL-12, or PBS, respectively. Mice were euthanized at 4, 24, 48, and 72 hours post-injection and IL-12 cytokine levels in plasma and tumor were measured by ELISA for Mouse IL-12 (p70) (Biolegend, #433604). Mouse tissues were prepared for ELISA as follows: tumors were homogenized in cold lysis buffer (PBS with cocktail protease inhibitors (Roche, # 11697498001) and PMSF (Thermo Scientific, #36978)) using the Beadbug homogenizer system (Benchmark Scientific, #D1030); mouse ears were homogenized in cold lysis buffer using the AG Polytron PT1200 handheld homogenizer with 5mm probe (Kinematica). Tissue lysates were centrifuged at 13,000 rpm at 4 °C and supernatant was diluted in kit assay diluent and loaded onto ELISA plates. Mouse plasma and conditioned media were diluted in kit assay diluent. Absorbance was read on the µQuant plate reader (Biotek) according to kit instructions. Standard curves and cytokine concentrations were calculated in Microsoft Excel. Tumor and ear tissue protein concentrations were determined by standard BCA assay (ThermoFisher, #23225).

3.5.3 Protocol for bioactive markers of IL-12 delivery

After establishment of tumors, animals with similarly-size tumors were IT-injected with MSC-IL-12, Cargocyte-IL-12, or PBS, respectively, and harvested at 48 hours after IT injection to measure the mRNA expression of mouse IFN-γ, CXCL9 and PD-L1 by Real-time RT-PCR. Total RNA was extracted from cultured cells or tissues with TRIzol (ThermoFisher, # 15596026) and purified with the RNeasy RNA purification kit (Qiagen, # 74104) according to manufacturer's

instructions. Purified RNA concentration was measured via Nanodrop (ThermoFisher) and cDNA was synthesized with an iScript cDNA synthesis kit (Bio-Rad, # 1708891). Quantitative RT-PCR was performed with PowerUp SYBR Green Master Mix kit (Applied Biosystems, A25742) on QuantStudio3 Real-Time PCR system (Applied Biosystems). Human or mouse hypoxanthine phosphoribosyltransferase 1 (HPRT1) gene was used as internal reference, respectively. Ratios of different mRNA levels compared to the reference mRNA were then calculated in Microsoft Excel. Primers used in this study are listed in Table 4.

3.5.4 Protocol for detection of tumor infiltrating leukocytes

After establishment of tumors, mice were IT-injected with MSC-IL-12, Cargocyte-IL-12, or PBS on Day 14, 17, and 19 (total of three injections). Tumors were harvested on Day 21 (48 hours after last IT injection) and dissociated with collagenase I solution (0.5 mg/ml collagenase (Sigma Aldrich, #C9891-100MG), 20 µg/ml DNase, 5% FBS in PBS) and analyzed by flow cytometry as previously described.[204] Briefly, 1M to 3M cells were stained for 30 minutes at 4°C in FACS tubes (Falcon, #352058) containing Fc block (anti-CD16/32), 100 µl staining buffer (PBS with 1% FBS), and the indicated antibody combinations (Table 5). Immediately prior to flow cytometry analysis, 7-AAD (Sigma, # SML1633) was added at 1 µg/ml. M1 macrophages were identified as $CD45^+/Ly6c^-/F4/80^+/MHC\ II^{high}$, while M2 macrophages were identified as $CD45^+/Ly6c^-/F4/80^+/MHC\ II^{lo}$. $CD8^+$ T cells were identified as $CD45.2^+/CD8^+/CD3^+/CD4^-$, while $CD4^+$ T cells were identified as $CD45.2^+/CD8^-/CD3^+/CD4^+$. NK cells were identified as $CD45^+/CD3^-/NK1.1^+$. For intracellular staining cells were permeabilized using the Intracellular Fixation & Permeabilization Buffer Set (ThermoFisher, #88-8824-00) according to the manufacturer's protocol. Regulatory T cells (Tregs) were identified as $CD45.2^+/CD4^+/CD25^+/Foxp3^+$.

In another experiment, similarly-treated tumors were fixed in 4% PFA and submitted to

the histology core at the Moores Cancer Center for immunohistochemical staining for anti-CD8a, anti-CD4 and anti-FoxP3 antibodies (Table 3). Images were taken on a Keyence BZ X810 microscope. Blood from these mice was submitted to the ACP Veterinary Diagnostic Laboratory at UCSD for complete blood count (Table 6) and blood chemistry screen analyses (Table 7).

3.6 Characterization of Cargocyte IL-12 production in vivo following intratumoral injection

Based on Cargocyte successful production of IL-12 in vitro, I hypothesized that Cargocytes would be able to produce detectable amounts of IL-12 in vivo, even in a harsh tumor microenvironment. Assuming successful production of IL-12, I predicted that tumors would have an increased number of infiltrating leukocytes, which would lead to decreased tumor burden.

When mice bearing SQ E0771 tumors were intratumorally (IT) injected with Cargocytes secreting IL-12, IL-12 was detectable in tumor tissues for 72 hours at levels parallel to MSCs secreting IL-12 (Fig. 7b). The animals did not show overt clinical signs of adverse events, and the level of IL-12 measured in plasma was consistent between MSC IL-12 and Cargocyte IL-12 (Fig. 7c). At 48 hours post-injection, these same tumors had increased levels of IFN-γ, PD-L1, and CXCL9, which are downstream activators from IL-12 (Fig 7d). Mice IT-injected with 3 doses of Cargocyte IL-12 showed a shift in leukocyte populations, with a relative increase in immunoreactive CD8+ (cytotoxic) T cells and decreased FoxP3+ (immunosuppressive) T regulatory (Treg) cells compared to PBS-treated control animals (Fig. 7e). Similarly, there was quantifiable increase in CD8+ and CD4+ T cells, increased M1/M2 macrophage ratio, decreased NK cells, and decreased FoxP3+/CD25+ Tregs (Fig. 7f).

3.7 Conclusions from short-term Cargocyte IL-12 intratumoral injections

Based on these results, Cargocytes effectively secreted immunomodulatory proteins in a diseased tissue to activate immune response pathways for the intended immune effector cells. The

ability to produce a complex cytokine like IL-12 in the harsh tumor microenvironment suggests that Cargocytes can deliver therapeutic products in vivo as an extension of their ability to produce IL-12 in vitro. By the induction of expression of downstream activators, it appears that the IL-12 produced by the Cargocytes was bioactive, similar to the IL-12 produced by the MSCs. This was further evidenced by the characterization of the immune cells present within the tumor. The relative increase in CD8+ T cells and decrease in FoxP3+Tregs compared to the PBS-treated tumors indicates that the leukocyte population shifted towards a more antitumor profile. Interestingly, Cargocytes secreting IL-12 had a significant increase in the number of CD8+ cells compared to MSCs secreting IL-12. While this does not provide conclusive evidence that Cargocytes performed better than MSCs as delivery vehicles, it does raise the interesting question as to why Cargocytes elicited more CD8+ cells. Contrary to my prediction, FACS analysis showed that this leukocyte shift was not due to an absolute increase in the total number of CD45+ leukocytes; rather, it was due to a redistribution of the numbers of different leukocyte types. This suggests that the IL-12 secretion did not recruit more leukocytes into the tumor, but instead led to selective recruitment and expansion of antitumor leukocytes. In this set of data, the decrease in NK cells in both MSC and Cargocyte-treated tumors was unexpected, as IL-12 is supposed to support NK cell activation and proliferation and aPD-1 can decrease NK cell exhaustion.[205] Further investigation into this finding is warranted.

Following production of IL-12 in vivo and documenting the immune response to Cargocyte IL-12 injections, the next step was to determine if Cargocytes in combination with a checkpoint inhibitor could affect overall tumor progression. This would indicate if the IL-12/aPD-1 was successful at not only stimulating the immune response, but reaching a threshold to overcome tumor burden and potentially lead to lasting antitumor immunity.

3.8 Materials and Methods for Cargocyte IL-12 survival and rechallenge experiments

For survival studies, animals with E0771 tumors received IT injections with MSC-IL-12, Cargocyte-IL-12, or PBS on Day 14, 17, 19 and 26 after tumor inoculation, followed by intraperitoneal injection of anti-mouse PD-1 or IgG control at 100 µl of 2.0 mg/ml in PBS on Day 20 and 27 (Fig. 8a). Animals were monitored frequently, and tumor size was measured with digital calipers and calculated using the formula Volume = (Width × Width × Length)/2. Tumor growth curves and mouse weight curves were generated in Excel. Animals were euthanized when tumors reached a 2 cm diameter in any dimension or had untreatable ulcers/skin irritation at the tumor site as per IUCAC guidelines. Kaplan-Meier survival curves were generated in GraphPad Prism8 and analyzed by the Mantel-Cox log-rank test.

Animals that survived at least 175 days post-tumor initiation and had no palpable tumor were re-challenged with 1E6 E0771 cells by subcutaneous injection in the contralateral flank (left) on Day 180. Age-matched, naïve control animals were injected at the same time. Tumor growth was monitored and measured as described above.

3.9 Antitumor effects of Cargocyte IL-12 combined with aPD-1

Since Cargocyte IL-12 were able to induce a shift if antitumor leukocyte profiles after 3 injections, I hypothesized that combining IL-12 and aPD-1 would lead to significant antitumor effects in the long term. I expected that combination therapy would entail an overall decrease in tumor growth and ultimately a better prognosis as measured by animal survival. For animals that survived, I predicted that they would have lasting tumor immunity characterized by rejection of future exposure to E0771 cells.

Animals that received a total of 4 Cargocyte IL-12 injections and 2 aPD-1 injections within a 2 week period had slowed tumor growth compared to animals receiving Cargocyte IL-12 alone

or aPD-1 alone (Fig. 8b,c). These animals did not appear to have adverse clinical effects, based on the change in weight for the duration of the experiment (Fig. 8d). Decreased tumor progression translated into a longer lifespan for the mouse, as seen in survival curves where animals receiving MSC IL-12 or Cargocyte IL-12 had better survival only when combined with aPD-1 (Fig. 8e). In fact, 40% of mice treated with combination Cargocyte IL-12 and aPD-1 had complete regression (no palpable tumors) for the remainder of the experiment (total >175d). These surviving animals were rechallenged with SQ E0771 cells in the contralateral flank to determine if lasting antitumor immunity was present. All rechallenged animals either had no tumor initiation or minimal tumor growth followed by rapid complete regression (Fig. 8e).

3.10 Conclusions from Cargocyte combination therapy

Animals receiving multiple doses of Cargocyte IL-12 not only experienced decreased tumor growth, but also had a 40% cure rate. While mouse studies do not always translate into similar human responses, this cure rate is remarkable because TNBC traditionally have relatively low overall response rates to standard of care treatment and current immunotherapies. Animals treated with MSC or Cargocytes and aPD-1 showed similar survival curves, which is interesting because in the short-term assay, Cargocyte IL-12 induced a stronger CD8+ response than MSC IL-12 treated animals. Regardless of the immunoprofile, MSCs and Cargocytes performed comparably in this dosing schedule for combination therapy.

Cargocyte IL-12 + aPD-1 animals that completely regressed also were able to reject E0771 cells when rechallenged in the contralateral flank. Although evaluation of tissues for leukocyte profiles was not part of the study design, it is assumed that the presence of CD4+ cells contributed to lasting tumor antitumor immunity. In future studies, it would be worthwhile to determine if altering the dosing schedule, such as providing aPD-1 concurrently with the IT Cargocyte IL-12

(instead of after it) would further increase the animal survival. If so, examining the immunoprofile of the tumor as it regresses or the site of rechallenge could provide valuable information about the mechanism by which Cargocytes are able to induce lasting antitumor immunity.

Chapter 3, in part, has been submitted for publication of the material as it may appear in Nature Biotechnology, H. Wang, C.N. Alarcón, B. Liu, F. Watson, S. Searles, C. Lee, J. Keys, W. Pi, D. Allen, J. Lammerding, J.D. Bui, and R.L. Klemke, 2020. The dissertation author was the co-primary investigator and co-first author of this paper.

Figure 7: Bioengineered Cargocytes producing bioactive IL-12 in a mouse TNBC model shifts the leukocyte populations towards an antitumor phenotype.

(**a**) Schematic of the workflow for bioengineering Cargocytes to express IL-12 cytokine and treat triple-negative breast cancer (TNBC) in immunocompetent mice. (**b**) Mice bearing E0771 tumors as in (a) were intratumorally (IT) injected with MSCs or Cargocytes transfected with mouse IL-12 mRNAs. Bar graph shows the level of IL-12 cytokine detected in the tumors by ELISA at indicated timeponts after IT injection. PBS, vehicle control; MSC-IL-12/Cargocyte-IL-12, hT-MSC or Cargocyte transfected with mIL-12 mRNA; Mean ± SEM; n=6 mice. (**c**) For mice treated as in (**b**), bar graph shows the concentration of secreted IL-12 cytokine in mouse plasma as determined by ELISA. Mean ± SEM; n=6. P value, two-way ANOVA with Dunnett's multiple comparisons test. (**d**) For mice treated as in (**b**), tumors were harvested and analyzed by real-time RT-PCR at 48hr post-IT injection. Graphs show the fold change (Log2) of the indicated mRNA markers compared to PBS group. Mean ± SEM; n=6 mice. (**e**) Established E0771 tumors were IT-injected on Day 14, 17 and 19. Tumors were harvested on Day 21. Light microscopy images of tumor sections stained with indicated immunohistochemical antibodies. Scale bar, 100μm. (**f**) For mice treated as in (**e**), tumors were harvested and analyzed by flow cytometry. %$CD8^+$ T cells, $100\times CD8^+CD4^-CD3^+CD45^+/CD45^+$; %$CD4^+$ T cells, $100\times CD8^-CD4^+CD3^+CD45^+/CD45^+$; M1Φ/M2Φ, $CD45^+Ly6c^-F4/80^+MHCII^{high}/CD45^+Ly6c^-F4/80^+MHC\ II^{low}$; %$Foxp3^+$ Treg cells, $100\times CD45.2^+CD4^+CD25^+Foxp3^+/CD45^+$; %NK cells, $100\times CD45^+CD3^-\ NK1.1^+/CD45^+$; %$CD45^+$ cells, $100\times CD45^+$/total cells. Mean ± SEM; n=6 mice.

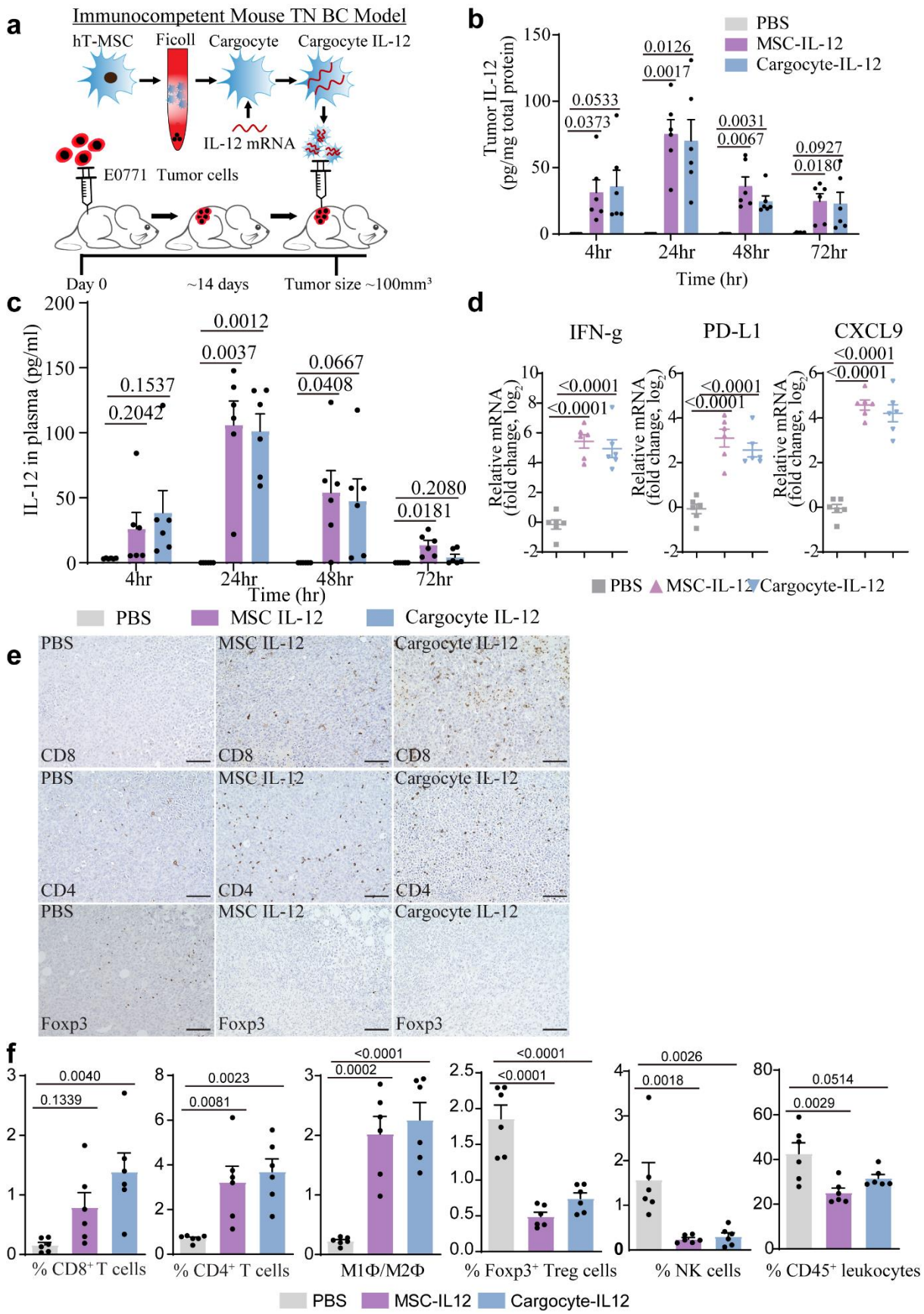
a
Immunocompetent Mouse TN BC Model
hT-MSC
Ficoll
Cargocyte
Cargocyte IL-12
IL-12 mRNA
E0771 Tumor cells
Day 0
~14 days
Tumor size ~100mm³
b
PBS
MSC-IL-12
Cargocyte-IL-12
Tumor IL-12 (pg/mg total protein)
0.0533
0.0373
0.0126
0.0017
0.0031
0.0067
0.0927
0.0180
4hr
24hr
48hr
72hr
Time (hr)
c
IL-12 in plasma (pg/ml)
0.1537
0.2042
0.0012
0.0037
0.0667
0.0408
0.2080
0.0181
Time (hr)
PBS
MSC IL-12
Cargocyte IL-12
d
IFN-g
PD-L1
CXCL9
Relative mRNA (fold change, log2)
<0.0001
PBS
MSC-IL-12
Cargocyte-IL-12
e
PBS
MSC IL-12
Cargocyte IL-12
CD8
CD4
Foxp3
f
% CD8⁺ T cells
% CD4⁺ T cells
M1Φ/M2Φ
% Foxp3⁺ Treg cells
% NK cells
% CD45⁺ leukocytes
PBS
MSC-IL12
Cargocyte-IL12

Figure 8: Intratumoral injection of bioengineered Cargocytes secreting IL-12 combined with administration of anti-PD-1 therapy caused TNBC tumor regression and antitumor immunity

(**a**) Graph shows the timeline of dosing scheme for combination therapy of IT-injected Cargocyte-IL-12 to pre-established E0771 tumors and intraperitoneal (IP) injection of anti-PD-1 antibody (aPD-1). (**b**) Graph shows tumor growth curve for animals treated as in (a). (**c**) Graph shows the Kaplan-Meier survival curve for mice treated as in (**a**). n=10 mice per group. P value, Mantel-Cox Log-rank test. (**d**) Graph shows tumor growth curve for mice treated as in (**a**) that survived >175d and had complete tumor regression, followed by re-challenge with E0771 cells in the contralateral flank. n=4 mice.

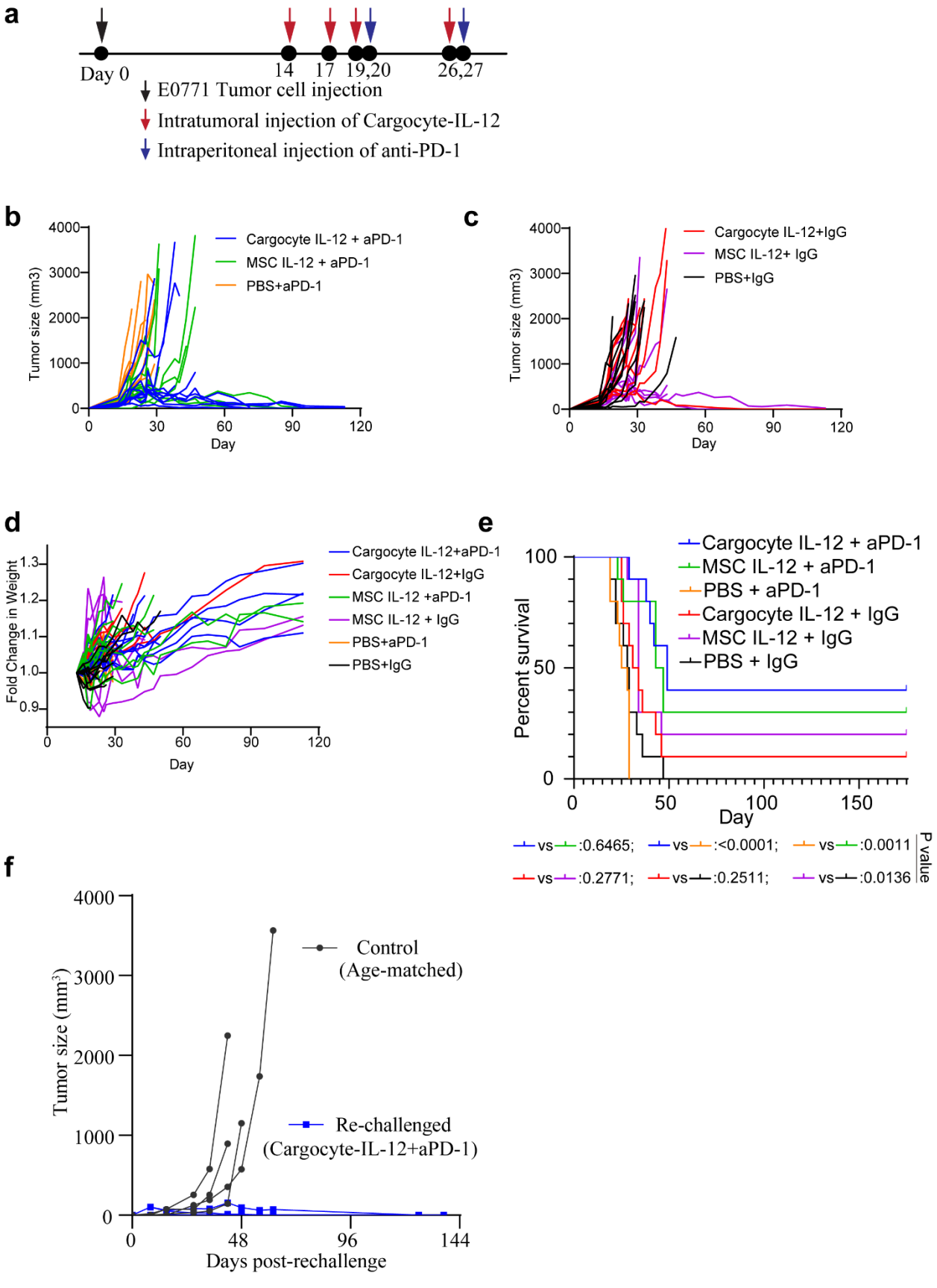
a
Day 0
14
17
19,20
26,27
E0771 Tumor cell injection
Intratumoral injection of Cargocyte-IL-12
Intraperitoneal injection of anti-PD-1
b
Tumor size (mm3)
Day
Cargocyte IL-12 + aPD-1
MSC IL-12 + aPD-1
PBS+aPD-1
c
Tumor size (mm3)
Day
Cargocyte IL-12+IgG
MSC IL-12+ IgG
PBS+IgG
d
Fold Change in Weight
Day
Cargocyte IL-12+aPD-1
Cargocyte IL-12+IgG
MSC IL-12 +aPD-1
MSC IL-12 + IgG
PBS+aPD-1
PBS+IgG
e
Percent survival
Day
Cargocyte IL-12 + aPD-1
MSC IL-12 + aPD-1
PBS + aPD-1
Cargocyte IL-12 + IgG
MSC IL-12 + IgG
PBS + IgG
vs :0.6465;
vs :<0.0001;
vs :0.0011
vs :0.2771;
vs :0.2511;
vs :0.0136
P value
f
Tumor size (mm3)
Days post-rechallenge
Control
(Age-matched)
Re-challenged
(Cargocyte-IL-12+aPD-1)

Table 3. List of lentiviruses and vectors

Name	**Company**	**Vector ID/Catalog**	**Promoter**	**Encoded gene**	**Drug Selection**
pLV-Hygro-EF1A hCXCR4	VectorBuilder	VB170808-1064dhz	EF1A	human CXCR4	50μg/ml hygromycin
pLV-EF1A mCcr2	VectorBuilder	VB171215-1221ybt	EF1A	mouse Ccr2	N/A
pLV-Puro-EFS mPsgl-1 P2A mFut7	VectorBuilder	VB170727-1187nrs	EFS	mouse PSGL-1 and Fut7	10μg/ml puromycin
rLV-Ubi-LifeAct RFP	Ibidi	#60141	Ubi (Ubiquitin)	LifeAct RFP fusion protein	10μg/ml puromycin
LentiBrite™ Histone H2B-GFP	MilliporeSigma	#17-10229	EF1	Histone H2B-GFP	N/A

Table 4. List of primers.

Primer Name for RT-PCR	**Sequence 5' to 3'**	**Target mRNA**
mCCL2 F	ATTGGGATCATCTTGCTGGT	mouse Ccl2
mCCL2 R	CCTGCTGTTCACAGTTGCC	
mIL6 F	ACCAGAGGAAATTTTCAATAGGC	mouse IL-6
mIL6 R	TGATGCACTTGCAGAAAACA	
mCxcl12 (SDF-1α) F	TTTCAGATGCTTGACGTTGG	mouse Cxcl12
mCxcl12 (SDF-1α) R	GCGCTCTGCATCAGTGA	
mCXCL9 F	GGAGTTCGAGGAACCCTAGTG	mouse Cxcl9
mCXCL9 R	GGGATTTGTAGTGGATCGTGC	
mSelP F	CCGGAGTGTGATCCTGGGA	mouse P-Selectin
mSelP R	TGTGCTGTAGTTATAGGTCCACG	
mSelE F	ATGAAGCCAGTGCATACTGTC	mouse E-Selectin
mSelE R	CGGTGAATGTTTCAGATTGGAGT	
hIDO1 F	GCCAGCTTCGAGAAAGAGTTG	human IDO1
hIDO1 R	ATCCCAGAACTAGACGTGCAA	
hPD-L1 F	TGTCAGTGCTACACCAAGGC	Human PD-L1
hPD-L1 R	ACAGCTGAATTGGTCATCCC	
mIFN-γ F	GCCACGGCACAGTCATTGA	mouse IFN γ
mIFN-γ R	TGCTGATGGCCTGATTGTCTT	
mTNF-α F	GCACCACCATCAAGGACTCA	mouse TNF-α
mTNF-α R	GAGGCAACCTGACCACTCTC	
mIL-1β F	GAAATGCCACCTTTTGACAGTG	mouse IL-1β
mIL-1β R	TGGATGCTCTCATCAGGACAG	
hHPRT1F	ACCCTTTCCAAATCCTCAGC	human HPRT1
hHPRT1R	GTTATGGCGACCCGCAG	
mHprt1 F	GAGGAGTCCTGTTGATGTTGCCAG	mouse Hprt1
mHprt1 R	GGCTGGCCTATAGGCTCATAGTGC	

Table 5: Antibody combinations.

Channel	Mix1 for Macrophage	Mix2 for T cells	Mix3 for NK cells	Mix4 for Treg cells
FITC	Ly6C Clone HK1.4 1:50			
PE	F4/80 Clone BM8 1:100	CD45.2 Clone 104 1:50		
Percp-Cy5.5	7-AAD	7-AAD	7-AAD	CD4 Clone :Clone GK1.5 1:100
PE/Cy7		CD3 Clone: 17A2 1:50	CD3 Clone: 17A2 1:50	CD25 Clone: PC61 1:100
APC	MHCII Clone M5/114.15.2 1:100	CD8 Clone: 53-6.7 1:50	NK1.1 Clone: PK136 1:50	FoxP3 Clone: FJK-16s 1:20
APC/Cy7	CD45 Clone: 30-F11 1:100	CD4 Clone: RM4-5 1:50	CD45 Clone: 30-F11 1:100	CD45 Clone: 30-F11 1:100

Table 6: Complete blood count analyses of mice for tumors harvested 48 hours after the last injection. Mean ± SEM, n=6 mice in each group. *, P<0.05, One-way ANOVA with Tukey's multiple comparisons test.

Cell Types	**Reference range**	**Cargocyte IL-12**	**MSC IL-12**	**PBS**
Red Blood Cell (1E9/mL)	6.36 - 9.42	8.434(±0.377)	7.21(±0.467)	8.675(±0.223)
White Blood Cell (1E6/mL)	1.8 - 10.7	9.216(±0.855)	7.56(±0.16)	9.21(±0.716)
Neutrophil (1E6/mL)	0.1 - 2.4	4.473(±0.372)	3.867(±0.19)	4.472(±0.387)
Lymphocyte (1E6/mL)	0.9 - 9.3	3.734(±0.857)	2.719(±0.234)	3.024(±0.382)
Monocyte (1E6/mL)	0.0 - 0.4	0.794(±0.067)*	0.684(±0.047)	0.585(±0.034)
Eosinophil (1E6/mL)	0.0 - 0.2	0.174(±0.046)	0.235(±0.058)	0.12(±0.029)
Basophil (1E6/mL)	0.0 - 0.2	0.045(±0.016)	0.059(±0.017)	0.034(±0.009)

Table 7: Serum chemistry analysis of mice for tumors harvested 48 hours after the last injection. Mean ± SEM, n=6 mice in each group. No significant differences between groups by one-way ANOVA with Tukey's multiple comparisons test.

Analyte	**Unit**	**Referenc e Range**	**Cargocyte IL-12**	**MSC IL-12**	**PBS**
Albumin	g/dL	2.5 - 4.8	4.084(±0.108)	4.017(±0.084)	4.317(±0.136)
Alkaline	U/L	62 - 209	78.667(±9.549)	66.834(±6.711	82.5(±10.204)
Alanine	U/L	28 - 132	44(±4.443)	88.667(±34.88	38.167(±2.949)
Amylase	U/L	1691 -	703.5(±29.178)	966.5(±103.78	804.334(±86.64
Bilirubin, total	mg/dL	0.1 - 0.9	0.3(±0)	0.367(±0.05)	0.317(±0.017)
Blood Urea	mg/dL	18 - 29	23.667(±0.844)	24.167(±0.946	21.5(±0.958)
Calcium	mg/dL	5.9 - 9.4	11.35(±0.313)	11.584(±0.312	11.934(±0.171)
Phosphorus	mg/dL	6.1 - 10.1	10.517(±0.515)	11.317(±0.498	11.167(±0.365)
Creatinine	mg/dL	0.2 - 0.8	0.334(±0.062)	0.284(±0.048)	0.234(±0.022)
Glucose	mg/dL	90 - 192	239.667(±13.36	225.167(±11.8	252.5(±5.807)
Sodium	mmol/	126 - 182	158.5(±3.274)	164.334(±3.50	165.667(±1.564
Potassium	mmol/	4.7 - 6.4	8.567(±0.136)	8.434(±0.067)	>8.5(±0)
Total Protein	g/dL	3.6 - 6.6	5.267(±0.089)	5.45(±0.139)	5.3(±0.078)
Globulin,	g/dL	N/A	1.017(±0.204)	1.4(±0.058)	1(±0.119)

Chapter 4: Cargocyte Anti-Inflammatory Therapeutic Potential in a Mouse Inflammation Model

There is no single gold standard for administration of cell-based therapies because each has strengths and limitations based on the type and location of the disease, timing of administration, and risks to either the cell or the patient.[206] Aside from local delivery of immunomodulatory cytokines, there can be both therapeutic benefits and practical advantages to administering cell based therapies systemically through intravenous (IV) infusion, which is minimally invasive and does not typically require specialized equipment, especially for repeated doses.[207, 208] As long as there are no major differences in the effects produced between local and systemically infused MSCs,[209-211] IV injections tend to be more convenient and also avoid the problem of cells locating and migrating to the intended target site. As discussed previously, cell bioengineering is one method to improve cell homing capabilities, for which I demonstrated in vitro feasibility of bioengineering Cargocytes with chemokine receptors that contributed to increased chemotaxis. Based on the in vitro results of this bioengineering and the demonstration that Cargocytes were able to have therapeutic effects in vivo in a tumor model, I hypothesized that the Cargocyte ability to perform in vitro chemotaxis would translate into improved in vivo migration.

4.1 Overcoming the problem of pulmonary passage in systemically-administered MSCs

Following IV injection, the majority of MSCs become entrapped in pulmonary capillaries for the first 24 hours, [212, 213] predominantly due to their relatively large size[214] and expression of integrins.[215] This first barrier to biodistribution is also a danger, as it can cause embolization. Methods of reducing in capillary trapping include reducing cell size, bioengineering to change or mask integrin expression, or repeat boluses.[213] One technique to reduce cell size is to culture cells in 3D,[216] such as in suspension rather than on 2D plastic plates where cell spreading can occur.

We selected the 3D hanging drop method[217] because of its straightforward workflow and reproducibility, although we found the yield of cultured MSCs would benefit from further optimization after dissociating spheroids into single-cell suspension. Although Cargocytes are already smaller than parental cells grown in traditional 2D culture (Fig. 2b), we predicted that Cargocytes generated from 3D-cultured cells would be even smaller and potentially pass through the lungs better than non-engineered cells.

4.2 The mouse acute, dermal ear inflammation model

The mouse ear swelling assay is a model for contact hypersensitivity or local anaphylaxis, which leads to acute (within 48 hours) and quantifiable erythema and edema of the mouse pinna (skin of the ear).[218] The test has low incidence of false positives, inflammation is both visible and measurable as an increase in ear thickness, and the contralateral ear serves as an internal control. While more commonly used for testing dermal drugs, solutions, antigens, photosensitivity, and epidermal immunobiology,[219] it has also been used with intradermal injection of irritants, endotoxins, and infectious parasites. The more invasive (non-topical) forms of this assay have reported technical variability in reproducibility,[220] but have included induction of infection through inoculation with bacterial agents.[221] In particular, bacterial lipopolysaccharide (LPS) has been used to acutely inflame the ear dermis as a model for MSC homing and intravital imaging.[222-225] In these models, vascular permeability was not a prerequisite for MSC extravasation, which was interpreted as a more active process.[222] We chose this model because it produced a localized, acute site of inflammation to which homing of bioengineered Cargocytes could be evaluated by multiple methods (reduction of inflammation, whole mount imaging, FACS analysis, intravital imaging, etc).

4.3 Effects of Interleukin 10 to treat inflammation

To reduce inflammation, some clinical trials have examined antagonists for pro-inflammatory cytokines,[226] and increased production or exogenous introduction of anti-inflammatory cytokines. IL-10 is a prototypical anti-inflammatory cytokine with pleiotropic roles in immunomodulation. It was originally described in 1989 as a cytokine synthesis inhibitory factor produced by CD4+Th2 cells that suppressed CD4+ Th1 cells,[227] but it is now known that almost every cell in both the innate and adaptive immune system is capable of expressing IL-10. Production of IL-10 primarily dampens the secretion of pro-inflammatory cytokines such as IL-1, IL-6, IL-12, TNF-α; GM-CSF and IFN-γ, but it can also decrease expression of co-stimulatory molecules, stimulate tissue repair, and induce B cell proliferation, differentiation, activation, and antibody production.[228] In the context of cancer, increased intratumoral expression of IL-10 in mouse models resulted in decreased tumorigenicity, whereas elevated levels of serum IL-10 in human cancer patients were either correlated with poor or good survival, entirely dependent on the type of tumor.[229] Overall, preclinical and clinical research of IL-10 therapies for inflammatory diseases or cancer has yielded either contradictory or only modest results,[159] likely due to its disease-specific or context-dependent action. Although IL-10 is an indisputably powerful immunomodulatory cytokine, the bioavailability, timing of administration during disease progression, and duration of local concentration all likely influence its ultimate efficacy,[159] and as of yet, no FDA-approved therapies exist.

While there are several methods to increase IL-10 stability for therapeutic delivery, such as through PEGylation, binding to fusion proteins, or secretion of IL-10 by bioengineered commensal bacteria,[162] specific delivery of IL-10 to the target site may improve its clinical efficacy. When IL-10 successfully binds its receptor, IL-10R, it signals through the JAK/STAT pathway to activate predominantly STAT3, although in some contexts it can also activate STAT1 and STAT5.[230] Both

humans and mice secrete IL-10 as noncovalently-linked homodimers and share ~73% sequence homology, although mIL-10 cannot activate human cells while hIL-10 can activate human and mouse cells.[231] In our experiments, Cargocytes bioengineered with homing receptors to sites of inflammation were transfected with synthesized human IL-10 mRNA (Fig. 9a) and tested in the mouse ear inflammation model. I hypothesized that bioengineered Cargocytes would pass through pulmonary vasculature to reach inflamed ears and deliver IL-10, ultimately resulting in reduced inflammation.

4.4 In vivo homing capability of bioengineered Cargocytes

Because Cargocytes have decreased size, ability to migrate in 3D, and potentially less lung trapping in the first 24 hours after IV injection, I hypothesized that Cargocytes bioengineered with homing receptors would be able to reach an in vivo site of inflammation in higher numbers compared to uninflamed sites and compared to non-engineered Cargocytes. In other words, Cargocyte in vitro chemotaxis would translate into improved in vivo homing. If these same Cargocytes are loaded with a therapeutic agent, such as an anti-inflammatory cytokine, they should be able to secrete IL-10 once they arrive at the target site. Since Cargocytes secrete functional IL-10 in vitro and 3D Cargocyte$^{Tri\text{-}E}$ home in vivo, I hypothesize that bioengineered Cargocytes will home and deliver IL-10, resulting in reduced inflammation.

4.5 Methods for Cargocyte homing and delivery of IL-10 in the ear inflammation model

4.5.1 Protocol for murine LPS-induced acute, dermal ear inflammation model

The LPS-induced model of dermal inflammation in the mouse pinna was established similar to previously described.[171, 225] Briefly, female BALB/cJ mice (8-12 weeks old) were anesthetized with isoflurane (VetOne, MWI 502017) and injected with 30 µg lipopolysaccharides (LPS, Sigma Aldrich, #L3024, in 30 µl saline) in the posterior/dorsal dermis of the right ear and

0.9% saline (Hospira NDC 0409-4888) in the control, contralateral ear. After 6 hours, mice were anesthetized for IV injection (tailvein or retro-orbital) of 1E6 MSCs or Cargocytes, or PBS (vehicle control) in 100 µl solution.

4.5.2 Protocol for 3D culturing of MSCs

Generation of 3D MSC spheroids in hanging drops was modified from previously published protocols.[217, 232] Briefly, MSCs were plated as drops on an inverted plastic dish lid (Olympus Plastics, #32-106) in 35 µl of CCM at 30,000 cells/drop. The lid was then replaced to cover the plate bottom containing 15 ml Dulbecco's phosphate-buffered saline (PBS, ThermoFisher, # 14190250) to prevent evaporation. Hanging drop cultures were grown at 37 °C for approximately 40 hours with 5% CO_2. To obtain single cell suspension, spheroids were collected into tubes and incubated with Accutase (Innovative Cell Technologies, # AT104-500) at RT for 20 minutes with gentle pipetting every 5 minutes. The cell-Accutase suspension was diluted with CCM, and dissociated spheroids were further treated with 100 µg/ml DNase I (Sigma Aldrich, #10104159001) for 10 minutes at 37 °C. Cells were passed through a 70 µm cell strainer (BioPioneer, # DGN258368) to obtain single cell suspensions used in the following described assays.

4.5.3 Protocol for FACS detection of IV-injected Cargocytes

For flow cytometry analyses, MSCs or Cargocytes were stained with 10 µM Vybrant DiD (Invitrogen, #V22887) following manufacturer's instructions prior to injection. Animals were euthanized 24 hours after MSC or Cargocyte injection. Ears were removed at the level of the base and the dorsal and ventral skin was peeled from the cartilage, then placed in 2 ml digestion buffer containing 0.1 mg/ml DNase I and 0.2 mg/ml Liberase TL (Sigma Aldrich, #5401020001) diluted in 1% FBS in RPMI media. After incubation at 37°C for 1 hour, ear skin was ground with a pestle

in a 70 µm cell strainer (Biopioneer, #DGN258368). When no large tissue pieces remained intact, strainers were washed with 2 ml of 1% FBS, 2 mM EDTA in PBS. Cells were then treated with 1X RBC lysis buffer (Biolegend, # 420301) for 2 minutes, washed with PBS, and stained with PE anti-mouse F4/80 Antibody and 7-AAD. Cells were analyzed by flow cytometry machine FACS Canto II (BD).

4.5.4 Protocol for whole mount immunostaining of mouse ears

For whole mount immunostaining of mouse ears, inflammation was initiated and treated in groups as described above. Mice were euthanized 24 hours after IV injection of Cargocyte$^{Tri\text{-}E}$, and ears were shaved, removed at the level of the base, and carefully dissected by peeling the dorsal skin surface from the underlying cartilage. Skin was fixed in 2% PFA on ice for 10 minutes, permeabilized in cold 100% methanol for 10 minutes and blocked in PBS with 20% FBS, 20% NGS (Normal goat serum, Jackson Immuno Research, # 005-000-121) and 0.2% Triton X-100 for 2 hours. The ears were then incubated with dye-conjugated primary antibodies in PBS with 10% FBS, 10% NGS and 0.2% Triton X-100 overnight. After washing in PBS with 0.2% Trion X-100 for at least 2 hours, the ears were post-fixed with 4% PFA and mounted in VECTASHIELD® Vibrance™ Antifade Mounting Medium (Vector Laboratories, # H-1700). Confocal images were taken in an Olympus FV-1000 microscope and maximum projection of Z stacks of fluorescent images were generated in ImageJ Fiji.

4.5.5 Protocols for assessing cytokine delivery in mouse ears

To test human IL-10 cytokine delivery efficiency, MSCs and Cargocytes were transfected with human IL-10 mRNA and IV-injected into the mice treated with LPS as described above. Animals were euthanized after 24 hours, and ears were minced and snap frozen in liquid nitrogen for ELISA analysis (Human IL-10 (Biolegend, #430604)). A separate batch of animals treated in

the same manner were euthanized at 48 hours after LPS injection. Mouse ears were fixed in 4% PFA and submitted to the histology core of Moores Cancer Center for tissue sections and H&E (Haemotoxylin and Eosin) staining, and additional mouse ears were harvested and snap frozen in liquid nitrogen for Real time RT-PCR analysis. The ear thickness was also measured in triplicate with a digital micrometer (Mitutoyo, # 293-831-30) prior to LPS injection and at the time of euthanasia (48 hours post LPS injection), and the change of ear thickness was used to monitor the inflammation status.

4.6 Cargocyte in vivo homing and delivery of an anti-inflammatory cytokine

Mouse ears inflamed with LPS were confirmed to have elevated expression of the chemokines and adhesion ligands (SDF-1α, Ccl2 and P-Selectin, Fig.9b) that correspond to the bioengineered MSC lines I created with chemokine receptors and endothelial adhesion molecules (CXCR4, CCR2, PSGL-1, or all 3 markers). When cells were grown in 3D, their size in suspension was decreased compared to cells grown in 2D, and Cargocytes generated from these 3D-cultured cells were the smallest of all cells and Cargocytes (Fig. 9c). Following 3D culture and IV injection into mice, MSCs expressing at least 1 bioengineered marker each had increased presence in the inflamed ear compared to non-engineered hT-MSCs, while $MSC^{Tri\text{-}E}$ simultaneously expressing all 3 markers were the highest (Fig. 9d). $MSC^{Tri\text{-}E}$ were then used to generate $Cargocyte^{Tri\text{-}E}$, which displayed both superior homing to the inflamed ear (Fig. 9e) and the least amount of trapping in the lungs (Fig. 9f). Importantly, 3D $Cargocyte^{Tri\text{-}E}$ were detected outside of vessel lumina and within ear connective tissue by immunostaining with specific antibodies against human mitochondria and nuclei (Fig. 9g). Animals treated with 3D $Cargocyte^{Tri\text{-}E}$ had the highest amount of IL-10 measured in the inflamed ear compared to the uninflamed ear (Fig. 10a), and the lowest amount produced in the blood (Fig. 10b). This production of IL-10 was correlated with a decrease

in inflammation as seen by less edema and leukocyte infiltrations of the ear (Fig. 10c), and decreased ear thickness and decreased production of the inflammatory cytokines IL-6, IL-1β and TNF-α (Fig. 10d).

4.7 Conclusions from Cargocyte in vivo homing and cytokine delivery

Consistent with previous literature, 3D-culturing of cells resulted in reduced cell size, and further decreased Cargocyte size as a strategy to improve passage through pulmonary vasculature. The MSCs bioengineered with individual chemokine receptors not only had improved chemotaxis in vitro, but each of the single-engineered MSCs had better homing in vivo compared to the non-engineered hT-MSCs. However, $MSC^{Tri\text{-}E}$ demonstrated superior homing, suggesting that the combined expression of all 3 markers allowed for cooperative advantages in homing to the target site for which they were bioengineered. In these experiments, the mouse D1 cell line (ATCC® CRL-12424™), which are BM MSCs originally isolated from BALB/c mice, were used as a syngeneic control for the human hT-MSCs and Cargocytes. Although mouse MSCs are smaller than human, bioengineered Cargocytes still had better homing, suggesting that the combination of size and bioengineering improved the ability of the cells to home to the ear.

Cargocytes did actually reach the inflamed ears more selectively than uninflamed ears, and were able to produce IL-10 at the designated site with a clear biologic effect. This indicates that Cargocytes can be bioengineered to home to diseased tissues in vivo, and deliver therapeutic payloads. This payload delivery was specific, as there was relatively low amounts present in the blood, and higher amounts present in the inflamed ear, likely because these Cargocytes were able to quickly reach the inflamed ear and then deliver the cargo. It is important to note that IL-10 did not completely ablate the inflammation, but rather reduced the total peak of inflammation, which can be expected in complex immunomodulatory diseases in which addition of one cytokine may

not be enough to fully reverse a disease state.

One important finding is that Cargocytes were detected outside of vessel walls, suggesting that they are neither passively trapped in nor leaking from inflamed vessels. While we cannot definitely prove that Cargocytes extravasated from the vasculature, these results are an intriguing indicator that Cargocytes are capable of active migration in 3D. Together, this data shows for the first time that enucleated cells can be extensively bioengineered to specifically home to designated diseased tissue and deliver treatment in vivo following systemic administration.

Chapter 4, in part, has been submitted for publication of the material as it may appear in Nature Biotechnology, H. Wang, C.N. Alarcón, B. Liu, F. Watson, S. Searles, C. Lee, J. Keys, W. Pi, D. Allen, J. Lammerding, J.D. Bui, and R.L. Klemke, 2020. The dissertation author was the co-primary investigator and co-first author of this paper.

Figure 9: Cargocytes bioengineered with chemokine receptors and adhesion molecules have improved homing to sites of inflammation in vivo.

(**a**) Schematic of the workflow for using bioengineered Cargocytes to treat LPS-induced acute ear inflammation in a mouse model. (**b**) Mouse ears were harvested and analyzed by real-time RT-PCR at 6 hours or 24 hours after LPS injection. Graphs show the fold change (Log2) of the indicated mRNA markers in LPS-treated ears at indicated time points and normalized to saline-treated ear (Control). Mean ± SEM, n=3 mice. P values, one-way ANOVA with Tukey's multiple comparisons test. (**c**) Bar graph shows the average diameter of indicated MSCs or Cargocytes in suspension. hT-MSC, MSC cultured on traditional 2D plastic dishes prior to enucleation; D1 MSCs, mouse BM-derived cell line grown on traditional 2D plastic dishes prior to enucleation; 3D hT-MSC, MSCs cultured in 3D as hanging drops prior to enucleation. Mean ± SEM; n=80 individual cells/Cargocytes. P value, two-tailed unpaired t-test. (**d**) Mice were injected with LPS in the right ear and saline in the left, followed 6 hours later by IV injection of DiD-labeled, 3D-cultured MSCs. Bar graphs show the number of $DiD^{+}F4/80^{-}$ cells out of 1E5 total cells harvested from mouse ears 24h post-injection and detected by flow cytometry. All MSCs were cultured as 3D hanging drops prior to injection. MSC, hT-MSC, non-engineered; $3D\text{-}MSC^{Tri\text{-}E\ C19}$, Triple (CXCR4/CCR2/PSGL-1) engineered MSC Clone 19. Mean ± SEM, n=6 mice; each point represents one mouse. P values, one-way ANOVA with Tukey's multiple comparisons test. (**e**) Mice treated as in (**d**) were IV-injected with indicated MSCs or Cargocytes labeled with DiD. Bar graphs show the average numbers of $DiD^{+}F4/80^{-}$ MSCs or Cargocytes out of 1E5 total cell harvested from mouse ears at 24h post injection and detected by flow cytometry. D1 MSC/Cargocyte, mouse D1 2D-cultured MSC/Cargocyte; 3D-MSC/Cargocyte, 3D-cultured hT-MSC/Cargocyte; $3D\text{-}MSC^{Tri\text{-}E\ C19}$, Triple (CXCR4/CCR2/PSGL-1) engineered MSC Clone 19; $3D\text{-}Cargocyte^{Tri\text{-}E\ C19}$, $3D\text{-}MSC^{Tri\text{-}E\ C19}$ derived Cargocyte. Mean ± SEM, n=6 mice; each point represents one mouse. P values, one-way ANOVA with Tukey's multiple comparisons test. (**f**) Mice treated as in (**d**) were IV-injected with $3D\text{-}Cargocyte^{Tri\text{-}E\ C19}$. After 24hr, mouse ears were harvested and whole-mount stained with anti-mouse CD31 (green), anti-human Mitochondrial (red), and anti-human nucleus antigen (blue). Confocal images from Olympus FV1000 were analyzed with Fiji ImageJ. Maximum projection of Z-stacks of images of ears from the same mouse were shown. Arrows point to human Cargocyte, and arrowheads point to human nuclei. Scale bar, 20μm.

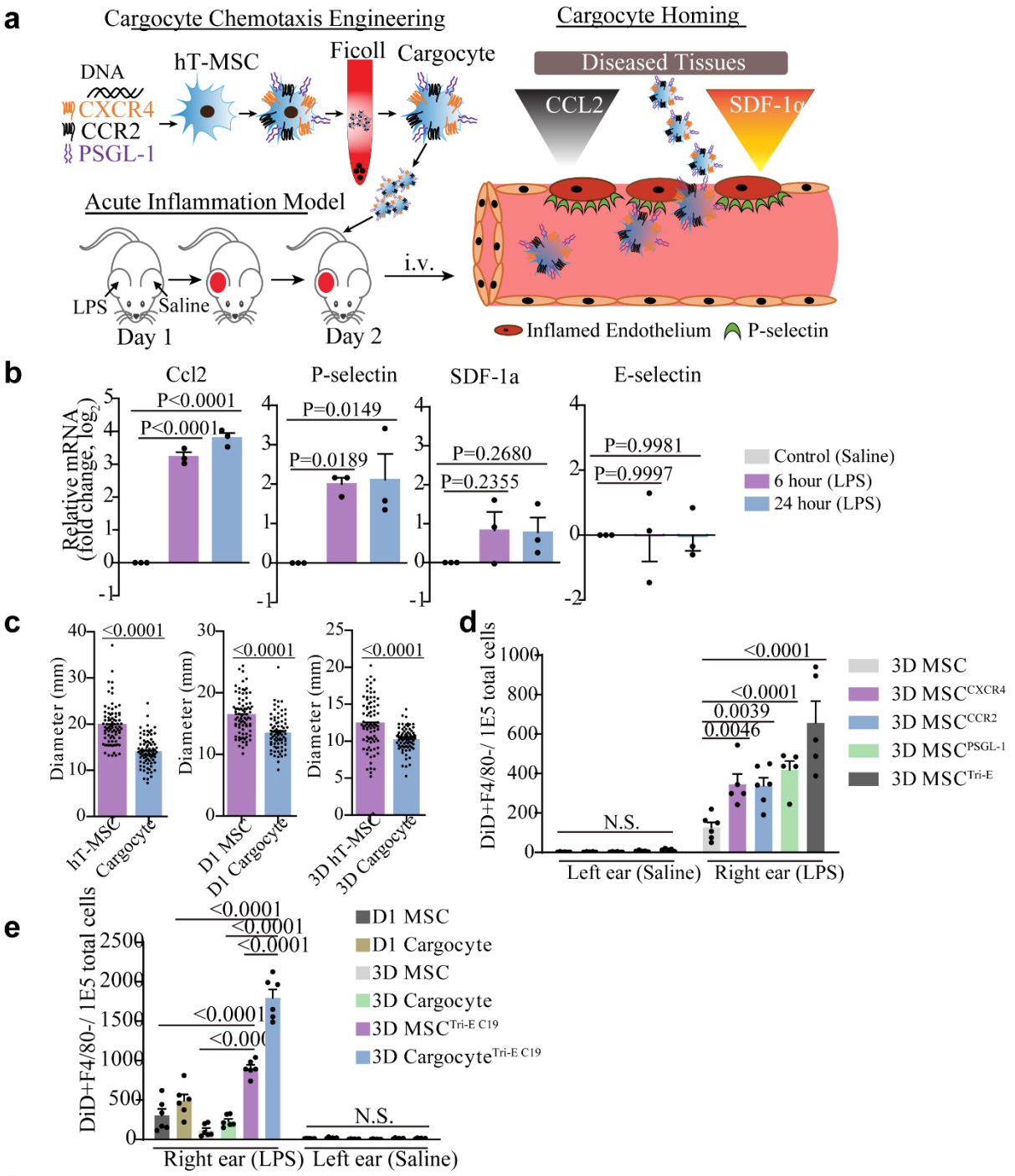
a
Cargocyte Chemotaxis Engineering
Cargocyte Homing
DNA
CXCR4
CCR2
PSGL-1
hT-MSC
Ficoll
Cargocyte
Diseased Tissues
CCL2
SDF-1α
Acute Inflammation Model
LPS
Saline
Day 1
Day 2
i.v.
Inflamed Endothelium
P-selectin
b
Ccl2
P-selectin
SDF-1a
E-selectin
Relative mRNA (fold change, log2)
P<0.0001
P<0.0001
P=0.0149
P=0.0189
P=0.2680
P=0.2355
P=0.9981
P=0.9997
Control (Saline)
6 hour (LPS)
24 hour (LPS)
c
Diameter (mm)
<0.0001
hT-MSC
Cargocyte
D1 MSC
D1 Cargocyte
3D hT-MSC
3D Cargocyte
d
DiD+F4/80-/ 1E5 total cells
<0.0001
<0.0001
0.0039
0.0046
N.S.
3D MSC
3D MSCCXCR4
3D MSCCCR2
3D MSCPSGL-1
3D MSCTri-E
Left ear (Saline)
Right ear (LPS)
e
DiD+F4/80-/ 1E5 total cells
<0.0001
<0.0001
<0.0001
<0.0001
<0.000
N.S.
D1 MSC
D1 Cargocyte
3D MSC
3D Cargocyte
3D MSCTri-E C19
3D CargocyteTri-E C19
Right ear (LPS)
Left ear (Saline)
f
Right ear (LPS)
Left ear (Saline)
CD31
huMito
huNucleus

Figure 10: Bioengineered Cargocytes home to inflamed ears and deliver IL-10 to reduce ear inflammation.

(**a**) Mice treated as in (**9d**) were IV-injected with indicated cells or Cargocytes transfected with human IL-10 mRNA. Bar graph shows the level of human IL-10 protein detected by ELISA from indicated mouse ears at 24hr post-injection. Mean ± SEM, n=6 mice; each point represents 1 mouse. All statistics are one-way two-way ANOVA with Tukey's multiple comparisons test. Adjusted P values shown above the bars. (**b**) Mice were treated as in (**a**). Bar graph shows the concentration of secreted human IL-10 cytokine in the mouse plasma as detected by ELISA. Mean ± SEM; n=6 mice. (**c**) Mice treated as in (**a**) were harvested at 48hr post-injection and processed for hematoxylin and eosin staining. Light microscopy images of representative ears from at least 2 independent experiments shown. (**d**) Mice treated as in (**a**) had ears harvested and analyzed by real-time RT-PCR 48hr after LPS injection. Graphs show the fold change (Log2) of the indicated mRNA markers between LPS-treated (right) and saline-treated (left) ears. All the data are representative for at least 2 independent experiments. Mean ± SEM, n=6 mice; each point represents 1 mouse. All statistics are one-way ANOVA with Tukey's multiple comparisons test. Adjusted P values shown above the bars.

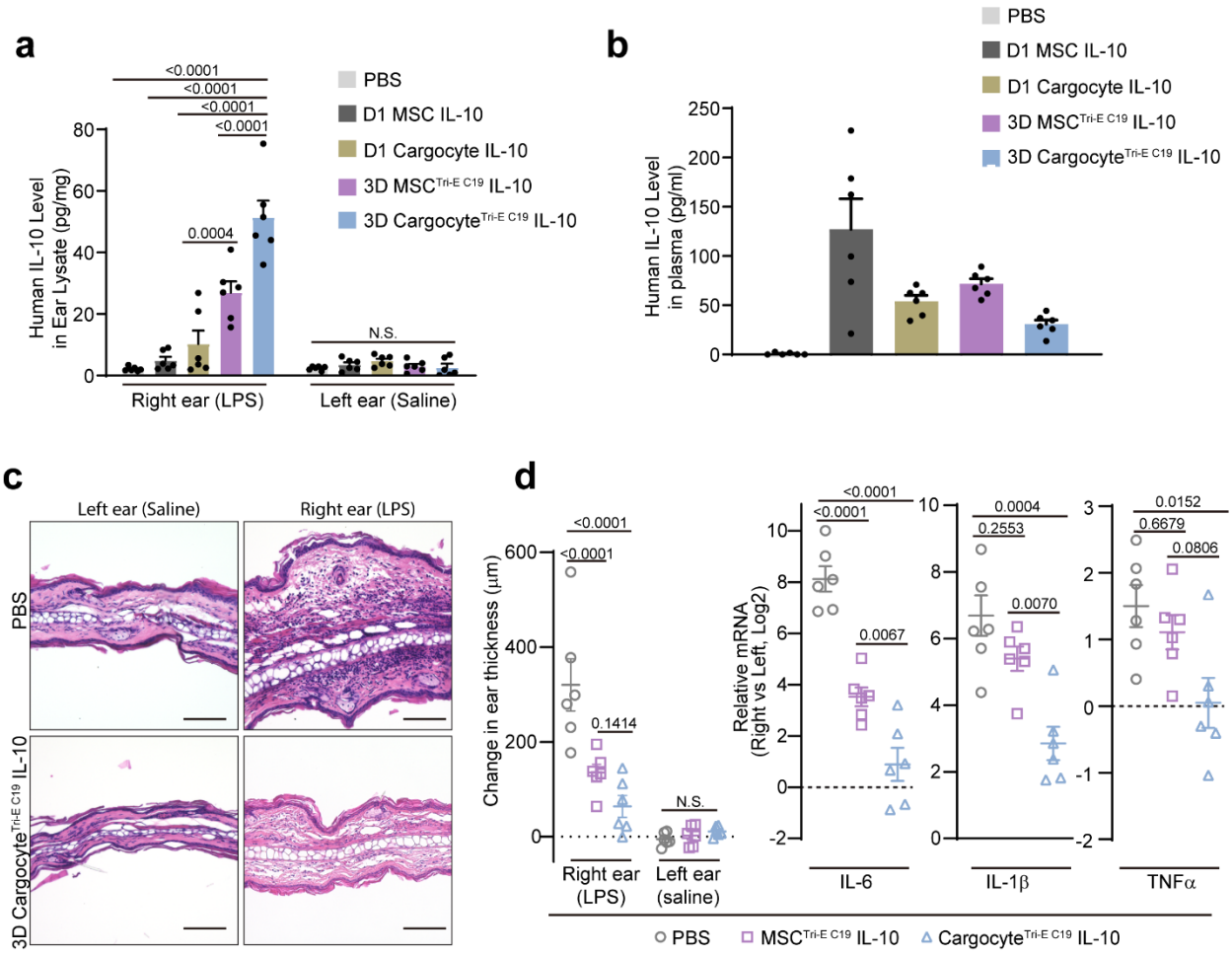
a
b
c
d
PBS
D1 MSC IL-10
D1 Cargocyte IL-10
3D MSC Tri-E C19 IL-10
3D Cargocyte Tri-E C19 IL-10
Human IL-10 Level in Ear Lysate (pg/mg)
Human IL-10 Level in plasma (pg/ml)
Right ear (LPS)
Left ear (Saline)
N.S.
0.0004
Left ear (Saline)
Right ear (LPS)
Change in ear thickness (μm)
Relative mRNA (Right vs Left, Log2)
0.1414
0.0067
0.0070
0.2553
0.6679
0.0806
0.0152
IL-6
IL-1β
TNFα
Right ear (LPS)
Left ear (saline)

Chapter 5 Discussion of Cargocyte findings

5.1 Importance of addressing problems in the cell based therapy field

With the ever-growing promise and potential of cell-based therapies to treat previously untreatable or inaccessible diseases, it is understandably an area of intense clinical research. Great strides have been made in coming to terms with the limitations of the field; namely, that cells are not drugs and therefore do not inherently behave in the same dose-response, controlled manner. Of particular importance is the realization that the protocols for manipulating and handling the cells can have just as much influence on clinical outcome as intrinsic factors of the cell itself. Additionally, as more information becomes available about the behavior of cells in different disease contexts, it becomes more likely to identify patients who would most benefit from cell-based therapies. Despite the awesome opportunities and occasional high-profile successes represented in cell-based therapies, there are still substantial barriers to mainstream clinical applications for a majority of disease. Addressing these barriers is crucial to making progress in the utility of these therapies. Several key obstacles include cell heterogeneity, controllability over in vivo homing and behavior, overall therapeutic efficacy, and patient safety. Bioengineering, and in particular, genetic editing, is positioned to have a high impact in overcoming some of these problems, while concurrently introducing new problems on its own. Ideally, the power of bioengineering could be safely incorporated into enhancing the therapeutic potential of cell-based therapies, although primary cell senescence during ex vivo expansion somewhat limits this possibility. It was this course of thinking that led us to consider the use of bioengineered, enucleated Cargocytes as an alternative approach to traditional cell-based therapies.

5.2 Key features of MSC-derived Cargocytes

In the present study, I enucleated a variety of cell types but focused on development of

enucleated MSCs based on their endogenous therapeutic properties and extensive use in clinical trials. By adapting and optimizing an enucleation protocol for cells in suspension, high numbers of high purity Cargocytes were available for experimental use. Consistent with previous literature documenting enucleated cells' ability to survive for several days, maintain receptors, translate proteins, and migrate, I found that Cargocytes survived for up to 72 hours without a nucleus, produced exogenous proteins from synthesized mRNAs, retained cell surface receptor expression for 48 hours, and migrated in 2D and 3D in vitro.

Based on these properties, I investigated the ability to bioengineer Cargocytes both pre- and post-enucleation with therapeutic functions, such as secretion of cytokines, expression of chemokine receptors, and expression of endothelial adhesion molecules. By validating the in vitro capabilities of the bioengineering to enhance Cargocyte protein production and chemotaxis, I next examined if these functions extrapolated to in vivo performance.

In a mouse TNBC model, intratumoral injection of Cargocytes secreting IL-12 produced detectable IL-12 within the tumor that shifted the leukocyte profile to characteristic antitumor populations, particularly in increased CD8+ T cells and decreased FoxP3+ Tregs. When combined with the PD-1 checkpoint inhibitor, 40% of mice had complete tumor regression and lasting antitumor immunity upon tumor rechallenge. This indicates that Cargocytes effectively produce and deliver bioactive cytokines in a local disease microenvironment. In a mouse ear inflammation model, IV injection of Cargocytes secreting IL-10 were able to home to the site of inflammation and deliver IL-10 that reduced the overall inflammation present. These experiments demonstrated that Cargocytes can be bioengineered to more specifically home to target tissues to produce a therapeutic effect.

Taken together, these studies provide convincing proof-of-concept frameworks for developing

additional bioengineered functions of Cargocytes in other disease models. In particular, the relative ease with which pre-and post-enucleation bioengineering is possible affords the opportunity to reverse-engineer Cargocytes to the tissue of interest, such as the Cargocytes$^{Tri\text{-}E}$ presented here.

5.3 Limitations of the present study

The largest limitation to the current experiments is that Cargocyte purity was ~95% instead of closer to 100%, which raises the possibility that small numbers of bioengineered cells contaminated the population. Since we see the absence of the nucleus as one of the main safety advantages of the Cargocyte platform, 95% is not clinical grade. To improve the absolute purity of Cargocytes, we performed proof-of-concept FACS sorting to remove contaminant nucleated cells and karyoplasts, first with staining by vital dye (Vybrant Dyecycle Green), and also by bioengineering an MSC line with lentiviral induction of GFP production tagged to the histone 2B (H2B MilliporeSigma (#17-10229)), in which production of GFP is only possible in the cell when the nucleus is present. By this method, we were able to generate Cargocytes of 99.999% purity (Fig. 11a) whose viability kinetics (Fig. 11b) were almost identical to the non-sorted Cargocytes used in the majority of the present experiments. Additionally, these sorted Cargocytes had strong migration towards FBS (Fig. 11c), similar to the capabilities of unsorted Cargocytes. Based on these results, I concluded that the observed performance of unsorted Cargocyte at levels either equal to or surpassing nucleated cells cannot be attributed solely to the presence of <5% nucleated cells in the population. It is important that Cargocytes can be reliably sorted to a very high purity for future clinical prototypes.

Another limitation is that the immunogenicity of Cargocytes in vivo was not fully explored. In these experiments, tumor-bearing animals received multiple injections of bioengineered Cargocytes, which always brings up the concern about developing antibodies against a cell

therapy. While this is a valid concern, a full toxicologic investigation into the dosing and immunogenicity of Cargocytes was outside of the scope of this project and the lab's capabilities, and was therefore not performed in the present study. However, animals receiving multiple IT injections of Cargocyte-IL-12 did not show overt clinical signs of adverse events and did not have significant weight changes (Fig. 8d). and preliminary data shows that Cargocytes do not induce significant changes in complete blood count (Table 6) or serum chemistry values (Table 7) between MSC, Cargocyte, and PBS injected animals in the short term. Additionally, mice IV-injected with Cargocytes did not have increased inflammatory markers in plasma at 4 and 24 hours post-injection (Table 8). Finally, in over 300 animals injected IT or IV, no evidence of animal morbidity or mortality was noted by clinical observation or gross examination of tissues. However, further studies are warranted to understand the full immunogenic profile of Cargocytes.

5.4 Unique advantages that Cargocytes provide in cell-based therapies:

The Cargocyte platform is a novel approach to cell-based therapies because it unifies a pre-existing technology (enucleation) with an emerging technology (bioengineering) to circumvent several problems in the field. While descriptions of the biology of enucleated cells have been around for over 40 years, to my knowledge, the potential of artificially enucleated cells that are bioengineered and transplanted for in vivo therapeutic use has not yet been explored.

One of the advantages of the Cargocyte platform is the relative ease in executing various bioengineering strategies at multiple points in the workflow, which allows for Cargocytes to be reverse-engineered and even bioengineered on multiple levels to produce a customized Cargocyte with specifically enhanced functions. One significant advantage is that the lack of a nucleus provides a defined lifespan during which therapies can be delivered in vivo. This means that the timeframe of the therapy can be controlled and better predicted, suggesting that delivery of product

might be more reproducible. Additionally, without the ability to undergo de novo synthesis, Cargocytes should not be reprogrammed in disease microenvironments, compared to the conversion of MSCs to cancer-promoting entities in some studies. I produced Cargocytes from a variety of species and cell origins, and any one of these could be further developed for specific therapeutic use. Although full toxicologic studies have not been performed, theoretically, the absence of DNA both avoids concerns about oncogenesis and reduces the risk of immune responses to modified DNA. Finally, because Cargocytes retain a cell membrane and functional organelles, they have more active cell-like functions compared to other membrane-derived particles like exosomes, extracellular vesicles, nanoghosts, or nanoparticles. In fact, we found that Cargocytes produce membrane particles of a size and morphology consistent with extracellular vesicles (data not shown), which makes them potentially even more useful than exosomes and nanoparticles.

5.5 Potential uses of Cargocytes

As a stand-alone therapy, Cargocytes are most suitable as cell vehicles to home to target tissues for the transient delivery of therapeutic products, such as drugs or biologics. The dosing of the treatment could be modified by pulsed administration or variable administration of different types of Cargocytes. We have begun investigating their ability to propagate and deliver viruses for gene delivery or oncolytic virus therapy (data not shown). While we used lentiviral transduction to create different lines of MSCs, other more current gene-editing technologies like CRISPR-Cas9 and transposons are obviously of interest for specific cellular modifications. Cargocytes may be developed as fusion partners to transfer cellular material to host tissues.

As an adjuvant therapy, I envision that Cargocytes would be most beneficial as a means to prime tissue microenvironments prior to standard-of-care therapies. Modulation and specifically

immunomodulation of the disease microenvironment has huge potential to affect the overall success of the therapy. As seen with the Cargocyte IL-12 + aPD-1 experiments, combination therapies that target a disease from multiple angles are becoming the future of cancer therapies because of cancer's propensity to adapt to or escape immune regulation. In this vein, it must be stated that I do not anticipate that Cargocytes will replace current cell-based therapies, since no one therapy is perfect or can perfectly address the needs and concerns of any given patient or disease.

5.6 Limitations of Cargocytes

Because Cargocytes are not able to truly regenerate or proliferate on their own, they will not be a primary vehicle for cell engraftment in regenerative medicine therapies. Since they survive for 72 hours, they are also not suitable for as therapies which require sustained, continuous release of a product depot. However, I estimate that their transient effects can be prolonged by repeat pulsing with Cargocytes of similar or multiple types of therapeutic products, or by delivery of a product with a long half-life. If a therapy relies on a cell's ability to respond to microenvironmental input, Cargocytes will not be able to perform de novo gene synthesis and will not respond in the immediate context.

5.7 Future Directions

In these proof-of-concept works, Cargocytes were shown to have impressive in vitro and in vivo capabilities, given that they are enucleated cells. However, there are many remaining questions about their basic immunobiology, pharmacodynamics, and applications. For example, the mechanism by which Cargocytes die is unknown, but it likely involves non-nuclear mediated caspase pathways. It is therefore unknown if Cargocyte death produces its own set of antigenic or immunogenic mediators that could influence immunoregulation. We have performed basic

biodistribution studies looking at entrapment of Cargocytes in the lungs; additional biodistribution studies are in progress to further characterize where else in the body they accumulate outside of the target tissue. As mentioned previously, the immunogenicity of Cargocytes may be an important clinical barrier, although the ability to bioengineer Cargocytes may provide a way to work around the specific antigenicity. Examining additional cell types, additional bioengineering strategies, additional disease models, and additional therapeutic agents is also of interest.

Overall, the Cargocyte platform introduces a host of new possibilities to explore in the development of more effective, reliable, and safe cell-based therapies.

Chapter 5, in part, has been submitted for publication of the material as it may appear in Nature Biotechnology, H. Wang, C.N. Alarcón, B. Liu, F. Watson, S. Searles, C. Lee, J. Keys, W. Pi, D. Allen, J. Lammerding, J.D. Bui, and R.L. Klemke, 2020. The dissertation author was the co-primary investigator and co-first author of this paper.

Figure 11: Cargocytes can be sorted to very high purity

(a) Graphs show flow cytometry analyses of $MSC^{H2B\text{-}GFP}$ (H2B-GFP lentivirus-engineered MSC), Non-sorted $Cargocyte^{H2B\text{-}GFP}$ ($Cargocyte^{H2B\text{-}GFP}$ before FACS sorting) and Sorted $Cargocyte^{H2B\text{-}GFP}$ ($Cargocyte^{H2B\text{-}GFP}$ after FACS sorting) **(b)** Graphs show the percentage of viable MSCs or Cargocytes versus initial population over time. Sorted MSC Control, FACS sorted $MSC^{H2B\text{-}GFP}$; Cargocytes and Karyoplast/MSC were separated from enucleated $MSC^{H2B\text{-}GFP}$ based on GFP expression. Mean ± SEM; n=6 biological replicates. **(c)** MSCs $^{H2B\text{-}GFP}$ or sorted Cargocytes $^{H2B\text{-}GFP}$ migrated in Boyden chambers towards FBS gradients. Bar graph represents the ratio of migrated MSCs or Cargocytes versus loading control. Mean ± SEM; n=15 independent fields from 5 biological replicates. P value, two-way ANOVA with Tukey's multiple comparisons test. All data were representative for 2 independent experiments.

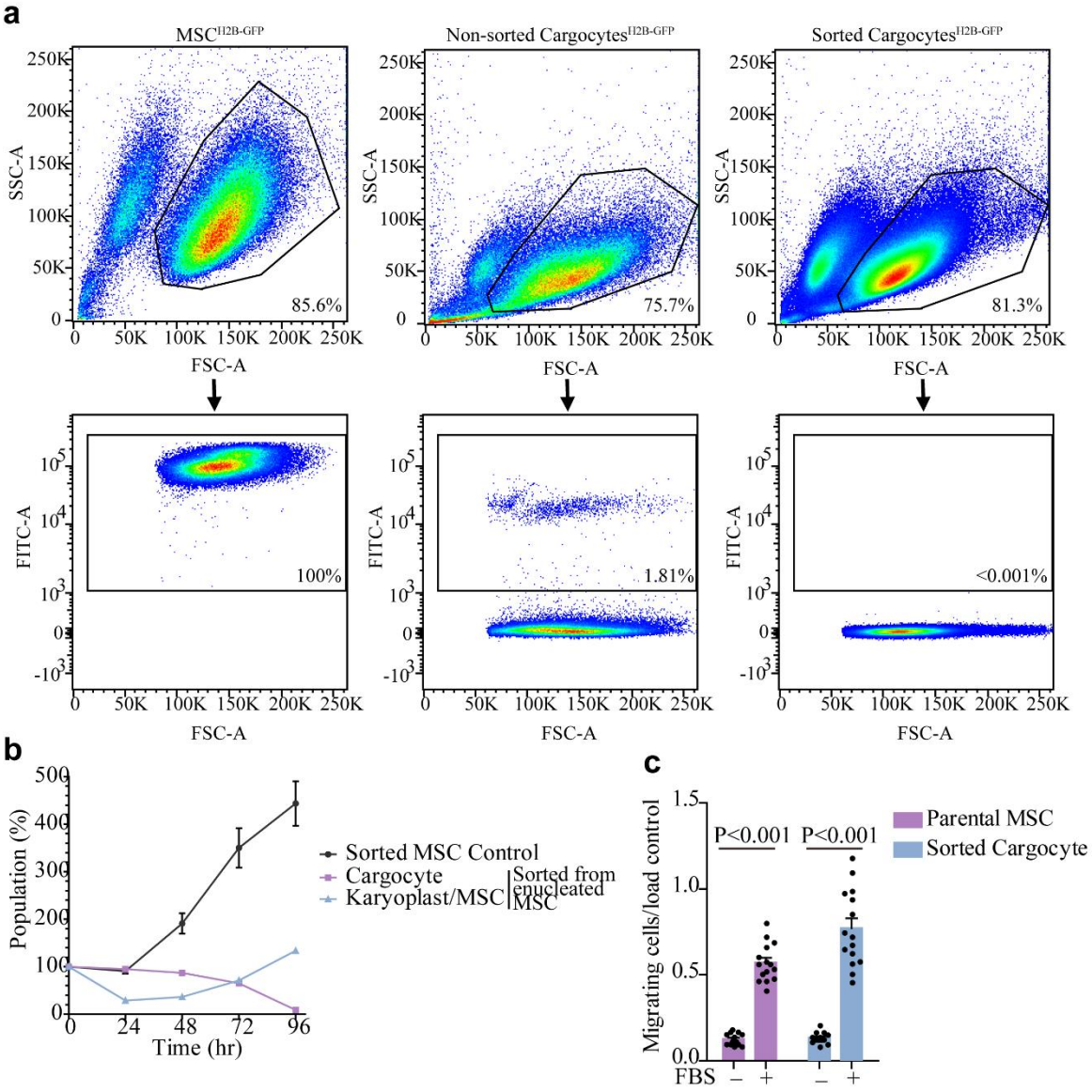
a
MSC^H2B-GFP
Non-sorted Cargocytes^H2B-GFP
Sorted Cargocytes^H2B-GFP
SSC-A
FSC-A
85.6%
75.7%
81.3%
FITC-A
100%
1.81%
<0.001%
b
Population (%)
Time (hr)
Sorted MSC Control
Cargocyte
Karyoplast/MSC
Sorted from enucleated MSC
c
Migrating cells/load control
P<0.001
P<0.001
Parental MSC
Sorted Cargocyte
FBS

Table 8. Plasma cytokine concentrations (pg/ml) in mice after IV injection of MSCs or Cargocytes. Cytokine concentrations in mouse (BalB/c) plasma were measured at 4 hours or 24 hours after IV injection of MSCs or Cargocytes (1E6 cells per mouse). Mean ± SEM, n=3 mice in each group. ***, P<0.001, One-way ANOVA with Tukey's multiple comparisons test. Zero value = undetectable level.

Time point	Cytokine (Pg/ml)	Cargocyte	MSC	PBS	Un-injected
4 hours	IL-1β	2.083 (±2.083)	5.208 (±2.756)	0	0
	TNFα	0	0	0	0
	IL-6	10.949 (±5.380)	48.565 (±6.101)***	0	0
	IFNγ	0	0	0	0
24 hours	IL-1β	0	0	0	0
	TNFα	0	0	0	0
	IL-6	0	33.02 (±21.55)	0	0
	IFNγ	0	0	0	0

References

1. Cytonus Therapeutics Inc. "Cytonus Therapeutics." https://cytonus.com/.
2. Stambler, I. The unexpected outcomes of anti-aging, rejuvenation, and life extension studies: an origin of modern therapies. *Rejuvenation Res* **17**, 297-305 (2014).
3. Henig, I. & Zuckerman, T. Hematopoietic stem cell transplantation-50 years of evolution and future perspectives. *Rambam Maimonides Med J* **5**, e0028-e0028 (2014).
4. Heathman, T.R., Nienow, A.W., McCall, M.J., Coopman, K., Kara, B. & Hewitt, C.J. The translation of cell-based therapies: clinical landscape and manufacturing challenges. *Regen Med* **10**, 49-64 (2015).
5. Mason, C., Brindley, D.A., Culme-Seymour, E.J. & Davie, N.L. Cell therapy industry: billion dollar global business with unlimited potential. *Regen Med* **6**, 265-272 (2011).
6. Ruprecht, V., Monzo, P., Ravasio, A., Yue, Z., Makhija, E., Strale, P.O., Gauthier, N., Shivashankar, G.V., Studer, V., Albiges-Rizo, C. & Viasnoff, V. How cells respond to environmental cues – insights from bio-functionalized substrates. *Journal of Cell Science* **130**, 51 (2017).
7. Fischbach, M.A., Bluestone, J.A. & Lim, W.A. Cell-based therapeutics: the next pillar of medicine. *Sci Transl Med* **5**, 179ps177 (2013).
8. ClinicalTrials.gov. "ClinicalTrials.gov." https://clinicaltrials.gov/ct2/results/details?cond=&term=%22cell+therapy%22&cntry=&state=&city=&dist=&Search=Search.
9. Golchin, A. & Farahany, T.Z. Biological Products: Cellular Therapy and FDA Approved Products. *Stem Cell Rev Rep* **15**, 166-175 (2019).
10. U.S. Food and Drug Administration Office of Tissue and Advanced Therapies. "Approved Cellular and Gene Therapy Products." 12/26/19. https://www.fda.gov/vaccines-blood-biologics/cellular-gene-therapy-products/approved-cellular-and-gene-therapy-products.
11. Silverman, L.I., Flanagan, F., Rodriguez-Granrose, D., Simpson, K., Saxon, L.H. & Foley, K.T. Identifying and Managing Sources of Variability in Cell Therapy Manufacturing and Clinical Trials. *Regenerative Engineering and Translational Medicine* **5**, 354-361 (2019).
12. Lynch, M.D. & Watt, F.M. Fibroblast heterogeneity: implications for human disease. *The Journal of Clinical Investigation* **128**, 26-35 (2018).
13. Altschuler, S.J. & Wu, L.F. Cellular Heterogeneity: Do Differences Make a Difference? *Cell* **141**, 559-563 (2010).
14. Cazaux, M., Grandjean, C.L., Lemaître, F., Garcia, Z., Beck, R.J., Milo, I., Postat, J., Beltman, J.B., Cheadle, E.J. & Bousso, P. Single-cell imaging of CAR T cell activity in vivo reveals extensive functional and anatomical heterogeneity. *The Journal of Experimental Medicine* **216**, 1038-1049 (2019).

15. Di Carlo, D. Technologies for the Directed Evolution of Cell Therapies. *SLAS Technol* **24**, 359-372 (2019).

16. Brenner, M.J., Cho, J.H., Wong, N.M.L. & Wong, W.W. Synthetic Biology: Immunotherapy by Design. *Annual Review of Biomedical Engineering* **20**, 95-118 (2018).

17. Saudemont, A., Jespers, L. & Clay, T. Current Status of Gene Engineering Cell Therapeutics. *Frontiers in Immunology* **9**, 153 (2018).

18. Themeli, M., Riviere, I. & Sadelain, M. New cell sources for T cell engineering and adoptive immunotherapy. *Cell Stem Cell* **16**, 357-366 (2015).

19. Sarkar, D., Spencer, J.A., Phillips, J.A., Zhao, W., Schafer, S., Spelke, D.P., Mortensen, L.J., Ruiz, J.P., Vemula, P.K., Sridharan, R., Kumar, S., Karnik, R., Lin, C.P. & Karp, J.M. Engineered cell homing. *Blood* **118**, e184-e191 (2011).

20. Guo, X.R., Yang, Z.S., Tang, X.J., Zou, D.D., Gui, H., Wang, X.L., Ma, S.N., Yuan, Y.H., Fang, J., Wang, B., Zhang, L., Sun, X.Y., Warnock, G.L., Dai, L.J. & Tu, H.J. The application of mRNA-based gene transfer in mesenchymal stem cell-mediated cytotoxicity of glioma cells. *Oncotarget* **7**, 55529-55542 (2016).

21. Lee, A.S., Tang, C., Rao, M.S., Weissman, I.L. & Wu, J.C. Tumorigenicity as a clinical hurdle for pluripotent stem cell therapies. *Nature medicine* **19**, 998-1004 (2013).

22. Herberts, C.A., Kwa, M.S.G. & Hermsen, H.P.H. Risk factors in the development of stem cell therapy. *J Transl Med* **9**, 29-29 (2011).

23. Zakrzewski, W., Dobrzyński, M., Szymonowicz, M. & Rybak, Z. Stem cells: past, present, and future. *Stem Cell Research & Therapy* **10**, 68 (2019).

24. U.S. Food and Drug Administration. "FDA Warns About Stem Cell Therapies." 12-28-19. https://www.fda.gov/consumers/consumer-updates/fda-warns-about-stem-cell-therapies.

25. Paludan, S.R. Activation and Regulation of DNA-Driven Immune Responses. *Microbiology and Molecular Biology Reviews* **79**, 225 (2015).

26. Atianand, M.K. & Fitzgerald, K.A. Molecular Basis of DNA Recognition in the Immune System. *The Journal of Immunology* **190**, 1911 (2013).

27. Deacon, D.H., Hogan, K.T., Swanson, E.M., Chianese-Bullock, K.A., Denlinger, C.E., Czarkowski, A.R., Schrecengost, R.S., Patterson, J.W., Teague, M.W. & Slingluff, C.L. The use of gamma-irradiation and ultraviolet-irradiation in the preparation of human melanoma cells for use in autologous whole-cell vaccines. *BMC Cancer* **8**, 360 (2008).

28. Inui, S., Minami, K., Ito, E., Imaizumi, H., Mori, S., Koizumi, M., Fukushima, S., Miyagawa, S., Sawa, Y. & Matsuura, N. Irradiation strongly reduces tumorigenesis of human induced pluripotent stem cells. *Journal of Radiation Research* **58**, 430-438 (2017).

29. Yu, S., Yi, M., Qin, S. & Wu, K. Next generation chimeric antigen receptor T cells: safety strategies to overcome toxicity. *Mol Cancer* **18**, 125-125 (2019).

30. Jones, B.S., Lamb, L.S., Goldman, F. & Di Stasi, A. Improving the safety of cell therapy products by suicide gene transfer. *Frontiers in Pharmacology* **5**, 254 (2014).

31. Smith, J. & Valton, J. A universal suicide switch for chimeric antigen receptor T cell adoptive therapies. *Journal of Clinical Oncology* **34**, 7039-7039 (2016).

32. MacCorkle, R.A., Freeman, K.W. & Spencer, D.M. Synthetic activation of caspases: Artificial death switches. *Proceedings of the National Academy of Sciences* **95**, 3655 (1998).

33. Fedoročko, P., Egyed, A. & Vacek, A. Irradiation induces increased production of haemopoietic and proinflammatory cytokines in the mouse lung. *International Journal of Radiation Biology* **78**, 305-313 (2002).

34. Cao, F., Drukker, M., Lin, S., Sheikh, A.Y., Xie, X., Li, Z., Connolly, A.J., Weissman, I.L. & Wu, J.C. Molecular Imaging of Embryonic Stem Cell Misbehavior and Suicide Gene Ablation. *Cloning and Stem Cells* **9**, 107-117 (2007).

35. Li, G.P., White, K.L. & Bunch, T.D. Review of enucleation methods and procedures used in animal cloning: state of the art. *Cloning Stem Cells* **6**, 5-13 (2004).

36. Carter, S.B. Effects of cytochalasins on mammalian cells. *Nature* **213**, 261-264 (1967).

37. Ladda, R.L. & Estensen, R.D. Introduction of a heterologous nucleus into enucleated cytoplasms of cultured mouse L-cells. *Proc Natl Acad Sci U S A* **67**, 1528-1533 (1970).

38. Poste, G. Anucleate mammalian cells: applications in cell biology and virology. *Methods Cell Biol* **7**, 211-249 (1973).

39. Prescott, D.M., Myerson, D. & Wallace, J. Enucleation of mammalian cells with cytochalasin B. *Exp Cell Res* **71**, 480-485 (1972).

40. Prescott, D.M. & Kirkpatrick, J.B. Mass enucleation of cultured animal cells. *Methods Cell Biol* **7**, 189-202 (1973).

41. Wright, W.E. The production of mass populations of anucleate cytoplasms. *Methods Cell Biol* **7**, 203-210 (1973).

42. Ege, T., Hamberg, H., Krondahl, U., Ericsson, J. & Ringertz, N.R. Characterization of minicells (nuclei) obtained by cytochalasin enucleation. *Exp Cell Res* **87**, 365-377 (1974).

43. Ege, T. & Ringertz, N.R. Preparation of microcells by enucleation of micronucleate cells. *Exp Cell Res* **87**, 378-382 (1974).

44. Follett, E.A. A convenient method for enucleating cells in quantity. *Exp Cell Res* **84**, 72-78 (1974).

45. Miller, R.A. & Ruddle, F.H. Enucleated neuroblastoma cells form neurites when treated with dibutyryl cyclic AMP. *J Cell Biol* **63**, 295-299 (1974).

46. Sethi, K.K. & Brandis, H. Protection of mice from malignant tumor implants by enucleated tumor cells. *J Natl Cancer Inst* **53**, 1175-1176 (1974).

47. Sethi, K.K. & Brandis, H. Introduction of mouse L cell nucleus into heterologous mammalian cells. *Nature* **250**, 225-226 (1974).

48. Veomett, G., Prescott, D.M., Shay, J. & Porter, K.R. Reconstruction of mammalian cells from nuclear and cytoplasmic components separated by treatment with cytochalasin B. *Proc Natl Acad Sci U S A* **71**, 1999-2002 (1974).

49. Lucas, J.J. & Kates, J.R. The construction of viable nuclear-cytoplasmic hybrid cells by nuclear transplantation. *Cell* **7**, 397-405 (1976).

50. Veomett, G., Shay, J., Hough, P.V. & Prescott, D.M. Large-scale enucleation of mammalian cells. *Methods Cell Biol* **13**, 1-6 (1976).

51. Wright, W.E. & Hayflick, L. Formation of anucleate and multinucleate cells in normal and SV 40 transformed WI-38 by cytochalasin B. *Exp Cell Res* **74**, 187-194 (1972).

52. Croce, C.M. & Koprowski, H. Enucleation of cells made simple and rescue of SV40 by enucleated cells made even simpler. *Virology* **51**, 227-229 (1973).

53. Goldman, R.D., Pollack, R. & Hopkins, N.H. Preservation of normal behavior by enucleated cells in culture. *Proc Natl Acad Sci U S A* **70**, 750-754 (1973).

54. Pollack, R. & Goldman, R. Synthesis of infective poliovirus in BSC-1 monkey cells enucleated with cytochalasin B. *Science* **179**, 915-916 (1973).

55. Schroder, C.H. & Hsie, A.W. Morphological transformation of enucleated Chinese hamster ovary cells by dibutyryl adenosine 3',5'-monophosphate and hormones. *Nat New Biol* **246**, 58-60 (1973).

56. Wise, G.E. & Prescott, D.M. Ultrastructure of enucleated mammalian cells in culture. *Exp Cell Res* **81**, 63-72 (1973).

57. Ege, T., Krondahl, U. & Ringertz, N.R. Introduction of nuclei and micronuclei into cells and enucleated cytoplasms by Sendai virus induced fusion. *Exp Cell Res* **88**, 428-432 (1974).

58. Goldman, R.D. & Pollack, R. Uses of enucleated cells. *Methods Cell Biol* **8**, 123-143 (1974).

59. Pollack, R., Goldman, R.D., Conlon, S. & Chang, C. Properties of enucleated cells. II. Characteristic overlapping of transformed cells is reestablished by enucleates. *Cell* **3**, 51-54 (1974).

60. Shay, J.W., Porter, K.R. & Prescott, D.M. The surface morphology and fine structure of CHO (Chinese hamster ovary) cells following enucleation. *Proc Natl Acad Sci U S A* **71**, 3059-3063 (1974).

61. Goldman, R.D., Pollack, R., Chang, C.M. & Bushnell, A. Properties of enucleated cells. III. Changes in cytoplasmic architecture of enucleated BHK21 cells following trypsinization and replating. *Exp Cell Res* **93**, 175-183 (1975).

62. Shay, J.W., Gershenbaum, M.R. & Porter, K.R. Enucleation of CHO cells by means of cytochalasin B and centrifugation: the topography of enucleation. *Exp Cell Res* **94**, 47-55 (1975).

63. Wigler, M.H. & Weinstein, I.B. A preparative method for obtaining enucleated mammalian cells. *Biochem Biophys Res Commun* **63**, 669-674 (1975).

64. GE Healthcare in Cell Preparation, Data File 18-1158-27 AB Edn. 2/2007 (General Electric Company, 2007).

65. Rickwood, D. in Centrifugal Separations in Molecular and Cell Biology. (eds. G.D. Birnie & D. Rickwood) 219-250 (Butterworth-Heinemann, 1978).

66. Siroky, J. Comparison of the coverslip and the discontinuous Percoll density gradient methods of enucleation of mouse cells. *General physiology and biophysics* **3**, 119-126 (1984).

67. Bossart, W., Loeffler, H. & Bienz, K. Enucleation of cells by density gradient centrifugation. *Exp Cell Res* **96**, 360-366 (1975).

68. Wigler, M.H., Neugut, A.I. & Weinstein, I.B. Enucleation of mammalian cells in suspension. *Methods Cell Biol* **14**, 87-93 (1976).

69. Bruno, J. & Lucas, J.J. Polypeptide synthesis in enucleated mouse fibroblasts. *Cell Biol Int Rep* **7**, 651-659 (1983).

70. Ber, R., Fenyo, E.M. & Klein, G. Cell surface antigen expression in cytoplasts and karyoplasts of mouse L cells. *Cancer Lett* **5**, 69-73 (1978).

71. Graham, D.M., Andersen, T., Sharek, L., Uzer, G., Rothenberg, K., Hoffman, B.D., Rubin, J., Balland, M., Bear, J.E. & Burridge, K. Enucleated cells reveal differential roles of the nucleus in cell migration, polarity, and mechanotransduction. *J Cell Biol* **217**, 895-914 (2018).

72. Follett, E.A., Pringle, C.R., Wunner, W.H. & Skehel, J.J. Virus replication in enucleate cells: vesicular stomatitis virus and influenza virus. *J Virol* **13**, 394-399 (1974).

73. Yamamoto, D., Coimbra, V.C., Okuda, K. & Rabinovitch, M. Enucleated L929 mouse fibroblasts support invasion and multiplication of Shigella flexneri 5a. *Braz J Med Biol Res* **39**, 749-758 (2006).

74. Wilkins, H.M., Carl, S.M. & Swerdlow, R.H. Cytoplasmic hybrid (cybrid) cell lines as a practical model for mitochondriopathies. *Redox Biol* **2**, 619-631 (2014).

75. Malawista, S.E. & De Boisfleury Chevance, A. The cytokineplast: purified, stable, and functional motile machinery from human blood polymorphonuclear leukocytes. *J Cell Biol* **95**, 960-973 (1982).

76. Keller, H.U. & Bessis, M. Chemotaxis and phagocytosis in anucleated cytoplasmic fragments of human peripheral blood leucocytes. *Nouv Rev Fr Hematol* **15**, 439-446 (1975).

77. Keller, H.U. & Bessis, M. Migration and chemotaxis of anucleate cytoplasmic leukocyte fragments. *Nature* **258**, 723-724 (1975).

78. Malawista, S.E., Montgomery, R.R. & Van Blaricom, G. Microbial killing by human neutrophil cytokineplasts: similar suppressive effects of reversible and irreversible inhibitors of nitric oxide synthase. *J Leukoc Biol* **60**, 753-757 (1996).

79. Shay, J.W. Cell enucleation, cybrids, reconstituted cells, and nuclear hybrids. *Methods Enzymol* **151**, 221-237 (1987).

80. Poste, G. & Reeve, P. Enucleation of mammalian cells by cytochalasin B. II. Formation of hybrid cells and heterokaryons by fusion of anucleate and nucleated cells. *Exp Cell Res* **73**, 287-294 (1972).

81. G, R., RD, C. & TE, H. Cytoplasts as therapy for experimental neonatal sepsis. *Clinical Research* **33**, A418 (1985).

82. Caplan, A.I. Mesenchymal stem cells. *Journal of orthopaedic research : official publication of the Orthopaedic Research Society* **9**, 641-650 (1991).

83. Friedenstein, A.J., Chailakhjan, R.K. & Lalykina, K.S. The development of fibroblast colonies in monolayer cultures of guinea-pig bone marrow and spleen cells. *Cell and tissue kinetics* **3**, 393-403 (1970).

84. Charbord, P. Bone marrow mesenchymal stem cells: historical overview and concepts. *Hum Gene Ther* **21**, 1045-1056 (2010).

85. Gadkari, R., Zhao, L., Teklemariam, T. & Hantash, B.M. Human embryonic stem cell derived-mesenchymal stem cells: an alternative mesenchymal stem cell source for regenerative medicine therapy. *Regen Med* **9**, 453-465 (2014).

86. da Silva Meirelles, L., Chagastelles, P.C. & Nardi, N.B. Mesenchymal stem cells reside in virtually all post-natal organs and tissues. *J Cell Sci* **119**, 2204-2213 (2006).

87. Lv, F.J., Tuan, R.S., Cheung, K.M. & Leung, V.Y. Concise review: the surface markers and identity of human mesenchymal stem cells. *Stem Cells* **32**, 1408-1419 (2014).

88. Crisan, M., Yap, S., Casteilla, L., Chen, C.W., Corselli, M., Park, T.S., Andriolo, G., Sun, B., Zheng, B., Zhang, L., Norotte, C., Teng, P.N., Traas, J., Schugar, R., Deasy, B.M., Badylak, S., Buhring, H.J., Giacobino, J.P., Lazzari, L., Huard, J. & Peault, B. A perivascular origin for mesenchymal stem cells in multiple human organs. *Cell Stem Cell* **3**, 301-313 (2008).

89. de Souza, L.E., Malta, T.M., Kashima Haddad, S. & Covas, D.T. Mesenchymal Stem Cells and Pericytes: To What Extent Are They Related? *Stem Cells Dev* **25**, 1843-1852 (2016).

90. Dominici, M., Le Blanc, K., Mueller, I., Slaper-Cortenbach, I., Marini, F., Krause, D., Deans, R., Keating, A., Prockop, D. & Horwitz, E. Minimal criteria for defining multipotent mesenchymal stromal cells. The International Society for Cellular Therapy position statement. *Cytotherapy* **8**, 315-317 (2006).

91. Lee, D.K. & Song, S.U. Immunomodulatory mechanisms of mesenchymal stem cells and their therapeutic applications. *Cell Immunol* **326**, 68-76 (2018).

92. Kyurkchiev, D., Bochev, I., Ivanova-Todorova, E., Mourdjeva, M., Oreshkova, T., Belemezova, K. & Kyurkchiev, S. Secretion of immunoregulatory cytokines by mesenchymal stem cells. *World J Stem Cells* **6**, 552-570 (2014).

93. Choi, J.R., Yong, K.W. & Nam, H.Y. Current Status and Perspectives of Human Mesenchymal Stem Cell Therapy. *Stem Cells Int* **2019**, 4762634 (2019).

94. Caplan, A.I. Mesenchymal Stem Cells: Time to Change the Name! *Stem Cells Transl Med* **6**, 1445-1451 (2017).

95. Ankrum, J.A., Ong, J.F. & Karp, J.M. Mesenchymal stem cells: immune evasive, not immune privileged. *Nat Biotechnol* **32**, 252-260 (2014).

96. Yong, K.W., Safwani, W.K.Z.W., Xu, F., Zhang, X., Choi, J.R., Abas, W.A.B.W., Omar, S.Z., Azmi, M.A.N., Chua, K.H. & Pingguan-Murphy, B. Assessment of tumourigenic potential in long-term cryopreserved human adipose-derived stem cells. *Journal of Tissue Engineering and Regenerative Medicine* **11**, 2217-2226 (2017).

97. Gruenloh, W., Kambal, A., Sondergaard, C., McGee, J., Nacey, C., Kalomoiris, S., Pepper, K., Olson, S., Fierro, F. & Nolta, J.A. Characterization and in vivo testing of mesenchymal stem cells derived from human embryonic stem cells. *Tissue engineering. Part A* **17**, 1517-1525 (2011).

98. Lopez-Iglesias, P., Blazquez-Martinez, A., Fernandez-Delgado, J., Regadera, J., Nistal, M. & Miguel, M.P. Short and long term fate of human AMSC subcutaneously injected in mice. *World J Stem Cells* **3**, 53-62 (2011).

99. Kusuma, G.D., Carthew, J., Lim, R. & Frith, J.E. Effect of the Microenvironment on Mesenchymal Stem Cell Paracrine Signaling: Opportunities to Engineer the Therapeutic Effect. *Stem Cells Dev* **26**, 617-631 (2017).

100. Gnecchi, M., Danieli, P., Malpasso, G. & Ciuffreda, M.C. Paracrine Mechanisms of Mesenchymal Stem Cells in Tissue Repair. *Methods Mol Biol* **1416**, 123-146 (2016).

101. Wilson, A., Hodgson-Garms, M., Frith, J.E. & Genever, P. Multiplicity of Mesenchymal Stromal Cells: Finding the Right Route to Therapy. *Frontiers in Immunology* **10**, 1112 (2019).

102. McLeod, C.M. & Mauck, R.L. On the origin and impact of mesenchymal stem cell heterogeneity: new insights and emerging tools for single cell analysis. *European cells & materials* **34**, 217-231 (2017).

103. Katsara, O., Mahaira, L.G., Iliopoulou, E.G., Moustaki, A., Antsaklis, A., Loutradis, D., Stefanidis, K., Baxevanis, C.N., Papamichail, M. & Perez, S.A. Effects of donor age, gender, and in vitro cellular aging on the phenotypic, functional, and molecular characteristics of mouse bone marrow-derived mesenchymal stem cells. *Stem Cells Dev* **20**, 1549-1561 (2011).

104. Phinney, D.G., Kopen, G., Righter, W., Webster, S., Tremain, N. & Prockop, D.J. Donor variation in the growth properties and osteogenic potential of human marrow stromal cells. *Journal of Cellular Biochemistry* **75**, 424-436 (1999).

105. Russell, A.L., Lefavor, R., Durand, N., Glover, L. & Zubair, A.C. Modifiers of mesenchymal stem cell quantity and quality. *Transfusion* **58**, 1434-1440 (2018).

106. Banfi, A., Muraglia, A., Dozin, B., Mastrogiacomo, M., Cancedda, R. & Quarto, R. Proliferation kinetics and differentiation potential of ex vivo expanded human bone marrow stromal cells: Implications for their use in cell therapy. *Experimental hematology* **28**, 707-715 (2000).

107. Roobrouck, V.D., Ulloa-Montoya, F. & Verfaillie, C.M. Self-renewal and differentiation capacity of young and aged stem cells. *Experimental Cell Research* **314**, 1937-1944 (2008).

108. Stenderup, K., Justesen, J., Clausen, C. & Kassem, M. Aging is associated with decreased maximal life span and accelerated senescence of bone marrow stromal cells. *Bone* **33**, 919-926 (2003).

109. Siddappa, R., Licht, R., van Blitterswijk, C. & de Boer, J. Donor variation and loss of multipotency during in vitro expansion of human mesenchymal stem cells for bone tissue engineering. *Journal of orthopaedic research : official publication of the Orthopaedic Research Society* **25**, 1029-1041 (2007).

110. Siegel, G., Kluba, T., Hermanutz-Klein, U., Bieback, K., Northoff, H. & Schafer, R. Phenotype, donor age and gender affect function of human bone marrow-derived mesenchymal stromal cells. *BMC Med* **11**, 146 (2013).

111. James, S., Fox, J., Afsari, F., Lee, J., Clough, S., Knight, C., Ashmore, J., Ashton, P., Preham, O., Hoogduijn, M., Ponzoni, R.D.A.R., Hancock, Y., Coles, M. & Genever, P. Multiparameter Analysis of Human Bone Marrow Stromal Cells Identifies Distinct Immunomodulatory and Differentiation-Competent Subtypes. *Stem Cell Reports* **4**, 1004-1015 (2015).

112. Rennerfeldt, D.A., Raminhos, J.S., Leff, S.M., Manning, P. & Van Vliet, K.J. Emergent heterogeneity in putative mesenchymal stem cell colonies: Single-cell time lapsed analysis. *PLoS One* **14**, e0213452 (2019).

113. O'Connor, K.C. Molecular Profiles of Cell-to-Cell Variation in the Regenerative Potential of Mesenchymal Stromal Cells. *Stem Cells Int* **2019**, 5924878 (2019).

114. Kern, S., Eichler, H., Stoeve, J., Klüter, H. & Bieback, K. Comparative Analysis of Mesenchymal Stem Cells from Bone Marrow, Umbilical Cord Blood, or Adipose Tissue. *STEM CELLS* **24**, 1294-1301 (2006).

115. Strioga, M., Viswanathan, S., Darinskas, A., Slaby, O. & Michalek, J. Same or Not the Same? Comparison of Adipose Tissue-Derived Versus Bone Marrow-Derived Mesenchymal Stem and Stromal Cells. *Stem Cells and Development* **21**, 2724-2752 (2012).

116. Mattar, P. & Bieback, K. Comparing the Immunomodulatory Properties of Bone Marrow, Adipose Tissue, and Birth-Associated Tissue Mesenchymal Stromal Cells. *Frontiers in Immunology* **6**, 560 (2015).

117. Mohamed-Ahmed, S., Fristad, I., Lie, S.A., Suliman, S., Mustafa, K., Vindenes, H. & Idris, S.B. Adipose-derived and bone marrow mesenchymal stem cells: a donor-matched comparison. *Stem Cell Research & Therapy* **9**, 168 (2018).

118. Schellenberg, A., Stiehl, T., Horn, P., Joussen, S., Pallua, N., Ho, A.D. & Wagner, W. Population dynamics of mesenchymal stromal cells during culture expansion. *Cytotherapy* **14**, 401-411 (2012).

119. Selich, A., Daudert, J., Hass, R., Philipp, F., von Kaisenberg, C., Paul, G., Cornils, K., Fehse, B., Rittinghausen, S., Schambach, A. & Rothe, M. Massive Clonal Selection and Transiently Contributing Clones During Expansion of Mesenchymal Stem Cell Cultures

Revealed by Lentiviral RGB-Barcode Technology. *STEM CELLS Translational Medicine* **5**, 591-601 (2016).

120. Yang, Y.-H.K., Ogando, C.R., Wang See, C., Chang, T.-Y. & Barabino, G.A. Changes in phenotype and differentiation potential of human mesenchymal stem cells aging in vitro. *Stem Cell Research & Therapy* **9**, 131 (2018).

121. Whitfield, M.J., Lee, W.C.J. & Van Vliet, K.J. Onset of heterogeneity in culture-expanded bone marrow stromal cells. *Stem Cell Research* **11**, 1365-1377 (2013).

122. Neuhuber, B., Swanger, S.A., Howard, L., Mackay, A. & Fischer, I. Effects of plating density and culture time on bone marrow stromal cell characteristics. *Experimental hematology* **36**, 1176-1185 (2008).

123. Huang, Y., Li, Q., Zhang, K., Hu, M., Wang, Y., Du, L., Lin, L., Li, S., Sorokin, L., Melino, G., Shi, Y. & Wang, Y. Single cell transcriptomic analysis of human mesenchymal stem cells reveals limited heterogeneity. *Cell Death & Disease* **10**, 368 (2019).

124. de Witte, S.F.H., Lambert, E.E., Merino, A., Strini, T., Douben, H., O'Flynn, L., Elliman, S.J., de Klein, A., Newsome, P.N., Baan, C.C. & Hoogduijn, M.J. Aging of bone marrow- and umbilical cord-derived mesenchymal stromal cells during expansion. *Cytotherapy* **19**, 798-807 (2017).

125. Yong, K.W., Choi, J.R., Dolbashid, A.S. & Wan Safwani, W.K.Z. Biosafety and bioefficacy assessment of human mesenchymal stem cells: what do we know so far? *Regen Med* **13**, 219-232 (2018).

126. Parsha, K., Mir, O., Satani, N., Yang, B., Guerrero, W., Mei, Z., Cai, C., Chen, P.R., Gee, A., Hanley, P.J., Aronowski, J. & Savitz, S.I. Mesenchymal stromal cell secretomes are modulated by suspension time, delivery vehicle, passage through catheter, and exposure to adjuvants. *Cytotherapy* **19**, 36-46 (2017).

127. Uccelli, A., Moretta, L. & Pistoia, V. Mesenchymal stem cells in health and disease. *Nature reviews. Immunology* **8**, 726-736 (2008).

128. Wei, X., Yang, X., Han, Z.-p., Qu, F.-f., Shao, L. & Shi, Y.-f. Mesenchymal stem cells: a new trend for cell therapy. *Acta Pharmacologica Sinica* **34**, 747-754 (2013).

129. Shah, K. Mesenchymal stem cells engineered for cancer therapy. *Advanced drug delivery reviews* **64**, 739-748 (2012).

130. Momin, E.N., Vela, G., Zaidi, H.A. & Quiñones-Hinojosa, A. The Oncogenic Potential of Mesenchymal Stem Cells in the Treatment of Cancer: Directions for Future Research. *Curr Immunol Rev* **6**, 137-148 (2010).

131. El-Badawy, A., Ghoneim, M.A., Gabr, M.M., Salah, R.A., Mohamed, I.K., Amer, M. & El-Badri, N. Cancer cell-soluble factors reprogram mesenchymal stromal cells to slow cycling, chemoresistant cells with a more stem-like state. *Stem Cell Research & Therapy* **8**, 254 (2017).

132. Berger, L., Shamai, Y., Skorecki, K.L. & Tzukerman, M. Tumor Specific Recruitment and Reprogramming of Mesenchymal Stem Cells in Tumorigenesis. *Stem Cells* **34**, 1011-1026 (2016).

133. Kalluri, R. & Zeisberg, M. Fibroblasts in cancer. *Nature reviews. Cancer* **6**, 392-401 (2006).

134. Quante, M., Tu, S.P., Tomita, H., Gonda, T., Wang, S.S., Takashi, S., Baik, G.H., Shibata, W., Diprete, B., Betz, K.S., Friedman, R., Varro, A., Tycko, B. & Wang, T.C. Bone marrow-derived myofibroblasts contribute to the mesenchymal stem cell niche and promote tumor growth. *Cancer Cell* **19**, 257-272 (2011).

135. CellTrials.org. "MSC Trials 2011-2018." 12/24/19. https://celltrials.org/public-cells-data/msc-trials-2011-2018/65.

136. Digirolamo, C.M., Stokes, D., Colter, D., Phinney, D.G., Class, R. & Prockop, D.J. Propagation and senescence of human marrow stromal cells in culture: a simple colony-forming assay identifies samples with the greatest potential to propagate and differentiate. *British journal of haematology* **107**, 275-281 (1999).

137. Zuk, P.A., Zhu, M., Mizuno, H., Huang, J., Futrell, J.W., Katz, A.J., Benhaim, P., Lorenz, H.P. & Hedrick, M.H. Multilineage cells from human adipose tissue: implications for cell-based therapies. *Tissue Eng* **7**, 211-228 (2001).

138. Sterodimas, A., de Faria, J., Nicaretta, B. & Pitanguy, I. Tissue engineering with adipose-derived stem cells (ADSCs): Current and future applications. *Journal of Plastic, Reconstructive & Aesthetic Surgery* **63**, 1886-1892 (2010).

139. Elman, J.S., Li, M., Wang, F., Gimble, J.M. & Parekkadan, B. A comparison of adipose and bone marrow-derived mesenchymal stromal cell secreted factors in the treatment of systemic inflammation. *J Inflamm (Lond)* **11**, 1-1 (2014).

140. Huang, S.J., Fu, R.H., Shyu, W.C., Liu, S.P., Jong, G.P., Chiu, Y.W., Wu, H.S., Tsou, Y.A., Cheng, C.W. & Lin, S.Z. Adipose-derived stem cells: isolation, characterization, and differentiation potential. *Cell Transplant* **22**, 701-709 (2013).

141. Kuhbier, J.W., Weyand, B., Radtke, C., Vogt, P.M., Kasper, C. & Reimers, K. Isolation, characterization, differentiation, and application of adipose-derived stem cells. *Advances in biochemical engineering/biotechnology* **123**, 55-105 (2010).

142. American Type Culture Collection. "ASC52telo, hTERT immortalized adipose derived Mesenchymal stem cells (ATCC® SCRC-4000™)." 12-31-19. https://www.atcc.org/products/all/SCRC-4000.aspx.

143. Wolbank, S., Stadler, G., Peterbauer, A., Gillich, A., Karbiener, M., Streubel, B., Wieser, M., Katinger, H., van Griensven, M., Redl, H., Gabriel, C., Grillari, J. & Grillari-Voglauer, R. Telomerase immortalized human amnion- and adipose-derived mesenchymal stem cells: maintenance of differentiation and immunomodulatory characteristics. *Tissue engineering. Part A* **15**, 1843-1854 (2009).

144. Miyagi-Shiohira, C., Kurima, K., Kobayashi, N., Saitoh, I., Watanabe, M., Noguchi, Y., Matsushita, M. & Noguchi, H. Cryopreservation of Adipose-Derived Mesenchymal Stem Cells. *Cell Medicine* **8**, 3-7 (2015).

145. Bhattacharyya, D., Hammond, A.T. & Glick, B.S. High-quality immunofluorescence of cultured cells. *Methods Mol Biol* **619**, 403-410 (2010).

146. Kramer, N., Walzl, A., Unger, C., Rosner, M., Krupitza, G., Hengstschläger, M. & Dolznig, H. In vitro cell migration and invasion assays. *Mutation Research/Reviews in Mutation Research* **752**, 10-24 (2013).

147. Davidson, P.M., Sliz, J., Isermann, P., Denais, C. & Lammerding, J. Design of a microfluidic device to quantify dynamic intra-nuclear deformation during cell migration through confining environments. *Integrative biology : quantitative biosciences from nano to macro* **7**, 1534-1546 (2015).

148. Keys, J., Windsor, A. & Lammerding, J. Assembly and Use of a Microfluidic Device to Study Cell Migration in Confined Environments. *Methods Mol Biol* **1840**, 101-118 (2018).

149. Dorland, Y.L., Cornelissen, A.S., Kuijk, C., Tol, S., Hoogenboezem, M., van Buul, J.D., Nolte, M.A., Voermans, C. & Huveneers, S. Nuclear shape, protrusive behaviour and in vivo retention of human bone marrow mesenchymal stromal cells is controlled by Lamin-A/C expression. *Scientific Reports* **9**, 14401 (2019).

150. Dinarello, C.A. Historical insights into cytokines. *Eur J Immunol* **37 Suppl 1**, S34-S45 (2007).

151. Whiteside, T.L. Cytokines and cytokine measurements in a clinical laboratory. *Clinical and diagnostic laboratory immunology* **1**, 257-260 (1994).

152. Vazquez-Lombardi, R., Roome, B. & Christ, D. Molecular Engineering of Therapeutic Cytokines. *Antibodies* **2** (2013).

153. Spangler, J.B., Moraga, I., Mendoza, J.L. & Garcia, K.C. Insights into Cytokine–Receptor Interactions from Cytokine Engineering. *Annual Review of Immunology* **33**, 139-167 (2015).

154. Shimabukuro-Vornhagen, A., Gödel, P., Subklewe, M., Stemmler, H.J., Schlößer, H.A., Schlaak, M., Kochanek, M., Böll, B. & von Bergwelt-Baildon, M.S. Cytokine release syndrome. *Journal for ImmunoTherapy of Cancer* **6**, 56 (2018).

155. Labusca, L., Herea, D.D. & Mashayekhi, K. Stem cells as delivery vehicles for regenerative medicine-challenges and perspectives. *World journal of stem cells* **10**, 43-56 (2018).

156. Biotechnologies, T. "Custom mRNA synthesis." https://www.trilinkbiotech.com/custom-mrna-synthesis.

157. Kozak, M. Pushing the limits of the scanning mechanism for initiation of translation. *Gene* **299**, 1-34 (2002).

158. Lasek, W., Zagozdzon, R. & Jakobisiak, M. Interleukin 12: still a promising candidate for tumor immunotherapy? *Cancer Immunol Immunother* **63**, 419-435 (2014).

159. Saxena, A., Khosraviani, S., Noel, S., Mohan, D., Donner, T. & Hamad, A.R. Interleukin-10 paradox: A potent immunoregulatory cytokine that has been difficult to harness for immunotherapy. *Cytokine* **74**, 27-34 (2015).

160. Del Vecchio, M., Bajetta, E., Canova, S., Lotze, M.T., Wesa, A., Parmiani, G. & Anichini, A. Interleukin-12: biological properties and clinical application. *Clin Cancer Res* **13**, 4677-4685 (2007).

161. Ma, X., Yan, W., Zheng, H., Du, Q., Zhang, L., Ban, Y., Li, N. & Wei, F. Regulation of IL-10 and IL-12 production and function in macrophages and dendritic cells. *F1000Res* **4**, F1000 Faculty Rev-1465 (2015).

162. Wang, X., Wong, K., Ouyang, W. & Rutz, S. Targeting IL-10 Family Cytokines for the Treatment of Human Diseases. *Cold Spring Harb Perspect Biol* **11** (2019).

163. Teixido, J., Martinez-Moreno, M., Diaz-Martinez, M. & Sevilla-Movilla, S. The good and bad faces of the CXCR4 chemokine receptor. *Int J Biochem Cell Biol* **95**, 121-131 (2018).

164. Won, Y.W., Patel, A.N. & Bull, D.A. Cell surface engineering to enhance mesenchymal stem cell migration toward an SDF-1 gradient. *Biomaterials* **35**, 5627-5635 (2014).

165. Bakos, E., Thaiss, C.A., Kramer, M.P., Cohen, S., Radomir, L., Orr, I., Kaushansky, N., Ben-Nun, A., Becker-Herman, S. & Shachar, I. CCR2 Regulates the Immune Response by Modulating the Interconversion and Function of Effector and Regulatory T Cells. *The Journal of Immunology* **198**, 4659 (2017).

166. Yoshimura, T. The chemokine MCP-1 (CCL2) in the host interaction with cancer: a foe or ally? *Cell Mol Immunol* **15**, 335-345 (2018).

167. Huang, Y., Wang, J., Cai, J., Qiu, Y., Zheng, H., Lai, X., Sui, X., Wang, Y., Lu, Q., Zhang, Y., Yuan, M., Gong, J., Cai, W., Liu, X., Shan, Y., Deng, Z., Shi, Y., Shu, Y., Zhang, L., Qiu, W., Peng, L., Ren, J., Lu, Z. & Xiang, A.P. Targeted homing of CCR2-overexpressing mesenchymal stromal cells to ischemic brain enhances post-stroke recovery partially through PRDX4-mediated blood-brain barrier preservation. *Theranostics* **8**, 5929-5944 (2018).

168. Harjunpää, H., Llort Asens, M., Guenther, C. & Fagerholm, S.C. Cell Adhesion Molecules and Their Roles and Regulation in the Immune and Tumor Microenvironment. *Frontiers in Immunology* **10** (2019).

169. Ullah, I., Subbarao, R.B. & Rho, G.J. Human mesenchymal stem cells - current trends and future prospective. *Biosci Rep* **35** (2015).

170. Ruster, B., Gottig, S., Ludwig, R.J., Bistrian, R., Muller, S., Seifried, E., Gille, J. & Henschler, R. Mesenchymal stem cells display coordinated rolling and adhesion behavior on endothelial cells. *Blood* **108**, 3938-3944 (2006).

171. Levy, O., Zhao, W., Mortensen, L.J., Leblanc, S., Tsang, K., Fu, M., Phillips, J.A., Sagar, V., Anandakumaran, P., Ngai, J., Cui, C.H., Eimon, P., Angel, M., Lin, C.P., Yanik, M.F. & Karp, J.M. mRNA-engineered mesenchymal stem cells for targeted delivery of interleukin-10 to sites of inflammation. *Blood* **122**, e23-32 (2013).

172. Lo, C.Y., Weil, B.R., Palka, B.A., Momeni, A., Canty, J.M. & Neelamegham, S. Cell surface glycoengineering improves selectin-mediated adhesion of mesenchymal stem cells (MSCs) and cardiosphere-derived cells (CDCs): Pilot validation in porcine ischemia-reperfusion model. *Biomaterials* **74**, 19-30 (2016).

173. Liao, W., Pham, V., Liu, L., Riazifar, M., Pone, E.J., Zhang, S.X., Ma, F., Lu, M., Walsh, C.M. & Zhao, W. Mesenchymal stem cells engineered to express selectin ligands and IL-10 exert enhanced therapeutic efficacy in murine experimental autoimmune encephalomyelitis. *Biomaterials* **77**, 87-97 (2016).

174. Lee, K.L., Kuo, Y.C., Ho, Y.S. & Huang, Y.H. Triple-Negative Breast Cancer: Current Understanding and Future Therapeutic Breakthrough Targeting Cancer Stemness. *Cancers (Basel)* **11** (2019).

175. Sugiura, K. & Stock, C.C. Studies in a tumor spectrum. I. Comparison of the action of methylbis (2-chloroethyl)amine and 3-bis(2-chloroethyl)aminomethyl-4-methoxymethyl -5-hydroxy-6-methylpyridine on the growth of a variety of mouse and rat tumors. *Cancer* **5**, 382-402 (1952).

176. Dunham, L.J. & Stewart, H.L. A survey of transplantable and transmissible animal tumors. *J Natl Cancer Inst* **13**, 1299-1377 (1953).

177. Ewens, A., Mihich, E. & Ehrke, M.J. Distant metastasis from subcutaneously grown E0771 medullary breast adenocarcinoma. *Anticancer Res* **25**, 3905-3915 (2005).

178. Johnstone, C.N., Smith, Y.E., Cao, Y., Burrows, A.D., Cross, R.S., Ling, X., Redvers, R.P., Doherty, J.P., Eckhardt, B.L., Natoli, A.L., Restall, C.M., Lucas, E., Pearson, H.B., Deb, S., Britt, K.L., Rizzitelli, A., Li, J., Harmey, J.H., Pouliot, N. & Anderson, R.L. Functional and molecular characterisation of EO771.LMB tumours, a new C57BL/6-mouse-derived model of spontaneously metastatic mammary cancer. *Dis Model Mech* **8**, 237-251 (2015).

179. Crosby, E.J., Wei, J., Yang, X.Y., Lei, G., Wang, T., Liu, C.X., Agarwal, P., Korman, A.J., Morse, M.A., Gouin, K., Knott, S.R.V., Lyerly, H.K. & Hartman, Z.C. Complimentary mechanisms of dual checkpoint blockade expand unique T-cell repertoires and activate adaptive anti-tumor immunity in triple-negative breast tumors. *Oncoimmunology* **7**, e1421891 (2018).

180. Van Gundy, Z.C., Markowitz, J., Baker, J.D., Strange, H.R. & Papenfuss, T.L. An In vitro Model System to Generate Breast Cancer MDSCs and Study Immune Cell Interactions in Immunocompetent C57bl/6 Mice. *journal of cancer biology and research* **2** (2014).

181. Pearce, J.V., Farrar, J.S., Lownik, J.C., Ni, B., Chen, S., Kan, T.W. & Celi, F.S. E0771 and 4T1 murine breast cancer cells and interleukin 6 alter gene expression patterns but do not induce browning in cultured white adipocytes. *Biochem Biophys Rep* **18**, 100624 (2019).

182. Kobayashi, M., Fitz, L., Ryan, M., Hewick, R.M., Clark, S.C., Chan, S., Loudon, R., Sherman, F., Perussia, B. & Trinchieri, G. Identification and purification of natural killer cell stimulatory factor (NKSF), a cytokine with multiple biologic effects on human lymphocytes. *J Exp Med* **170**, 827-845 (1989).

183. Stern, A.S., Podlaski, F.J., Hulmes, J.D., Pan, Y.C., Quinn, P.M., Wolitzky, A.G., Familletti, P.C., Stremlo, D.L., Truitt, T., Chizzonite, R. & et al. Purification to homogeneity and partial characterization of cytotoxic lymphocyte maturation factor from human B-lymphoblastoid cells. *Proc Natl Acad Sci U S A* **87**, 6808-6812 (1990).

184. Ding, Q., Lu, P., Xia, Y., Ding, S., Fan, Y., Li, X., Han, P., Liu, J., Tian, D. & Liu, M. CXCL9: evidence and contradictions for its role in tumor progression. *Cancer medicine* **5**, 3246-3259 (2016).

185. Cheng, X., Zhao, Z., Ventura, E., Gran, B., Shindler, K.S. & Rostami, A. The PD-1/PD-L pathway is up-regulated during IL-12-induced suppression of EAE mediated by IFN-gamma. *J Neuroimmunol* **185**, 75-86 (2007).

186. Colombo, M.P. & Trinchieri, G. Interleukin-12 in anti-tumor immunity and immunotherapy. *Cytokine & growth factor reviews* **13**, 155-168 (2002).

187. Car, B.D., Eng, V.M., Lipman, J.M. & Anderson, T.D. The toxicology of interleukin-12: a review. *Toxicologic pathology* **27**, 58-63 (1999).

188. Mahvi, D.M., Henry, M.B., Albertini, M.R., Weber, S., Meredith, K., Schalch, H., Rakhmilevich, A., Hank, J. & Sondel, P. Intratumoral injection of IL-12 plasmid DNA – results of a phase I/IB clinical trial. *Cancer Gene Therapy* **14**, 717-723 (2007).

189. Aznar, M.A., Tinari, N., Rullán, A.J., Sánchez-Paulete, A.R., Rodriguez-Ruiz, M.E. & Melero, I. Intratumoral Delivery of Immunotherapy—Act Locally, Think Globally. *The Journal of Immunology* **198**, 31 (2017).

190. Marabelle, A., Kohrt, H., Caux, C. & Levy, R. Intratumoral Immunization: A New Paradigm for Cancer Therapy. *Clinical Cancer Research* **20**, 1747 (2014).

191. Marabelle, A., Andtbacka, R., Harrington, K., Melero, I., Leidner, R., de Baere, T., Robert, C., Ascierto, P.A., Baurain, J.F., Imperiale, M., Rahimian, S., Tersago, D., Klumper, E., Hendriks, M., Kumar, R., Stern, M., Öhrling, K., Massacesi, C., Tchakov, I., Tse, A., Douillard, J.Y., Tabernero, J., Haanen, J. & Brody, J. Starting the fight in the tumor: expert recommendations for the development of human intratumoral immunotherapy (HIT-IT). *Ann Oncol* **29**, 2163-2174 (2018).

192. Tugues, S., Burkhard, S.H., Ohs, I., Vrohlings, M., Nussbaum, K., Vom Berg, J., Kulig, P. & Becher, B. New insights into IL-12-mediated tumor suppression. *Cell Death Differ* **22**, 237-246 (2015).

193. Darvin, P., Toor, S.M., Sasidharan Nair, V. & Elkord, E. Immune checkpoint inhibitors: recent progress and potential biomarkers. *Experimental & Molecular Medicine* **50**, 165 (2018).

194. Li, X., Li, M., Lian, Z., Zhu, H., Kong, L., Wang, P. & Yu, J. Prognostic Role of Programmed Death Ligand-1 Expression in Breast Cancer: A Systematic Review and Meta-Analysis. *Targeted oncology* **11**, 753-761 (2016).

195. Kwa, M.J. & Adams, S. Checkpoint inhibitors in triple-negative breast cancer (TNBC): Where to go from here. *Cancer* **124**, 2086-2103 (2018).

196. Garris, C.S., Arlauckas, S.P., Kohler, R.H., Trefny, M.P., Garren, S., Piot, C., Engblom, C., Pfirschke, C., Siwicki, M., Gungabeesoon, J., Freeman, G.J., Warren, S.E., Ong, S., Browning, E., Twitty, C.G., Pierce, R.H., Le, M.H., Algazi, A.P., Daud, A.I., Pai, S.I., Zippelius, A., Weissleder, R. & Pittet, M.J. Successful Anti-PD-1 Cancer Immunotherapy

Requires T Cell-Dendritic Cell Crosstalk Involving the Cytokines IFN-gamma and IL-12. *Immunity* **49**, 1148-1161 e1147 (2018).

197. Marra, A., Viale, G. & Curigliano, G. Recent advances in triple negative breast cancer: the immunotherapy era. *BMC medicine* **17**, 90-90 (2019).

198. Miyashita, M., Sasano, H., Tamaki, K., Hirakawa, H., Takahashi, Y., Nakagawa, S., Watanabe, G., Tada, H., Suzuki, A., Ohuchi, N. & Ishida, T. Prognostic significance of tumor-infiltrating CD8+ and FOXP3+ lymphocytes in residual tumors and alterations in these parameters after neoadjuvant chemotherapy in triple-negative breast cancer: a retrospective multicenter study. *Breast cancer research : BCR* **17**, 124 (2015).

199. Vikas, P., Borcherding, N. & Zhang, W. The clinical promise of immunotherapy in triple-negative breast cancer. *Cancer Manag Res* **10**, 6823-6833 (2018).

200. Hu, W., Wang, G., Huang, D., Sui, M. & Xu, Y. Cancer Immunotherapy Based on Natural Killer Cells: Current Progress and New Opportunities. *Frontiers in immunology* **10**, 1205-1205 (2019).

201. Yang, M., McKay, D., Pollard, J.W. & Lewis, C.E. Diverse Functions of Macrophages in Different Tumor Microenvironments. *Cancer Research* **78**, 5492 (2018).

202. Kaira, K., Yamaguchi, O., Yoshimura, K., Mouri, A., Shiono, A., Nishihara, F., Miura, Y., Shinomiya, S., Hashimoto, K., Murayama, Y., Kitano, S., Kobayashi, K. & Kagamu, H. CD4+ T-cell immunity predicts long-lasting antitumor immunity after PD-1 blockade therapy. *Journal of Clinical Oncology* **37**, 2545-2545 (2019).

203. Wang, H., Lapek, J., Fujimura, K., Strnadel, J., Liu, B., Gonzalez, D.J., Zhang, W., Watson, F., Yu, V., Liu, C., Melo, C.M., Miller, Y.I., Elliott, K.C., Cheresh, D.A. & Klemke, R.L. Pseudopodium-enriched atypical kinase 1 mediates angiogenesis by modulating GATA2-dependent VEGFR2 transcription. *Cell Discov* **4**, 26 (2018).

204. Bui, J.D., Uppaluri, R., Hsieh, C.S. & Schreiber, R.D. Comparative analysis of regulatory and effector T cells in progressively growing versus rejecting tumors of similar origins. *Cancer Res* **66**, 7301-7309 (2006).

205. Bi, J. & Tian, Z. NK Cell Exhaustion. *Frontiers in immunology* **8**, 760-760 (2017).

206. Caplan, H., Olson, S.D., Kumar, A., George, M., Prabhakara, K.S., Wenzel, P., Bedi, S., Toledano-Furman, N.E., Triolo, F., Kamhieh-Milz, J., Moll, G. & Cox, C.S. Mesenchymal Stromal Cell Therapeutic Delivery: Translational Challenges to Clinical Application. *Frontiers in Immunology* **10**, 1645 (2019).

207. De Becker, A. & Riet, I.V. Homing and migration of mesenchymal stromal cells: How to improve the efficacy of cell therapy? *World J Stem Cells* **8**, 73-87 (2016).

208. Wysoczynski, M., Khan, A. & Bolli, R. New Paradigms in Cell Therapy: Repeated Dosing, Intravenous Delivery, Immunomodulatory Actions, and New Cell Types. *Circ Res* **123**, 138-158 (2018).

209. Kanazawa, M., Atsuta, I., Ayukawa, Y., Yamaza, T., Kondo, R., Matsuura, Y. & Koyano, K. The influence of systemically or locally administered mesenchymal stem cells on tissue repair in a rat oral implantation model. *Int J Implant Dent* **4**, 2-2 (2018).

210. Huang, S., Xu, L., Zhang, Y., Sun, Y. & Li, G. Systemic and Local Administration of Allogeneic Bone Marrow-Derived Mesenchymal Stem Cells Promotes Fracture Healing in Rats. *Cell Transplantation* **24**, 2643-2655 (2015).

211. Kallmeyer, K., André-Lévigne, D., Baquié, M., Krause, K.-H., Pepper, M.S., Pittet-Cuénod, B. & Modarressi, A. Fate of systemically and locally administered adipose-derived mesenchymal stromal cells and their effect on wound healing. *STEM CELLS Translational Medicine* **n/a** (2019).

212. Leibacher, J. & Henschler, R. Biodistribution, migration and homing of systemically applied mesenchymal stem/stromal cells. *Stem Cell Res Ther* **7**, 7 (2016).

213. Fischer, U.M., Harting, M.T., Jimenez, F., Monzon-Posadas, W.O., Xue, H., Savitz, S.I., Laine, G.A. & Cox, C.S., Jr. Pulmonary passage is a major obstacle for intravenous stem cell delivery: the pulmonary first-pass effect. *Stem Cells Dev* **18**, 683-692 (2009).

214. Schrepfer, S., Deuse, T., Reichenspurner, H., Fischbein, M.P., Robbins, R.C. & Pelletier, M.P. Stem cell transplantation: the lung barrier. *Transplantation proceedings* **39**, 573-576 (2007).

215. Wang, S., Guo, L., Ge, J., Yu, L., Cai, T., Tian, R., Jiang, Y., Zhao, R. & Wu, Y. Excess Integrins Cause Lung Entrapment of Mesenchymal Stem Cells. *Stem Cells* **33**, 3315-3326 (2015).

216. Zanetti, A., Grata, M., Etling, E.B., Panday, R., Villanueva, F.S. & Toma, C. Suspension-Expansion of Bone Marrow Results in Small Mesenchymal Stem Cells Exhibiting Increased Transpulmonary Passage Following Intravenous Administration. *Tissue Eng Part C Methods* **21**, 683-692 (2015).

217. Bartosh, T.J. & Ylostalo, J.H. Preparation of Anti-Inflammatory Mesenchymal Stem/Precursor Cells (MSCs) Through Sphere Formation Using Hanging-Drop Culture Technique. *Current Protocols in Stem Cell Biology* **28**, 2B.6.1-2B.6.23 (2014).

218. Gad, S.C. The mouse ear swelling test (MEST) in the 1990s. *Toxicology* **93**, 33-46 (1994).

219. Gábor, M. THE MOUSE EAR AS A MODEL FOR CUTANEOUS IRRITATION. *Journal of Toxicology: Cutaneous and Ocular Toxicology* **21**, 191-202 (2002).

220. Thorne, P.S., Hawk, C., Kaliszewski, S.D. & Guiney, P.D. The noninvasive mouse ear swelling assay. I. Refinements for detecting weak contact sensitizers. *Fundamental and applied toxicology : official journal of the Society of Toxicology* **17**, 790-806 (1991).

221. Marino-Marmolejo, E.N., Flores-Hernández, F.Y., Flores-Valdez, M.A., García-Morales, L.F., González-Villegas, A.C. & Bravo-Madrigal, J. A quantitative model for dermal infection and oedema in BALB/c mice pinna. *BMC Microbiology* **16**, 290 (2016).

222. Teo, G.S.L., Yang, Z., Carman, C.V., Karp, J.M. & Lin, C.P. Intravital Imaging of Mesenchymal Stem Cell Trafficking and Association With Platelets and Neutrophils. *STEM CELLS* **33**, 265-277 (2015).

223. Mortensen, L.J., Levy, O., Phillips, J.P., Stratton, T., Triana, B., Ruiz, J.P., Gu, F., Karp, J.M. & Lin, C.P. Quantification of Mesenchymal Stem Cell (MSC) delivery to a target site using in vivo confocal microscopy. *PLoS One* **8**, e78145 (2013).

224. Sarkar, D., Zhao, W., Gupta, A., Loh, W.L., Karnik, R. & Karp, J.M. in Mesenchymal Stem Cell Assays and Applications. (eds. M. Vemuri, L.G. Chase & M.S. Rao) 505-523 (Humana Press, Totowa, NJ; 2011).

225. Corradetti, B., Taraballi, F., Martinez, J.O., Minardi, S., Basu, N., Bauza, G., Evangelopoulos, M., Powell, S., Corbo, C. & Tasciotti, E. Hyaluronic acid coatings as a simple and efficient approach to improve MSC homing toward the site of inflammation. *Scientific Reports* **7**, 7991 (2017).

226. Brunger, J.M., Zutshi, A., Willard, V.P., Gersbach, C.A. & Guilak, F. Genome Engineering of Stem Cells for Autonomously Regulated, Closed-Loop Delivery of Biologic Drugs. *Stem Cell Reports* **8**, 1202-1213 (2017).

227. Fiorentino, D.F., Bond, M.W. & Mosmann, T.R. Two types of mouse T helper cell. IV. Th2 clones secrete a factor that inhibits cytokine production by Th1 clones. *J Exp Med* **170**, 2081-2095 (1989).

228. Saraiva, M. & O'Garra, A. The regulation of IL-10 production by immune cells. *Nature Reviews Immunology* **10**, 170-181 (2010).

229. Ng, T.H., Britton, G.J., Hill, E.V., Verhagen, J., Burton, B.R. & Wraith, D.C. Regulation of adaptive immunity; the role of interleukin-10. *Front Immunol* **4**, 129 (2013).

230. Mannino, M.H., Zhu, Z., Xiao, H., Bai, Q., Wakefield, M.R. & Fang, Y. The paradoxical role of IL-10 in immunity and cancer. *Cancer Lett* **367**, 103-107 (2015).

231. Shouval, D.S., Ouahed, J., Biswas, A., Goettel, J.A., Horwitz, B.H., Klein, C., Muise, A.M. & Snapper, S.B. Interleukin 10 receptor signaling: master regulator of intestinal mucosal homeostasis in mice and humans. *Adv Immunol* **122**, 177-210 (2014).

232. Bartosh, T.J., Ylostalo, J.H., Mohammadipoor, A., Bazhanov, N., Coble, K., Claypool, K., Lee, R.H., Choi, H. & Prockop, D.J. Aggregation of human mesenchymal stromal cells (MSCs) into 3D spheroids enhances their antiinflammatory properties. *Proc Natl Acad Sci U S A* **107**, 13724-13729 (2010).